MICROCOPY RESOLUTION TEST CHART
NATIONAL BUREAU OF STANDARDS-1963-A

REPORT DOCUMENTATION PAGE		READ INSTRUCTIONS BEFORE COMPLETING FORM
1. REPORT NUMBER AFIT/CI/NR 86-172D	**2. GOVT ACCESSION NO.**	**3. RECIPIENT'S CATALOG NUMBER**
4. TITLE *(and Subtitle)* Multipixel, Multidimensional Laser Radar System Performance		**5. TYPE OF REPORT & PERIOD COVERED** THESIS/DISSERTATION
		6. PERFORMING ORG. REPORT NUMBER
7. AUTHOR(s) Martin B. Mark		**8. CONTRACT OR GRANT NUMBER(s)**
9. PERFORMING ORGANIZATION NAME AND ADDRESS AFIT STUDENT AT: Massachusetts Institute of Technology		**10. PROGRAM ELEMENT, PROJECT, TASK AREA & WORK UNIT NUMBERS**
11. CONTROLLING OFFICE NAME AND ADDRESS		**12. REPORT DATE** 1986
		13. NUMBER OF PAGES 141
14. MONITORING AGENCY NAME & ADDRESS(*if different from Controlling Office*)		**15. SECURITY CLASS.** *(of this report)* UNCLASS
		15a. DECLASSIFICATION/DOWNGRADING SCHEDULE

16. DISTRIBUTION STATEMENT *(of this Report)*

APPROVED FOR PUBLIC RELEASE; DISTRIBUTION UNLIMITED

17. DISTRIBUTION STATEMENT *(of the abstract entered in Block 20, if different from Report)*

18. SUPPLEMENTARY NOTES
APPROVED FOR PUBLIC RELEASE: IAW AFR 190-1

LYNN E. WOLAVER
Dean for Research and
Professional Development
AFIT/NR

DTIC
ELECTE
OCT 1 4 1986

19. KEY WORDS *(Continue on reverse side if necessary and identify by block number)*

20. ABSTRACT *(Continue on reverse side if necessary and identify by block number)*

ATTACHED ...

DD _{1 JAN 73} **1473**   EDITION OF 1 NOV 65 IS OBSOLETE

MULTIPIXEL, MULTIDIMENSIONAL LASER RADAR SYSTEM PERFORMANCE

by

CAPT MARTIN B. MARK, USAF

ABSTRACT

Laser radar analyses up to now generally fall into two categories. Single pixel analyses exist which cover receiver design, target statistics, atmospheric effects, and the resulting statistical performance characterizations like probabilities of detection (P_D) and false alarm (P_F). Multipixel analyses exist which use various ad hoc target recognition, identification, and feature extraction schemes based on intuitive insight or analogies to human perception. The limitation of these multipixel processors is it is difficult to quantitatively predict processor performance as a function of various system parameters and the resolving power in the measurement dimensions like range, Doppler shift, and angle. The single pixel performance equations can give quantitative answers to these questions, but only for single pixel measurements. This thesis bridges these two approaches by proposing physically realistic target, background, and radar models which allow us to incorporate the statistics for the single pixel measurements into multipixel probability density functions and derive quasi-optimal generalized likelihood ratio processors from the densities.

The thesis proposes simple but realistic models, then derives the multipixel density functions, the quasi-optimal multipixel processors, and P_D-P_F curves for the processors as a function of the radar parameters and measurement dimension resolving powers. The analyses are for a ranging radar, but duality arguments are presented which demonstrate how to apply the results directly to Doppler and range and Doppler radars. Some analyses are presented which show how the radar's resolution in range and angle measurement dimensions depend on each other through the radar equation for the carrier-to-noise ratio, how they interact to affect performance, and how it is possible to balance performance loss in one measurement dimension by improved resolution in another.

Thesis length: 141 pages

86 10 19 10

MULTIPIXEL, MULTIDIMENSIONAL LASER RADAR SYSTEM PERFORMANCE

by

CAPT MARTIN B. MARK, USAF

B. S. Electrical Engineering, Purdue University
(1979)

M. S. Electrical Engineering, Air Force Institute of Technology
(1980)

SUBMITTED TO THE DEPARTMENT OF
ELECTRICAL ENGINEERING AND COMPUTER SCIENCE
IN PARTIAL FULFILLMENT OF THE REQUIREMENTS
FOR THE DEGREE OF

DOCTOR OF PHILOSOPHY

at the

MASSACHUSETTS INSTITUTE OF TECHNOLOGY
August 1986

© Martin B. Mark, 1986

Signature of Author..
Department of Electrical Engineering and Computer Science
August 1986

Certified by..
Professor Jeffrey H. Shapiro
Thesis Supervisor

Accepted by...
Professor Arthur C. Smith
Chairman, Department Committee on Graduate Students

ACKNOWLEDGMENTS

First, I would like to thank my academic and thesis advisor, Prof Jeffrey
H. Shapiro. As a thesis advisor, his knowledge, patience, and ability to
clearly convey concepts have helped me through my research when I was
stymied. As an academic advisor, he always kept in mind my limited period
of time at MIT and helped me plan around it. I would like to thank Dr
Robert J. Hull for acting as a reader and, along with the other members of
the Lincoln Laboratory Opto-Radar Systems Group, for providing the use of
computers, real laser radar data when needed, and technical discussions on
the state of the art in this field. I thank my other reader, Prof David
H. Staelin, for helping me focus clearly on the problem statement when
preparing the drafts of the thesis. I also thank the current and past
members of the Optical Propagation and Communication Group at MIT for
their technical help and personal friendships.

I am most deeply thankful to my country and the US Air Force who permitted
me to spend these last three years of active duty doing nothing but
pursuing this degree. I look forward to repaying the investment they made
in me. In addition, I want to acknowledge the US Army for support under
contract DAAG29-84-K-0095.

Finally, I want to thank my wife, Lynn, for her patience, understanding,
and love. It isn't easy being married to a graduate student, particularly
one working under a strict deadline. In marrying me she gave up a big
wedding, a honeymoon, and a lot of time we could have spent together. I
am very grateful to her, thankful for her, and dedicate this thesis to
her.

For Lynn

TABLE OF CONTENTS

LIST OF FIGURES

I. INTRODUCTION

A. Laser Radar Overview

The development of lasers with sufficient stability, spectral purity, and power has allowed system designers to translate much of microwave radar design directly to the optical wavelength region [1]. Because their wavelength is so much shorter, laser radars offer spatial, angular, range, and Doppler shift resolutions far superior to those available with microwave systems. Although laser systems can take advantage of their increased resolution in any or all of these dimensions, the increased spatial and angular resolutions have particularly affected the way designers present data to the user. With beam diameters of a few centimeters at the radar optics exit aperture and beam angles measured in microradians, it is possible to scan the beam over the target and construct an image of the target, similar to a television (TV) image, from the radar returns. The color and intensity of the displayed image can represent reflected intensity, Doppler shift, range, or some combination of these signal dimensions [2].

With the shorter wavelength of laser systems, there comes a disadvantage as well. Because the wavelength is so short, most target surfaces are rough at dimensions on the order of the radar wavelength. So, they reflect the incident beam with an essentially random phase shift as a function of position on the target, producing a phenomenon known as laser speckle [3]. Laser speckle appears as a graininess in the image of the target due to self interference among the reflected wave's angular components. Since it is a self interference, it is independent of signal

strength. It appears even at very high carrier (reflected radar energy) to noise ratios. Any processing scheme should take into account both detection noise and speckle noise, both of which degrade image quality.

B. Image and Signal Processing

Laser radars (and some microwave radars as well) have sufficient spatial resolution that they can build images of targets by making spatially distributed measurements of the target with a beam of diameter much less than the target dimensions. Each spatially distinct element of the target is called a picture element, or pixel. Up to now, analyses for these high resolution radars have fallen into two general classes: single pixel statistical signal processing and multipixel image processing.

The single pixel processing work follows the traditional radar and communication system approaches [4]. This approach models the target and the radar, derives statistically optimal processors based on the models, and produces equations for the performance of the processors derived from the statistics. The advantages of this approach are twofold. First, the performance equations are in terms of the various laser system design parameters. This makes it easy to predict how performance will change as we vary the system parameters. Second, since the processors are statistically optimal, their performance measures must be bounds on the performance achievable with any other proposed processor. The disadvantage of this approach is it is a single pixel analysis. The processors don't use the information available to them from the spatially distributed measurements of several pixels.

The image processing approach, on the other hand, often draws on pattern recognition and image analysis theory from research in areas like remote sensing, machine vision, and artificial intelligence [5], [6]. This approach proposes intuitive algorithms based on these research fields, and the resulting ad hoc processors make little use of the statistics of the signals generating the images. The advantage of this approach is many of the processors seem to work quite well. The disadvantage is it is incapable of producing performance equations which allow system designers to predict how changes in the radar parameters will affect performance.

This thesis presents for the first time a method to perform statistical signal processing based on target and laser models like the single pixel approach just outlined, but which takes advantage of the multipixel nature of the targets. The result will be equations for the radar's performance against spatially distributed or multipixel targets in terms of the radar's design parameters. These equations are important because they give designers a method to perform trades among system parameters and predict the effect on system performance. With these equations it is possible, for instance, to trade intensity resolution with range resolution or spatial resolution with Doppler resolution and predict the effects on receiver performance. It is not possible to do this directly with the ad-hoc models. These equations also act as benchmarks against which we can compare the performance of the ad hoc image processing algorithms researchers will undoubtedly continue to pursue.

C. Problem Statement

We will study the classical radar detection problem [4]. In our detection

problem we will assume we are given a set of directions comprising an angular uncertainty region, Ω_u, and a corresponding swath of ranges representing a range uncertainty region, L_u, wherein a target may appear, as in Figure 1.1. There may or may not be a target in this uncertainty volume $\Omega_u L_u$ and, if there is, we don't know where it falls within the volume. Our task is to make measurements over the uncertainty volume with the laser radar and, based on the measurements, decide between two hypotheses: H_1, target present, and H_0, target absent. Although we will try to treat thoroughly general processors, the goal here is to derive tools to predict the performance of real systems. If necessary, we will make simplifying assumptions to get results which are useful for existing systems at the expense of complete generality in the analysis.

D. Thesis Organization

Chapter two of this thesis develops background information on laser radar systems and target statistical models. It derives a statistical model for the signal in the intermediate frequency (IF) system of the radar and imposes some IF pre-processing used in real laser radar systems. This chapter also takes the crucial step of presenting a model for the major characteristics of the target and its environment in a fashion which makes it possible to incorporate these characteristics into the statistical signal model.

Chapter three derives a joint probability density function for two of the most common radar measurements: range and intensity. Chapter three closes by considering the range-Doppler and range-range and Doppler dualities which make it possible to do the Doppler and range and Doppler

H_1: TARGET PRESENT

H_0: TARGET ABSENT

L_u

Ω_u
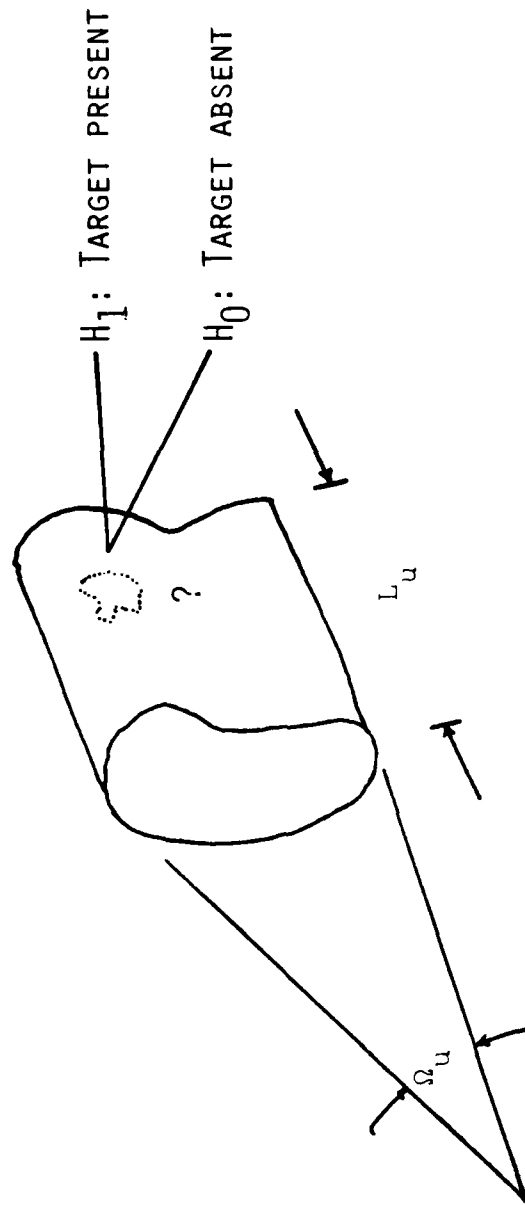
FIGURE 1.1

THE TARGET DETECTION PROBLEM

system analyses by direct analogy with the range system analysis.

Chapter four introduces the binary detection receiver and the generalized likelihood ratio and derives optimal and near optimal processors for several measurement models. Chapter five takes two of the most important processors from chapter four and derives equations to characterize their performance.

Chapter six presents numerical and graphical results for the equations in chapter five. These results demonstrate how the radar performance, in terms of probability of detection, P_D, and probability of false alarm, P_F, varies as a function of the laser design parameters, the target characteristics, and the type of radar used. Specifically, we will assess how performance varies as a function of radar resolution capabilities for several types of radars with laser sources of either constant average or peak power. The ultimate output of this analysis is the ability to predict for the first time what sets of design parameters will allow the radar to meet a given performance level against a multipixel target.

The final chapter summarizes the thesis, draws some conclusions, and outlines some areas where further research may be profitable.

II. LASER RADAR BACKGROUND

A. System Configuration

Figure 2.1 is the simplified block diagram of a coherent laser radar. This thesis considers only monostatic radars -- the transmitter's exit optics and the receiver's entrance optics are the same. This could be a ranging or Doppler radar (or both). The principal differences between these systems are the transmitted waveforms and the type of intermediate frequency (IF) processing. For a ranging system, the waveform is usually as short as possible to give good range resolution. For a Doppler system, the waveform may be continuous wave (CW) or a long pulse. It is possible to time-share both measurements with an appropriate choice of waveform [7]. The radar performs a raster scan of the transmitter beam as shown in figure 2.2. The scan rates are such that there is minimal beam overlap between adjacent pixels. The radar may be on a truck, an aircraft, or elsewhere. For the air-to-ground imaging situation, the radar is above and looking down on the target. This imposes a specific laser-target geometry, which we will introduce and exploit in section E of this chapter.

This thesis uses the laser radar systems in existence at MIT Lincoln Laboratory as examples of real systems when desiring to make theoretical models simpler or more realistic, or to use specific numerical values for design parameters. The Lincoln Laboratory systems use CO_2 lasers operating at a wavelength of 10.6 μm. These systems operate at relatively short ranges (on the order of a few kilometers) with modest aperture sizes (on the order of 10 to 20 centimeters) [8], [9]. The
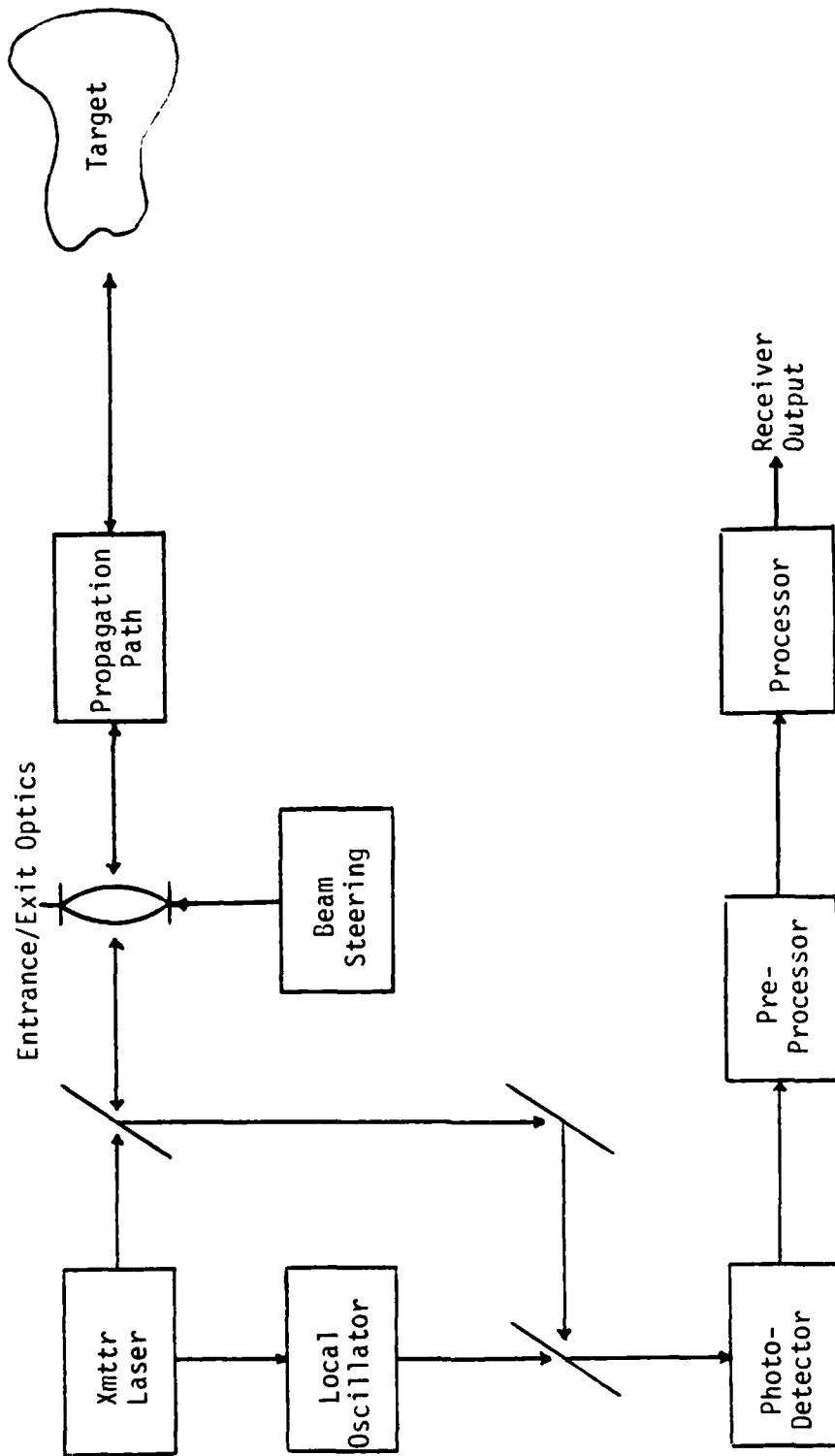
Figure 2.1
Laser Radar Block Diagram
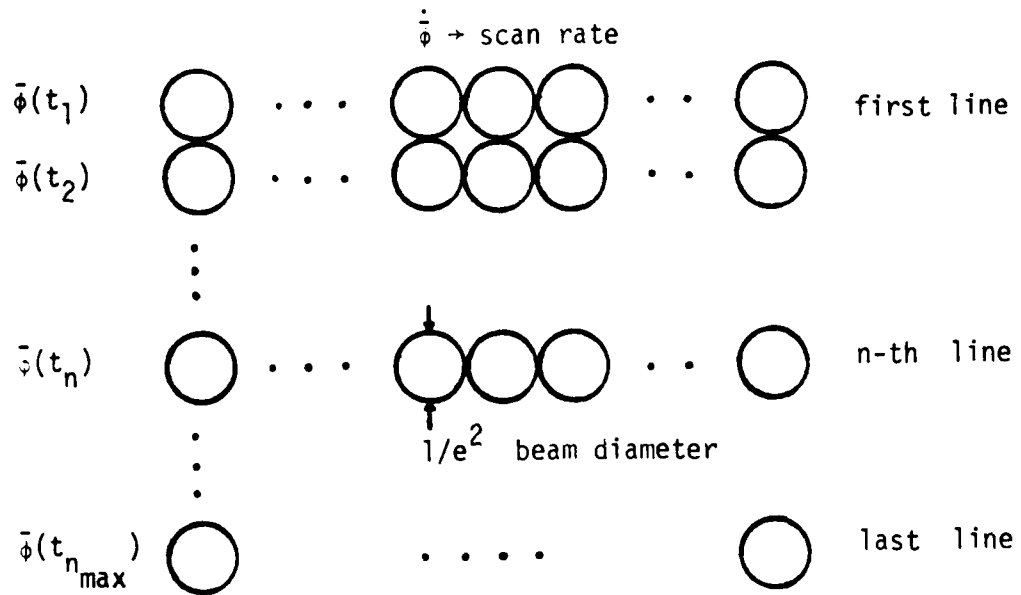
Figure 2.2

Radar Beam Raster Scan in Angle Space

aperture size, laser power level (up to a few watts [8], [9]), and detector sensitivity combine to limit the radar's range under any given set of atmospheric conditions. The aperture size is not larger because these systems are designed to investigate the design of primarily compact systems for air-to-ground applications. These systems also use heterodyne detection rather than direct detection. The advantages of a heterodyne system are that it increases the sensitivity of the detector because of the well known detection gain of a heterodyne system [10] and, since the local oscillator is coherent with the received optical signal, it preserves the relative phase variations of the received signal so the receiver can measure Doppler shifts in the optical carrier [10]. Since a direct detection receiver is not sensitive to the phase of the optical carrier, it cannot measure Doppler shifts. The disadvantage of a heterodyne system is the greater prominence of the speckle effect. In a direct detection system, it is possible to reduce the degree of speckle induced intensity variations by using a larger diameter detector to average over several speckle lobes. In a heterodyne system, the diffraction limited field-of-view makes it impossible to reduce speckle so easily [11].

To analyze this configuration, we will first model the target, then use Fourier optics to propagate the laser pulse to and from the target, and use tools from statistical communication theory to determine the statistics of the signal just before IF processing for a single pixel. Then we will discuss the pre-processors often used in laser radar systems and their advantages and, finally, present a model for the entire multipixel target and its surroundings.

B. Target Models

Real targets are themselves very complicated objects. However, this thesis' purpose is not to investigate the subtle differences between two trucks from the same assembly line, or two different trucks, or even a truck and a building. Accurate statistical modeling of real targets is the subject of other, ongoing research [12]. In this thesis, all targets will follow the purely diffuse speckle target model [3]. This model is very accurate for certain prepared test targets [13], [14] and quite accurate for at least the gross features of real targets. In the most general form of this model, the target has a complex reflection coefficient $\underline{T}(\ \bar{\rho},\ z,\ t\ )$ at every point in space and time ($\bar{\rho}$, z, t), where $\bar{\rho}$ is the transverse position vector (x, y) and $\underline{T}(\ *\ )$ is a four dimensional (space and time) complex Gaussian random process with independent, identically distributed real and imaginary parts [3]. Since $\underline{T}(\ *\ )$ is Gaussian, a second moment description completely characterizes its statistics. The moments are:

$$E[\ \underline{T}(\ \bar{\rho},\ z,\ t\ )\ ] = 0,$$

$$E[\ \underline{T}(\ \bar{\rho},\ z,\ t\ )\ \underline{T}(\ \bar{\rho}',\ z',\ t'\ )\ ] = 0, \quad\quad\quad (\ 2.1\ )$$

$$E[\ \underline{T}(\ \bar{\rho},\ z,\ t\ )\ \underline{T}^*(\ \bar{\rho}',\ z',\ t'\ )\ ] =$$

$$\lambda^2\ T_s(\ \bar{\rho},\ z,\ t-t'\ )\ \delta(\ \bar{\rho} - \bar{\rho}'\ )\ \delta(\ z-z'\ ).$$

The spatial impulse functions indicate the random structure of the target's surface decorrelates much faster than a distance of one wavelength λ at the laser frequency, $\nu_o = c\ /\ \lambda$. The spatial dependences in $T_s(\ *\ )$ indicate the target need not be uniform. The time dependence indicates the target may be moving, but this model assumes the motion is a stationary random process, hence the dependence on only the

time difference $t - t'$. This will be the model (often simplified) for all targets, background, clutter, or anything entering the radar's field of view (fov), including the no target case where $T_s(\bar{\rho}, z, t) = 0$.

C. IF Signal Derivation

In terms of the complex envelope of the optical signals at the optical frequency, ν_o, the IF signal out of the detector is proportional to the product of the complex field envelope of the reflected pulse and the local oscillator (LO) integrated over the detector surface. To get the reflected pulse's complex envelope, one must propagate the transmitted field to the target, multiply by the target reflection coefficient $\underline{T}(*)$ and propagate back to the receiver. In this thesis we will model atmospheric optical propagation as free-space diffraction modified only by extinction loss, which is a reasonable approach for compact CO_2 laser radars [24]. We shall assume the LO field pattern is matched to the transmitted field pattern, as is usually the case in such radars [14]. In practice, it is easier to use the antenna theorem [15] and back propagate the LO field to the target and perform the integration over the target surface rather than the detector surface. Define $\underline{\xi}(\bar{\rho}, z, t)$ as the normalized transmitted beam pattern at target range z. Here the time dependence t is due only to the beam scanning motion. We define another term, $\underline{s}(t)$, to contain the time dependence from the transmitter modulation. Now we can express the transmitted beam and back propagated LO beam at the target in terms of $\underline{\xi}(*)$ and $\underline{s}(t)$. Further define A_p and A_T as the optics aperture and target surface, respectively, and P_T as the transmitted power. Then the complex envelope of the IF signal at intermediate frequency ω_{IF} (radians/second) is $\underline{y}(t)$ [14]:

$$\underline{y}(\ t\ ) = \sqrt{P_T}\ \int_0^\infty dz\ \underline{s}(\ t\ -\ 2z/c\ )\ \int_{A_T} d\bar{\rho}\ \underline{\xi}(\ \bar{\rho}\ ,\ z,\ t\ -\ 2z/c\ )$$

$$\cdot\underline{T}(\ \bar{\rho}\ ,\ z,\ t\ -\ z/c\ )\ \underline{\xi}(\ \bar{\rho}\ ,\ z,\ t\ )\ +\ \underline{n}(\ t\ ),\qquad(\ 2.2\ )$$

where $\underline{n}(\ t\ )$, which represents the LO induced shot noise, is a stationary, zero-mean, circulo-complex Gaussian random process independent of $\underline{T}(\ *\ )$ with covariance function $E[\ \underline{n}(\ t\ )\ \underline{n}*(\ t'\ )\ ] = (\ h\ \nu_o\ /\ \eta\ )\ \delta(\ t\ -\ t'\ )$ [10]. Here $h\ \nu_o$ is the optical photon energy and η is the detector quantum efficiency. The first term in equation 2.2 is basically a delay-integral/heterodyne-overlap integral specification of the target-return component of $\underline{y}(\ t\ )$. The delay integral over z encompasses targets at all ranges while the overlap integral over A_T is the heterodyne integral for a particular range z. The equation includes all appropriate lag times. For the IF target return at time t from range z, the transmitted waveform was $\underline{s}(\ t\ -\ 2z/c\ )$. The first $\underline{\xi}(\ *\ )$ term is the transmitted beam shape that contributes to the target return at t from range z. The second $\underline{\xi}(\ *\ )$ term is the LO beam shape relevant to the target-return at t from range z; it has no time lag. The target term $\underline{T}(\ *\ )$ has a lag of only z/c seconds, the one-way time of flight from the target to the radar.

Now let us make the assumption $\underline{\xi}(\ \bar{\rho}\ ,\ z,\ t-2z/c\ ) \simeq \underline{\xi}(\ \bar{\rho}\ ,\ z,\ t\ )$ for all z such that $|\underline{\xi}(\ *\ )|$ makes an appreciable contribution to the integral. This is the assumption of negligible radar lag angle. It will make more physical sense after defining the transmitted field pattern in terms of a radar scanning motion in the next paragraph. For now, the IF waveform is:

$$\underline{y}(t) = \sqrt{P_T} \int_0^\infty dz \; \underline{s}(t - 2z/c) \int_{A_T} d\overline{\rho} \; \underline{T}(\overline{\rho}, z, t - z/c)$$

$$\cdot \; \underline{\xi}^2(\overline{\rho}, z, t - z/c) + \underline{n}(t). \qquad\qquad (2.3)$$

Although the transmitted beam pattern has been arbitrary so far, it is usually a collimated Gaussian beam with some pointing angle $\overline{\phi}(t)$ with respect to a reference direction (see figure 2.4). Thus, let us take $\underline{F}(\overline{\rho}, t)$, defined to be the normalized transmitted beam pattern at the radar, as follows:

$$\underline{F}(\overline{\rho}, t) = (\frac{8}{\pi d^2})^{1/2} \exp[-\frac{4|\overline{\rho}|^2}{d^2} + jk \; \overline{\rho} \cdot \overline{\phi}(t)] \qquad (2.4)$$

where $\qquad\qquad k = 2\pi / \lambda$ = wavenumber

and $\qquad\qquad d = e^{-2}$ beam intensity diameter at exit pupil.

Generally, $\overline{\phi}(t)$ is a linear scanning function, $\overline{\phi}(t) = \overline{\phi}(t_n) + \dot{\overline{\phi}} \cdot (t - t_n)$, for $t_n \leq t \leq t_n + T_\Delta$, where t_n and $\overline{\phi}(t_n)$ are the starting time and direction, respectively, for the n-th scan line, $\dot{\overline{\phi}}$ is the scan rate, and T_Δ is the time required to scan one line. This gives a raster scan arrangement like that in figure 2.2. (Note that because of flyback time, $t_{n+1} > t_n + T_\Delta$ generally prevails).

D. IF Pre-processing

Thus far we have made as few assumptions as possible in order to make the equation for $\underline{y}(t)$ as general as possible. These derivations give the statistics of the IF waveform directly out of the detector, but real processing systems (i.e., detection, identification, etc.) generally don't

deal with this IF waveform directly. Instead, some form of pre-processing usually exists between the IF and the signal processing [12], [13]. One reason for this intermediate step is the bandwidth disparity between the IF waveform and the bandwidth of recording and processing electronics. Typical research systems record the radar return data on tape for subsequent off line analysis and testing [12], [13]. It is difficult to record the data coming directly off of the detector because the IF frequency is in the tens of MHz and has a bandwidth of several MHz. Reducing this bandwidth is a prime reason why these systems employ pre-processing hardware prior to data recording. Reducing the quantity (and hence the bandwidth) of the data also makes it easier to process the data in real time, an important consideration for practical systems.

Scanning systems, such as the one we have specified, usually break the target into pixels and build an image of the target area from the pixels. The pre-processing electronics act on each individual pixel time element. For a ranging radar, the usual pre-processor examines the pixel time interval and selects the peak of the random waveform and records its intensity and time location relative to the start of the interval (corresponding to the target's range). For a Doppler radar system, the usual pre-processor Fourier transforms the received random waveform and then selects the peak in the frequency space and records its intensity and location (target velocity). These peak detection pre-processors reduce the entire random waveform over a time interval to two real random variables. Figure 2.3 is a schematic diagram of both pre-processors.

If the pixel dwell times are short compared to the time orders on which the
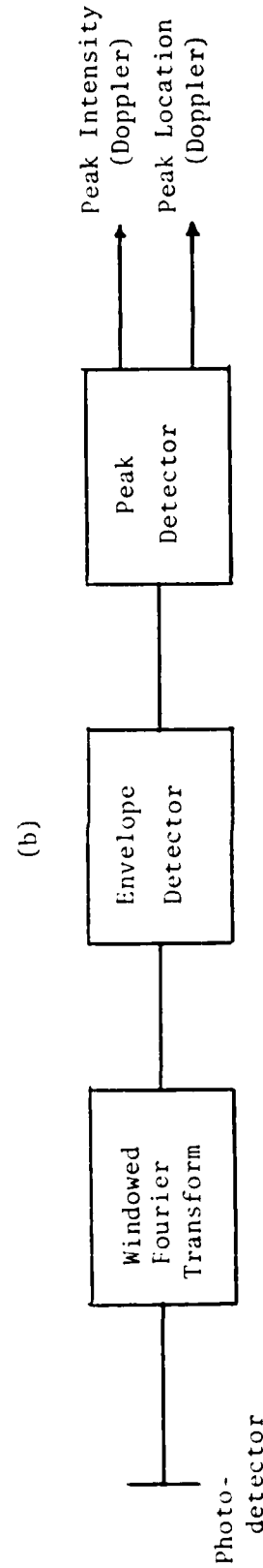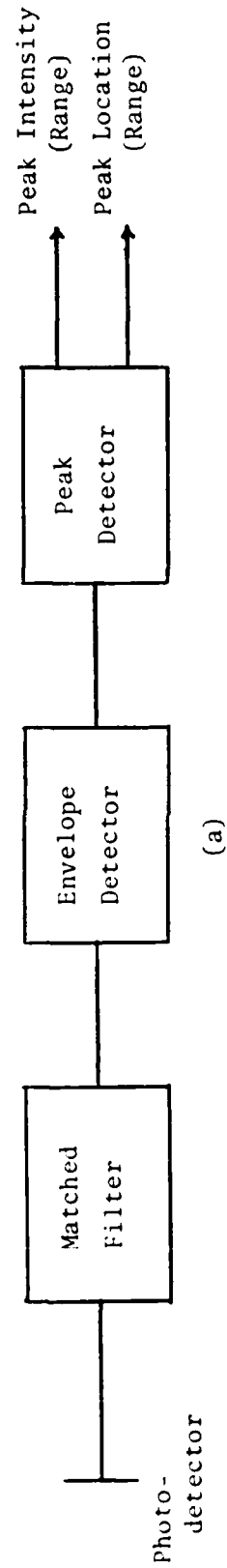
FIGURE 2.3
Pre-Processor Block Diagrams
(a) Range   (b) Doppler

target changes, there is little loss in optimality from dividing the waveform into pixels, but the peak detection may seem a bit ad-hoc. Actually, there is theoretical support for this type of pre-processing. In the case of a ranging radar and a non-range spread target observed on a single pixel, it is easy to show [4] that the maximum likelihood (ML) estimate of the target range corresponds to the peak of the matched filter output of the detector. So the pre-processor is essentially the ML range estimator, but remains fixed for all types of problems.

One could argue the virtues of working out performance measures on truly optimal receivers, given one goal is to examine the limits on the performance of laser radars. However, real radars are likely to continue to use some of the mentioned types of pre-processing for the reasons mentioned. Taking this pre-processing into account will give performance measures which are more realistic and closer to those researchers are likely to achieve. This thesis will use the matched filter, peak detector pre-processor model throughout. The signal analysis for the pre-processor will simply pick up where the analysis for $y(t)$ left off. None of the previous work goes to waste. Detailed single pixel peak detector analyses exist [23]. The analyses in this reference include thresholding in the pre-processor and the effect of the resulting dropouts. (When the intensity for a particular pixel is below the threshold, no data is recorded for that pixel and we say a dropout has occurred.) This thesis will not use thresholding in the pre-processor.

E. Frames and Subframes

The pixel is our basic unit of spatial measurement and we will shortly

derive the statistics for measurements taken on a single pixel. However, laser radars have resolutions such that interesting targets often take up more than a single pixel. We would like our receivers to use this spatially distributed information in an optimal or nearly optimal fashion to improve their performance. Since we have arranged our scanning geometry (see figure 2.2) so pixels are essentially non-overlapping, the pixel measurements will be independent thanks to the statistics of the target reflection coefficient $\underline{T}(*)$. Now we need a method to introduce the spatial relationships between the pixels into the statistical models.

We will adopt the down-looking geometry of figure 2.4 for our analysis of a single target at an unknown range and angular location within the radar's field of regard (total field of view). For this geometry, the radar always illuminates something. It may be the desired target (the vertical object in figure 2.4), or it may be the horizontal background. In either case, since the radar illuminates something, there is a target, or reflector element, return for each pixel. We will sometimes use the term target loosely to refe. to either target or background reflector elements. We will discuss figure 2.4 in more detail shortly.

We will assume we know the target shape and angular extent so we can tile the angular observation plane with M target shapes, each containing N pixels as in figure 2.5. We will call one observation of the entire observation plane (MN pixels) a frame and call each target shape a subframe (N pixels). The radar may stare in a particular direction long enough to take more than one frame of data (MN pixels), but we will consider only one frame at a time -- we won't try to use information from one frame to the
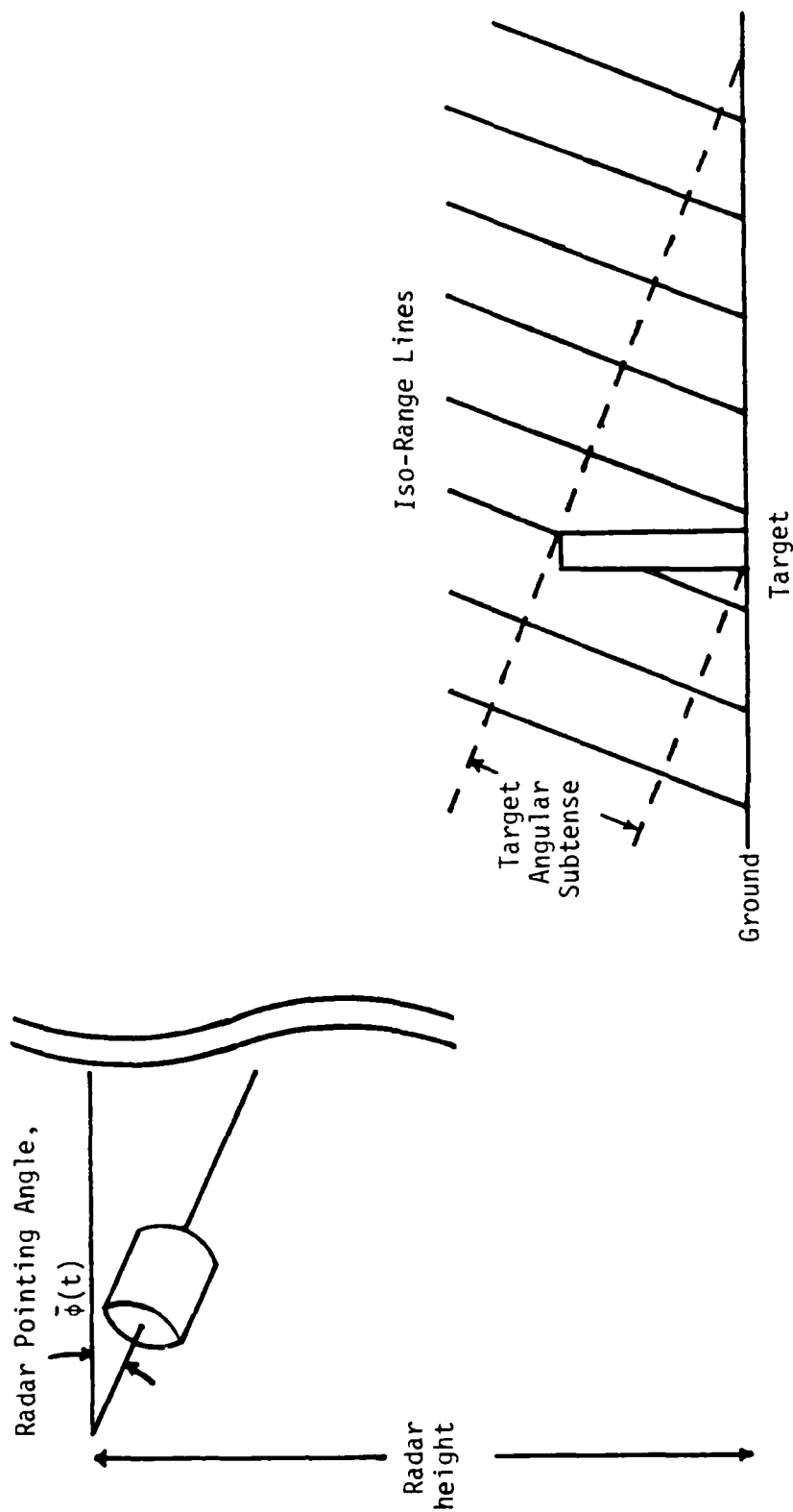
Figure 2.4

Laser-Target Geometry Model

next. We shall assume henceforth the target exactly aligns with one of the

subframes. This assumption will allow us to search the frame for the

target one subframe at a time with each subframe independent of all

others. Without this assumption, searching the frame for the target would

involve searching approximately MN subframes, each with many pixels in

common with several other adjacent subframes. That is, we would be sliding

the target shape as a window around the entire frame like the dotted target

outline in figure 2.5. Thus, the subframes would not be statistically

independent and this would considerably complicate the ultimate task of

computing receiver performance. This may seem a rather weak justification,

but we must consider our stated objective is to find useful performance

measures even at the expense of optimality if necessary. This is our model

of the target's angular characteristics. Now consider the target's range

characteristics.

We will begin our range model by assuming both the target and the

background are range unresolved. A range unresolved object is one where,

for each pixel, the radar beam illuminates only the target or the

background for each pixel (we ignore effects at the edges of the targets)

and the target or background has a sharply defined range relative to the

radar's range resolution. The iso-range lines on figure 2.4 are separated

by a distance equal to the radar's range resolution. True to the

assumption, the target's depth is much less than the radar's range

resolution distance. Under this model, the z-dependence of $\underline{T}(\bar{\rho} , z, t)$

is simply a Dirac delta function at the target or background range L:

$\underline{T}(\bar{\rho} , z, t) = \underline{T}(\bar{\rho} , L, t) \delta(z - L)$. Of course, this will make the z

integral in equation 2.3 trivial, but we will wait until the next chapter

1 frame,
M = 12 subframes

target not aligned
with subframes

target aligned
with subframes

target
appearance in
angle space:

1 subframe,
N = 20 pixels

target shape and size:
arbitrary but known
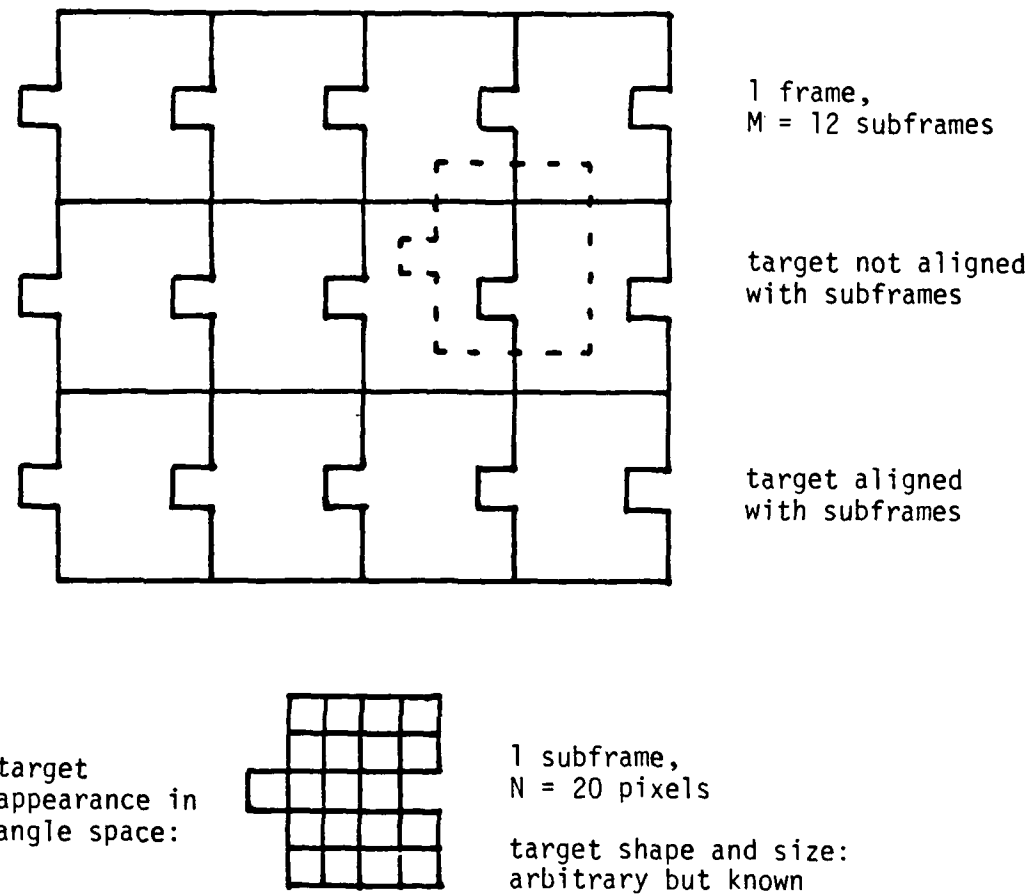
Figure 2.5

Target Subframe Model

to actually perform this integration. Another type of interesting target we won't consider in this thesis is the range spread target. Range spread targets are those whose geometry is such as to generate returns from a spread of distances in a single pixel. For example, a flat plate viewed at close to grazing incidence would produce a range spread return, as do aerosols and the edges of hard targets. The range unresolved assumption is reasonable for the 2-D pulsed imager compact CO_2 systems we are considering in this thesis [8], [9].

Examining figure 2.4 again, notice the down looking geometry will make the background appear to slope away from the radar at a known angle (the radar's pointing angle). If we know the radar's altitude, we can compute the range to the background accurately for a smooth background. So, we will assume we know the range to the background for each pixel in the frame. We will let any target in the frame be at an unknown range, but require it to be vertical. Most targets of interest easily meet this requirement. For a reasonably smooth background, each horizontal line of pixels in a subframe will be at the same range and adjacent lines will be at different ranges. The target, however, will have all its pixels in the subframe at the same range. Notice if the target sits on the ground, as in figure 2.4, its range is the same as the range for the nearest background pixel in the subframe. But since we know the range to every background pixel, we would know the target range, too. However, the target need not actually sit on the ground; it may be above the ground as well. As a result we must assume we don't know the target range. However, since the target can't be behind the ground, we know the background range is always more distant than the target.

This completes our model of the target's range and angular characteristics. We have introduced a model which is complex enough to be fairly realistic while being simple enough for analysis. We have made the model complex by allowing the target's angular position and range be unknown, by forcing the contiguous nature of the target into the subframe model, and introducing a background much like the target. Both target and background have unknown reflectivities. The model is simple by virtue of the relatively small number of free parameters in the model. These parameters are the target range and reflectivity, L_t and ρ_t, the background reflectivity, ρ_b, and the single subframe containing the target, m_o. The target size and shape are known and both background and target have uniform average reflectivity. Finally, all the pixels are independent as a result of the speckle statistics.

In the next chapter we will derive probability density functions for the pre-processor outputs, which are our measurement statistics, starting from the $\underline{y}(t)$ derivations in this chapter. In chapter four we will incorporate the target frame models above and the chapter three results into near optimal receiver processor equations.

III. RANGE-INTENSITY DENSITY FUNCTION

In the previous sections we were able to describe the statistics of the complex envelope of the detector's output exactly. It had a Gaussian density function with moments we could compute. This is a complete statistical description of the signal. The pre-processor is not linear, however, so its outputs are not Gaussian. Nevertheless, the joint range-intensity (or Doppler-intensity) probability density function (pdf) of the output random variables is a complete statistical description of those random variables. This chapter derives this joint density. We will perform the development in detail for a ranging radar; results for the Doppler and range-Doppler cases are handled via duality.

A. Signal Model

Figure 3.1 is a complex envelope model of the ranging radar receiver through the pre-processor. The last chapter derived an equation for $\underline{y}(t)$. For a ranging radar, the radar waveform $\underline{s}(t)$ will be periodic with period T, the pixel dwell time:

$$\underline{s}(t) = \sum_{n=-\infty}^{+\infty} \underline{b}(t - nT), \qquad (3.1)$$

where $\underline{b}(t)$ is some elementary waveform, non-zero only in the interval $[-T/2, +T/2]$. The filter $\underline{h}(t)$ is matched to the transmitter waveform $\underline{b}(t)$:

$$\underline{h}(t) = \underline{b}^*(T - t). \qquad (3.2)$$
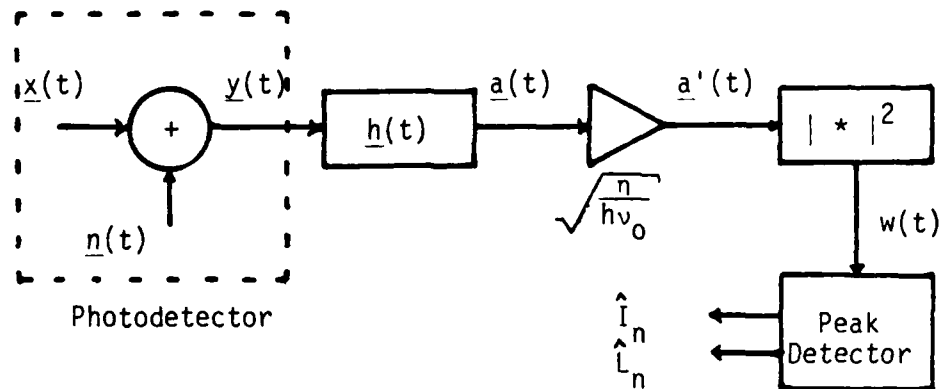
Figure 3.1

Radar Complex Envelope IF Signal Model

The next block is a square-law envelope detector. In many real systems this block would be a linear envelope detector because the linear detector has a smaller dynamic range at its output. The squared magnitude of a complex Gaussian random variable gives exponential statistics, whereas the linear magnitude gives Rayleigh statistics [16]. The two are related by a simple transformation, but the exponential statistics are easier to work with. The peak occurs at the same point in either case.

Substituting equation 3.1 for $\underline{s}(\ t\ )$ into equation 2.3 for $\underline{y}(\ t\ )$ gives:

$$\underline{y}(\ t\ ) = \sum_n \sqrt{P_T}\ \int_0^\infty dz\ \int_{A_T} d\overline{\rho}\ \underline{\xi}^2(\ \overline{\rho}\ ,\ z,\ t - z/c\ )$$

$$\cdot\ \underline{T}(\ \overline{\rho}\ ,\ z,\ t - z/c\ )\ \underline{b}(\ t - nT - 2z/c\ )\ +\ \underline{n}(\ t\ )\ .\qquad (\ 3.3\ )$$

The matched filter output is:

$$\underline{a}(\ t\ ) = \underline{y}(\ t\ )\ *\ \underline{h}(\ t\ )$$

$$= \underline{x}(\ t\ )\ *\ \underline{h}(\ t\ )\ +\ \underline{n}(\ t\ )\ *\ \underline{h}\ (\ t\ )$$

$$= \underline{a}_x(\ t\ )\ +\ \underline{a}_{noise}(\ t\ ),\qquad\qquad (\ 3.4\ )$$

where

$$\underline{a}_x(\ t\ ) = \sum_n \sqrt{P_T}\ \int_0^\infty dz\ \int_{A_T} d\overline{\rho} \int_{t - 3T/2}^{t - T/2} d\tau\ \underline{\xi}^2(\ \overline{\rho}\ ,\ z,\ \tau - z/c\ )$$

$$\cdot\ \underline{T}(\ \overline{\rho}\ ,\ z,\ \tau - z/c\ )\ \underline{b}(\ \tau - nT - 2z/c\ )\ \underline{b}^*(\ \tau - t + T\ )\ .\ (\ 3.5\ )$$

If the duration of $\underline{b}(\ t\ )$ is quite short compared to T, $\underline{T}(\ *\ )$ and $\underline{\xi}(\ *\ )$ will be approximately constant over the period of time $\underline{b}(\ t\ )$ is significant, even if they are not constant over the entire pixel dwell time. This short-duration pulse condition is the usual route to obtaining

good radar range resolution, although some microwave and optical radars use long duration high time–bandwidth product waveforms which undergo compression later in the receiver's IF system. This thesis will use the short pulse assumption, under which we can take the $\underline{T}(\ast)$ and $\underline{\xi}(\ast)$ terms out of the time integral, so that $\underline{a}_x(t)$ is approximately:

$$
\underline{a}_x(t) = \sum_n \sqrt{P_T} \int_0^\infty dz \int_{A_T} d\bar{p} \, \underline{\xi}^2(\bar{p}, z, nT + z/c)
$$

$$
\cdot \, \underline{T}(\bar{p}, z, nT + z/c) \int_{t - 3T/2}^{t - T/2} d\tau \, \underline{b}(\tau - nT - 2z/c) \, \underline{b}^*(\tau - t + T). \tag{3.6}
$$

Meanwhile, the noise component is:

$$
\underline{a}_{noise}(t) = \underline{n}(t) * \underline{h}(t) \tag{3.7}
$$

$$
= \int_{t - 3T/2}^{t - T/2} d\tau \, \underline{n}(\tau) \, \underline{b}^*(\tau - t + T) . \tag{3.8}
$$

Since $\underline{y}(t)$ is a zero–mean circulo–complex Gaussian random process and $\underline{h}(t)$ is a linear filter, $\underline{a}(t)$ is also a zero–mean circulo–complex Gaussian random process. Therefore, its magnitude squared process will have an exponential density function.

We will assume, as we did in proposing the model in the last chapter, that each pixel contains only one, range–unresolved reflector element (target or background). Again, for a range unresolved target, $\underline{T}(\bar{p}, z, t) = \underline{T}(\bar{p}, L_n, t) \, \delta(z - L_n)$ with the target at range L_n for the n-th pixel. Now the filtered signal return is:

$$\underline{a}_x(t) = \sum_n \sqrt{P_T} \int_{A_T} d\bar{\rho} \ \underline{\xi}^2(\bar{\rho} , L_n, nT + L_n/c) \ \underline{T}(\bar{\rho} , L_n, nT + L_n/c)$$

$$\cdot \int_{t - 3T/2}^{t - T/2} d\tau \ \underline{b}(\tau - nT - 2L_n/c) \ \underline{b}^*(\tau - t + T)$$

$$= \sum_n \sqrt{P_T} \ \underline{u}_n \ R_{\underline{bb}}(t - (n+1)T - 2L_n/c) \ , \qquad (\ 3.8 \ )$$

where $\underline{u}_n$ is a zero-mean circulo-complex Gaussian random variable arising from the ρ-integral and $R_{\underline{bb}}(x)$ is the autocorrelation function of $\underline{b}(t)$, arising from the τ-integral. Define for future use, $\tau_n \equiv (n+1)T + 2L_n/c$.

Finally, we divide $\underline{a}(t)$ by the square root of the $n(t)$ white noise spectral density, $h \nu_o / \eta$, to get a normalized signal:

$$\underline{a}'(t) = \underline{a}(t) / \sqrt{h \nu_o / \eta}$$

$$= \sqrt{\eta \ P_T / h\nu_o} \sum_n \underline{u}_n \ R_{\underline{bb}}(t - \tau_n) + \underline{v}(t)$$

$$= \sqrt{CNR} \sum_n \underline{u}_n' \ R_{\underline{bb}}(t - \tau_n) + \underline{v}(t) \qquad (\ 3.9 \ )$$

Here $\underline{v}(t)$ is the normalized noise process and $\underline{u}_n'$ is the normalized target return. It is easy to show these have moments:

$$E[\ \underline{u}_n' \ ] = 0 \qquad\qquad E[\ \underline{u}_n' \ \underline{u}_{n'}'^* \ ] = \delta_{nn'}$$

$$E[\ \underline{v}(t) \ ] = 0 \qquad\qquad E[\ |\underline{v}(t)|^2 \ ] = 1 \qquad (\ 3.10 \ )$$

$$E[\ \underline{u}_n' \ \underline{u}_{n'}' \ ] = 0 \qquad\qquad E[\ \underline{v}(t)^2 \ ] = 0.$$

Now all the physics of the transmitter power, LO induced shot noise, the beam patterns, the target reflectivity, and $1/L^2$ range losses are in the single, measurable parameter CNR, the carrier-to-noise ratio. Physically, CNR is the ratio of the average reflector element return power to the average LO shot noise power in the IF bandwidth. It is a quantity that is well known in microwave and optical radar theory. For the monostatic radar, resolved speckle target case of interest, CNR obeys the radar equation [17]:

$$CNR = \frac{\eta}{h \nu_0 B} \ P_T \ \rho \ \frac{A_p}{\pi L^2} \ e^{-2 \alpha L} \ \varepsilon_{opt} \ , \tag{3.11}$$

where B is the bandwidth of the IF filter, α is the atmospheric extinction coefficient, ε_{opt} is the radar optical efficiency, and ρ is the target reflectivity. The statement $E[\ \underline{u}_n' \underline{u}_{n'}'^* \ ] = \delta_{nn'}$ also implies all pixels are independent. This is true because, as stated earlier, the scanning assures minimal overlap of the beam between two pixels and the target surface has a very short correlation distance. Also, since the signal and detector noise are from different physical phenomena, they are independent: $E[\ \underline{u}_n' \ \underline{v}(\ t\ )\ ] = E[\ \underline{a}_x'(\ t\ )\ \underline{v}(\ t\ )\ ] = 0$. Because the pixels are independent, it is possible to examine them individually. From now on, the discussion will center on the density functions for a single pixel, so we will arbitrarily chosse the n = -1 pixel and drop the pixel subscript, n:

$$\underline{a}'(\ t\ ) = \sqrt{CNR} \ \underline{u}' \ R_{\underline{bb}}(\ t - \tau\ ) + \underline{v}(\ t\ ) \ , \tag{3.12}$$

$$\tau - \frac{T}{2} \ \le \ t \ \le \ \tau + \frac{T}{2} \ .$$

This equation also assumes for any specific time t, $\sum_{n} R_{\underline{bb}}(t - \tau_{n}) \simeq R_{\underline{bb}}(t - \tau_{n})$. This is a consequence of the short duration of the radar waveform $\underline{b}(t)$ compared to the dwell time T and the assumption of a range unresolved target. Put together, these assumptions assure there is only one return per dwell time and this return's time duration is much less than the dwell time. Now take the single pixel return through the squarer:

$$w(t) = |\underline{a}'(t)|^{2}$$

$$= CNR\ |\underline{u}'|^{2}\ |R_{\underline{bb}}(t - \tau)|^{2} + |\underline{v}(t)|^{2} +$$

$$2Re\{ \sqrt{CNR}\ \underline{u}'\ R_{\underline{bb}}(t - \tau)\ \underline{v}^{*}(t) \}. \qquad (3.13)$$

The intensity process $w(t)$ is a non-negative, non-stationary random process whose probability density function for any single time t is exponential.

B. Range-Intensity Density Function

The final step in our ranging radar pre-processor is to peak detect $w(t)$, generating the two random variables $\hat{I}$ and $\hat{L}$, the intensity and range, the $\hat{}$ meaning an estimated or measured quantity. We desire an expression for $\underline{p}_{\hat{I},\hat{L}}(x, y)$, the joint pdf of these random variables. To derive an expression for this pdf, we will examine $w(t)$ more carefully and construct a model for the waveform.

Suppose we wish to locate a target return time within the dwell time of T seconds. Then we define the range uncertainty interval as $L_{u} = cT/2$. If the pixel dwell time T is greater than the time corresponding to the range

uncertainty, $2L_u/c$, we will of course attempt to locate the target within the smaller time interval. At the risk of confusion, we will use the same notation, L_u and T, in either case. Figure 3.2 pictures the situation for T the full pixel dwell time for the $n = -1$ case we introduced in equation 3.12. In the absence of noise, $\underline{v}(t) = 0$, $w(t)$ has a peak value of CNR $\cdot$ $|\underline{u}'|^2$ at $t = \tau = \hat{\tau}$, where $\hat{\tau} = 2\hat{L}/c$ is the time delay associated with the range measurement $\hat{L}$, as sketched in figure 3.2(a) for an arbitrary $\underline{b}(t)$. If $\underline{v}(t) \neq 0$ but the CNR is very large, we might expect $w(t)$ to display only minor corruption from the noise, as in figure 3.2(b), so that $\hat{\tau} \simeq \tau$ would prevail. However, since $\underline{u}'$ is a random variable and $\underline{v}(t)$ is a random process, there may be intervals where, even at high CNRs, the realization of $|\underline{u}'|^2$ is very small while $\underline{v}(t)$ takes on a larger value somewhere in the interval. In this case, the peak in the interval occurs at some $\hat{\tau}$ far removed from τ, the location of the noise free peak. Figure 3.2(c) depicts this situation. The situation pictured in 3.2(c) is called an anomaly, designated by the event $\{ x_1 \}$. The situation in figure 3.2(b) is called no anomaly, designated by the event $\{ x_0 \}$. The statistics of $\hat{I}$ and $\hat{L}$ conditioned on x_0 and x_1 will be very different. The two events are mutually exclusive and collectively exhaustive, so $\Pr(x_0) + \Pr(x_1) = 1$.

The existence of anomalies is not unique to this problem; it is a feature of nonlinear estimation problems in general [4]. Another, related, feature of nonlinear estimation problems is the existence of a threshold effect. In classical nonlinear parameter estimation, the estimator's performance degrades gracefully as the CNR falls until it reaches some critical point, the threshold. Beyond the threshold, performance degrades
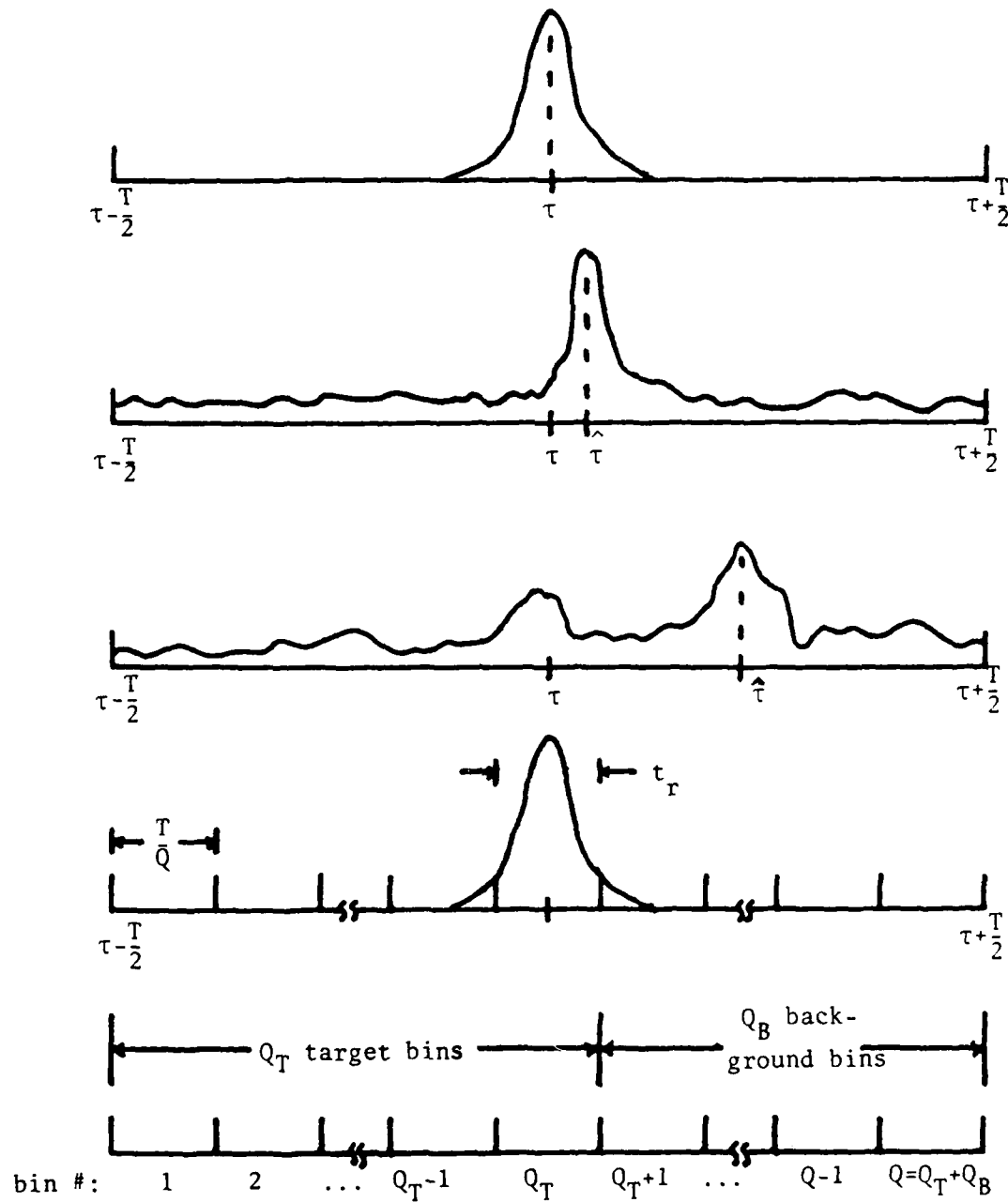
Figure 3.2

Peak Detection and Range Bin Model

more quickly as CNR falls [4]. This is a very general result in nonlinear estimation theory. For single pixel measurements of speckle targets, however, the threshold is not apparent [23]. For this case, the anomalies always occur and we are effectively always below threshold. For the case of multipixel speckle targets, however, there is a threshold effect [23], so we have taken some time to discuss the phenomenon here.

Both the signal portion of w(t) and the noise portion, $\underline{v}$(t), have widths or decorrelation times (see equation (3.7)) on the order of t_r, the width of the pulse $\underline{b}$(t). So, w(t) is approximately constant over time intervals less than t_r and points separated by greater than t_r are approximately statistically independent. Consequently, we will divide the interval T into an integer number of subintervals, Q, each of length $T/Q \simeq t_r$ and model w(t) as a sequence of Q independent exponentially distributed random variables as shown in figure 3.2(d) [12]. The random variables all have mean 1 when the reflector element is not in the bin and mean CNR + 1 when the reflector element is in the bin. Let's reiterate the Q bins need not cover the entire pixel dwell time of T seconds. Instead, the bins may cover only a subinterval of T in which the user is interested.

At this point we can overlay the range and subframe models from the last chapter onto the bin model. From figures 2.4 and 2.5 we can see the background bins must be the last (farthest range) bins and the target must fall in one of the remaining (nearest range) bins. We will divide the Q range bins into Q_T potential target range bins and Q_B background range bins as in figure 3.2(e). For a target, in the absence of noise,

$1 \leq \hat{Q} \leq Q_T$. For the background, in the absence of noise, $Q_T+1 \leq \hat{Q} \leq Q$, and $Q = Q_T + Q_B$.

The usual approach would be to estimate the range variable τ by first performing a global maximization by choosing the bin containing the peak and then performing a local maximization within that bin. The maximum value would be the intensity estimate for that pixel, $\hat{I}$, and its location will be the range estimate for that pixel, $\hat{\tau}$ (or $\hat{L} = c\hat{\tau}/2$). In general, it is this global/local approach [4] which produces the threshold effect mentioned above. As the CNR drops, the global estimator will make errors (anomalies) more frequently causing the local estimator's performance to degrade drastically. However, we have already noted that for the speckle target statistics, the anomalies dominate the error probabilities at all CNRs, so we need not worry about the threshold effect on a single pixel. In addition, we are going to concern ourselves only with global or coarse range estimates -- estimates of only the bin containing the target with no local maximization within a bin. It is possible to do the fine range maximization and derive the densities for the measurements [18], but they are more difficult to work with. Although the fine range results indicate processor performance more accurately, they provide no additional insight into the processor. Both processors exhibit the same qualitative dependences on the range and angular resolution parameters [18]. From here on, we will refer to the range measurement random variable by its bin number $\hat{Q} = 2\hat{L}/ct_r$.

We will use conditioning to compute the pdf $p_{\hat{I},\hat{Q}}(x, q)$:

$$p_{\hat{I},\hat{Q}}(x, q) \quad =$$

$$p_{\hat{I}|\hat{Q},\alpha_0}(x \mid q, \alpha_0) \, Pr(\hat{Q} = q \mid \alpha_0) \, Pr(\alpha_0) \; +$$

$$p_{\hat{I}|\hat{Q},\alpha_1}(x \mid q, \alpha_1) \, Pr(\hat{Q} = q \mid \alpha_1) \, Pr(\alpha_1) \; . \qquad (3.14)$$

The joint density function is also a mixed density function. The random variable $\hat{I}$ is continuous, while the random variable $\hat{Q}$ is discrete. Consequently, the probability function for $\hat{Q}$ is a probability mass function rather than a density function.

The first step in deriving the joint pdf is to compute the probability of no anomaly, $Pr(\alpha_0) = 1 - Pr(\alpha_1)$. Call the Q exponentially distributed random variables in our model Z_q for $q = 1$ to Q. Assume, with no loss in generality, the target is in bin number 1. Then event α_0 occurs if $Z_q \leq Z_1$ for all $q \neq 1$. Use the bin independence and directly integrate over the exponential densities of Z_1 and Z_q to obtain

$$Pr(\alpha_0) = Pr(Z_2 \leq Z_1, \ldots, Z_Q \leq Z_1)$$

$$= E_{Z_1}[\, Pr(Z_2 \leq Z_1 \mid Z_1)^{Q-1}\,] \qquad (3.15)$$

$$= E_{Z_1}[\, (1 - \exp(-Z_1))^{Q-1}\,]$$

$$= \frac{1}{CNR + 1} \frac{\Gamma(Q)\,\Gamma(\frac{1}{CNR+1})}{\Gamma(Q + \frac{1}{CNR+1})}$$

$$= a \frac{\Gamma(Q)\,\Gamma(a)}{\Gamma(Q+a)} \, ,$$

where the parameter a is $1 / (CNR + 1)$. This parameter recurs frequently in the $\hat{I}$ densities, so this shorthand is convenient. The reflector element CNR can be for the target or background. We will designate these CNRs as CNR_t and CNR_b, respectively, when we wish to make a distinction and write their corresponding a parameters a_t and a_b. For large CNR [4]:

$$Pr(\alpha_0) \doteq 1 - a (\log(Q) - 1 / 2Q + 0.577) . \quad (3.16)$$

Finding the density $p_{\hat{I}|\hat{Q},\alpha_1} (x \mid q, \alpha_1)$ requires using Bayes law and conditional random variables. With the bin model we have introduced, the conditioning on the range measurement $\hat{Q}$ corresponds to saying the peak intensity occurs in a particular bin, say the q-th bin, $\hat{Q} = q$. Conditioning on α_1 further requires $\hat{Q} = q \neq Q_i$, where Q_i, i = t, b, is the true target or background range bin, respectively. Call the random variable for the intensity in each bin, q, Z_q, as before. The desired density is the joint conditional density for all Q intensity values after integrating out all but the one where $\hat{Q} = q$:

$$p_{\hat{I}|\hat{Q},\alpha_1} (x \mid q, \alpha_1) = \int_0^\infty dx_1 \ldots \int_0^\infty dx_{q-1} \int_0^\infty dx_{q+1} \ldots \int_0^\infty dx_Q$$

$$p_{Z_1,\ldots,Z_Q|\hat{Q},\alpha_1} (x_1,\ldots,x_Q \mid q, \alpha_1) . \quad (3.17)$$

But:

$$p_{Z_1,\ldots,Z_Q|\hat{Q},\alpha_1} (x_1,\ldots,x_Q \mid q, \alpha_1) = \quad (3.18)$$

$$(Pr(\alpha_1 | Z_1 = x_1,\ldots,Z_Q = x_Q, \hat{Q} = q) \quad Pr(\hat{Q} = q | Z_1 = x_1,\ldots,Z_Q = x_Q)$$

$$\cdot \; \underline{p}_{Z_1,\ldots,Z_Q}(x_1,\ldots,x_Q) \;)$$

$$\overline{\qquad\qquad\qquad\qquad\qquad\qquad\qquad\qquad\qquad\qquad} \cdot$$

$$\Pr(\hat{Q}=q \mid \alpha_1) \, \Pr(\alpha_1)$$

The first and second terms in the numerator are both indicator functions: they are either 1 or 0 depending on the values of their conditioning variables. Together they force all $Q{-}1$ integrals to have upper limits of x_q. Since all the Z's are independent, the last term in the numerator is:

$$\underline{p}_{Z_1,\ldots,Z_Q}(x_1,\ldots,x_Q) = \underline{p}_{Z_{Q_i}}(x_{Q_i}) \prod_{\substack{q=1 \\ q \neq Q_i}}^{Q} \underline{p}_{Z_q}(x_q) \qquad (3.19)$$

where $\quad \underline{p}_{Z_j}(x) = \dfrac{1}{\overline{Z}_j} \exp\left(-\dfrac{x}{\overline{Z}_j}\right) u(x)$, $\quad \overline{Z}_j = \begin{cases} CNR + 1 & \text{for } j = Q_i \\ 1 & \text{for } j \neq Q_i \end{cases}$

The first term in the denominator is just $1 / (Q-1)$ since an anomaly is equally likely in any of the bins $Q \neq Q_i$. The integration is easy because of the indicator functions, yielding:

$$\underline{p}_{\hat{I}|\hat{Q},\alpha_1}(x \mid q, \alpha_1) = \frac{Q-1}{\Pr(\alpha_1)} \, e^{-x} \, (1 - e^{-ax}) \, (1 - e^{-x})^{Q-2}$$

$$\cdot \, u(x) \, (1 - \delta_{qQ_i}) \, . \qquad (3.20)$$

The calculation for $\underline{p}_{\hat{I}|\hat{Q},\alpha_0}(x \mid q, \alpha_0)$ is only slightly different:

$$\underline{p}_{\hat{I}|\hat{Q},\alpha_0}(x \mid q, \alpha_0) = \qquad\qquad\qquad\qquad\qquad (3.21)$$

$$= \int_0^\infty dx_1 \, \ldots \int_0^\infty dx_{q-1} \int_0^\infty dx_{q+1} \, \ldots \int_0^\infty dx_Q \; \delta_{qQ_i}$$

$$\frac{Pr(\ \alpha_0 \mid \hat{Q}=q, Z_1=x_1, \ldots, Z_Q=x_Q\ )\ p_{Z_1, \ldots, Z_Q | \hat{Q}}(\ x_1, \ldots, x_Q \mid q\ )}{Pr(\ \alpha_0\ )}$$

Again, $Pr(\ \alpha_0 \mid Q=q,\ Z_1=x_1, \ldots,\ Z_Q=x_Q\ )$ is an indicator function which forces the upper limits on the integrals to x_q. The result is:

$$p_{\hat{I} | \hat{Q}, \alpha_0}(\ x \mid q,\ \alpha_0\ ) = \frac{1}{Pr(\ \alpha_0\ )}\ a\ e^{-ax}\ (\ 1 - e^{-x}\ )^{Q-1}\ u(\ x\ )\ \delta_{qQ_i}.$$

$$(\ 3.22\ )$$

Turning to the probability mass functions for the range, under event α_1 any range outside the correct bin is equally likely, so:

$$Pr(\ \hat{Q} = q \mid \alpha_1\ ) = \frac{1}{Q-1}\ (\ 1 - \delta_{qQ_i}\ )\ ,$$

$$(\ 3.23\ )$$

where Q_i is again the noise free (true) target range bin.

The probability mass function $Pr(\ \hat{Q} = q \mid \alpha_0\ )$ is by far the most trivial. It is simply an indicator function:

$$Pr(\ \hat{Q} = q \mid \alpha_0\ ) = \delta_{qQ_i}$$

$$(\ 3.24\ )$$

Putting all the pieces together, the joint density is:

$$p_{\hat{I}, \hat{Q}}(\ x,\ q\ ) = a\ e^{-ax}\ (\ 1 - e^{-x}\ )^{Q-1}\ u(\ x\ )\ \delta_{qQ_i}\ +$$

$$(\ 3.25\ )$$

$$e^{-x}\ (\ 1 - e^{-ax}\ )\ (\ 1 - e^{-x}\ )^{Q-2}\ u(\ x\ )\ (\ 1 - \delta_{qQ_i}\ )\ .$$

The marginal densities are

$$p_{\hat{I}}(x) = a\, e^{-ax}\, (1 - e^{-x})^{Q-1}\, u(x) +$$

$$e^{-x}\, (1 - e^{-ax})\, (1 - e^{-x})^{Q-2}\, u(x) \qquad (3.26)$$

$$= \frac{d}{dx}\, [\, (1 - e^{-ax})\, (1 - e^{-x})^{Q-1}\,]\, u(x)\, ,$$

$$Pr(\hat{Q} = q) = Pr(\alpha_0)\, \delta_{qQ_i} + \frac{Pr(\alpha_1)}{Q - 1}\, (1 - \delta_{qQ_i})\, . \qquad (3.27)$$

C. Range–Doppler Duality

The previous derivations centered on intensity and range measurements. This section will demonstrate a duality between the range and Doppler shift measurements that will make it unnecessary to always repeat range-intensity analyses for Doppler-intensity radars.

The previous analysis, up to equation 3.3 for $\underline{y}(t)$, does not change. We will pick up the Doppler analysis from that point, but drop the n summation index and let n = -1 so as to deal with only one pixel (as we did in the range analysis). A well known result of Fourier transform theory tells us that in order to obtain good frequency resolution we require a long observation time. So, for a Doppler radar the duration of $\underline{b}(t)$ will generally be comparable to the pixel dwell time. Under this condition, almost any target is range unresolved, so we can let:

$$\underline{T}(\bar{\rho}, z, t - z/c) = \underline{T}(\bar{\rho}, t - z/c)\, \delta(z - (L + v_z t)) \qquad (3.28)$$

where v_z is the target's longitudinal velocity (only the longitudinal component contributes a Doppler shift). For simplicity, assume a transverse velocity of zero. Performing the z integration in the single pixel reflector element return integral then gives:

$$\underline{y}(t) = \sqrt{P_T} \int_{A_p} d\bar{\rho} \ \underline{\xi}(\bar{\rho}, L + v_z t, t - \frac{L + v_z t}{c}) \ \underline{T}(\bar{\rho}, t - \frac{L + v_z t}{c})$$

$$\cdot \underline{b}(t - \frac{2(L + v_z t)}{c}) + \underline{n}(t) \ . \tag{3.29}$$

If we perform the integrations to propagate the beam to the target, we find under the far field approximation:

$$\underline{\xi}(\bar{\rho}, z, t) = -\frac{k}{z} e^{2jkz} e^{jk|\bar{\rho}|^2/z} \frac{1}{\sqrt{2\pi} \ \sigma(z)}$$

$$\cdot \exp[-\frac{|\bar{\rho} - z \bar{\phi}(t)|^2}{2 \ \sigma(z)^2}], \tag{3.30}$$

$$\sigma(z) = \frac{2 \lambda z}{d} \gg d \ .$$

We will continue to use the assumptions the target changes little over a pixel dwell time, and that there is negligible radar lag angle. We shall also assume that the dwell time is short enough that only a relatively small fractional change occurs in the area the radar illuminates. Under these conditions we have that

$$\underline{\xi}^2(\bar{\rho}, z + v_z t, t)^2 \simeq \underline{\xi}(\bar{\rho}, z, t) e^{jkv_z t} \ , \tag{3.31}$$

and

$$\underline{y}(t) \simeq \sqrt{P_T} \, \underline{b}\left(t\left(1 - \frac{2v_z}{c}\right) - \frac{2L}{c}\right) e^{2jkv_z t}$$

$$\cdot \int_{A_P} d\bar{\rho} \, \underline{\varepsilon}^2(\bar{\rho}, z, t - \frac{L}{c}) \, \underline{T}(\bar{\rho}, t - \frac{L}{c}) + \underline{n}(t)$$

$$\simeq \sqrt{P_T} \, \underline{u} \, \underline{b}(t - \frac{2L}{c}) e^{2jkv_z t} + \underline{n}(t), \qquad (3.32)$$

where we used $2v_z \ll c$. Here $\underline{b}(*)$ is the delayed pulse, $\underline{u}$ is the speckle induced amplitude variations, and the exponential is the Doppler shift.

Now let us impose a pre-processor as before except instead of matched filtering $\underline{y}(t)$, perform a time-limited (windowed) Fourier transform. So the output of this transform will be:

$$\bar{a}(f) = FT_W\left\{ \frac{\eta}{h\nu_o} \underline{y}(t) \right\}$$

$$= \sqrt{CNR} \, \underline{u}' \int_{-\infty}^{+\infty} W(t) \, \underline{b}(t - \frac{2L}{c}) \, e^{j2kv_z t} \, e^{-j2\pi ft} \, dt$$

$$+ \bar{v}(f), \qquad (3.33)$$

where $\underline{u}'$ is $\underline{u}$ scaled to a unit variance and $W(t)$ is the window function, $W(t) = 0$ for $|t| > T/2$. The noise $\underline{\tilde{v}}(f)$ is a unit variance, zero mean, complex Gaussian random process. Continuing:

$$\underline{\bar{a}}'(f) = \sqrt{CNR} \, \underline{u}' \, [\, \tilde{W}(f - f_d) * \underline{\tilde{b}}(f - f_d)\,] \, e^{-j2\pi(f - f_d)t}$$

$$\qquad (3.34)$$

$$+ \underline{\tilde{v}}(f).$$

Note that if we choose $W(t)$ so that $\underline{W}(f) = \underline{b}^*(-f)$, the convolution becomes $R_{\underline{bb}}(f - f_d)$ and we have an exact analogy with the ranging radar result in equationn 3.18, except for the phase term. However, we can combine the phase term with $\underline{u}'$ without changing its statistics. So, we have demonstrated an exact analogy between the ranging and Doppler radar signals under the stated conditions. By using appropriate scaling factors, we can use all the range radar results in Doppler radar analyses. The Doppler $\hat{Q}$ measurement is $\hat{Q} = \hat{F} / f_r$ where the random variable $\hat{F}$ is the measured Doppler shift and f_r is the frequency resolution or Doppler bin width in Hz.

Although we have established a duality between the IF pre-processor output signals in ranging radars and Doppler radar, we must still demonstrate a duality between the target and background models for the two systems. We will still assume the down-looking radar geometry of figure 2.3. If the radar is moving parallel to the ground with velocity $\overline{v}$, we can use simple trigonometry to determine the projection of $\overline{v}$ onto the line of sight direction to the ground in terms of the radar's pointing angles, $\vec{\neg}(t)$. So, we can assume we know the longitudinal velocity of the background relative to the radar for each pixel. If the radar is stationary, we have the special case $\overline{v} = 0$ and all the background pixel velocities are 0. As long as the target moves with a constant longitudinal velocity with respect to the ground, its velocity will fall into a Doppler bin distinct from the background bins. However, since the target may move toward or away from the radar, it is not possible to place the Q_B background Doppler bins at either end of the Q total bins in general. Typically, one would arrange the frequency uncertainty interval, F_u, the dual of the range

uncertainty interval L_u, so it is centered around the background Doppler bins unless we have a priori knowledge of the sign of the target's Doppler shift.

D. Range-Range and Doppler Dulaity

In the previous section, we developed the duality between range radar and Doppler radar by putting both post-filtering waveforms into the form:

$$\underline{a}'(t) = \sqrt{CNR} \ \underline{u}' \ R_{\underline{bb}}(t - \tau) + \underline{v}(t) \tag{3.35}$$

with appropriate joint statistics for $\underline{u}'$ and $\underline{v}(t)$. However, for the peak detecting pre-processor we will deal with, this is a bit more stringent than we really require. Although certainly the statistics must be the same, the function $R_{\underline{bb}}(t)$ need not be an autocorrelation function.

For a receiver measuring both range and Doppler, the maximum likelihood processor is the ambiguity processor [19] which first extracts the time-frequency correlation function

$$\underline{a}'_{\underline{x}}(t_d, f_d) = \int_{-\infty}^{+\infty} dt \ \underline{y}(t) \ \underline{s}^*(t - t_d) \ e^{-j2\tau f_d t} \tag{3.36}$$

prior to envelope detection and peak detection. If we choose a transmitter waveform $\underline{s}(t)$ such that the ambiguity function $| \chi (t_d, f_d)|^2$, where

$$\chi (t_d, f_d) = \int_{-\infty}^{+\infty} dt \ \underline{s}(t) \ \underline{s}^*(t - t_d) \ e^{-j2\pi f_d t} \tag{3.37}$$

is the near ideal thumbtack, as Skolnik [20] calls it, shown in figure 3.3, then the pre-processor input is:

$$\underline{a}'(\, t, \, f \,) = \sqrt{CNR} \; \underline{u}' \; \chi (\, t, \, f \,) \; + \; \underline{v}(\, t, \, f \,) \qquad\qquad (\; 3.38 \;)$$

where $\underline{v}(\, t, \, f \,)$ is a zero mean, unit variance, complex Gaussian random process arising from the filtered local oscillator shot noise.

Now we divide the t-f plane into Q range-Doppler bins. The waveform $\underline{s}(\, t \,)$ sets the range and Doppler resolutions, through $\chi (\, t, \, f \,)$, and so the bin sizes. Simply mapping the 2-D array of Q bins onto the 1-D array of Q range bins makes the range-Doppler receiver based on equation 3.38 isomorphic to the range radar receiver based on the coarse range version of equation 3.12. Notice in both this and the range only processor, by using only coarse range, Doppler, or range and Doppler data, the exact form of the $R_{\underline{bb}}(\, * \,)$ or $\chi (\, * \,)$ functions are not very important as long as the noise free peak is unambiguous. If we had used fine range data as well, the analogy would need to be more stringent to translate the results. The exact shape of the correlation functions would need to be the same.

This establishes the duality in the IF signals, but we need to establish the duality between the range-Doppler model and the range model as well. This is very easy now that we have established the duality in the Doppler radar case. Taking a composite of the range and Doppler radar models we have already developed, we can segment the range-Doppler bins into a set of Q_B large range, low Doppler shift bins where the background returns must fall and the remaining Q_T bins where a target could occur, as shown
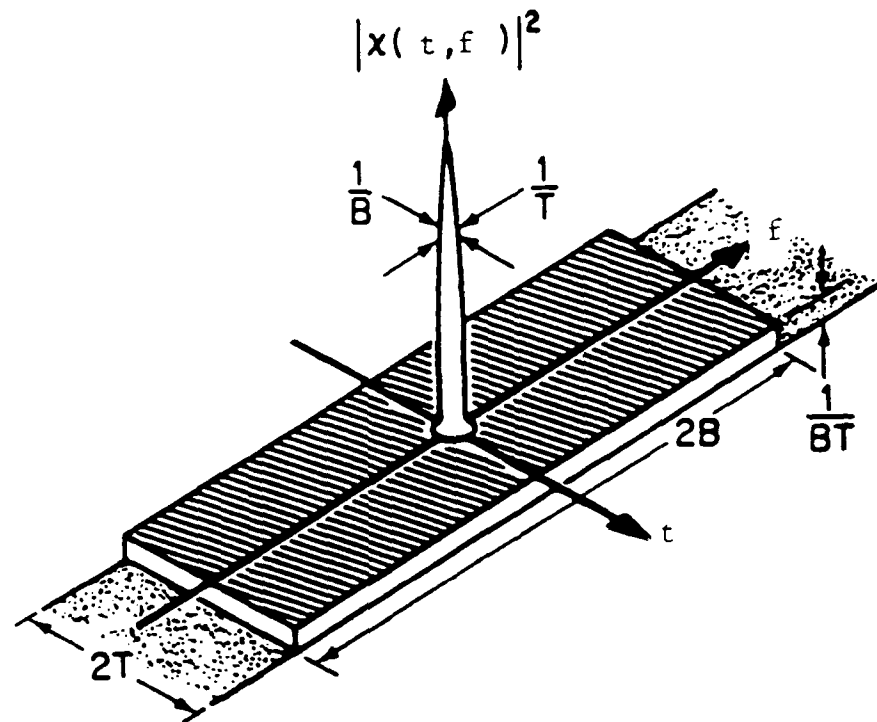
Figure 3.3

Thumbtack Ambiguity Function

in figure 3.4.

With the joint and marginal densities in hand, we can proceed with processor design in the next chapter. Using the dualities we just derived, we only need do this design once for the range receivers.

$$Q = Q_F Q_L$$

Range bin number:
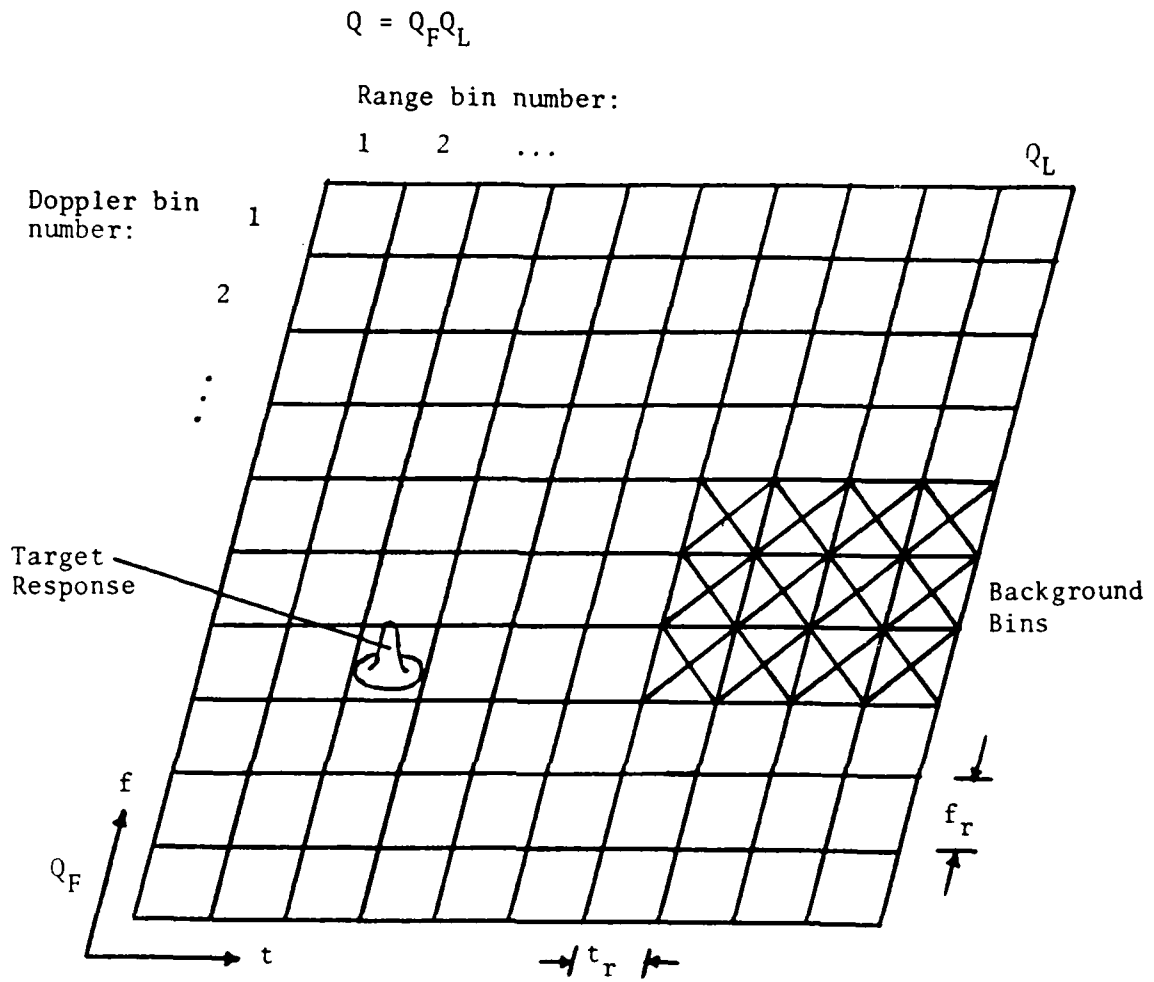
Figure 3.4

Range and Doppler Bin Model

IV. BINARY DETECTION RECEIVERS

A. The Neyman-Pearson Criterion

This thesis focuses on binary detection receivers which use the Neyman-Pearson criterion for detection [4]. The Neyman-Pearson approach is useful for deciding between two events whose a-priori probabilities are either unknown or, as in this case, not meaningful because they are not random phenomena. The problem here is to choose between two possible decisions: target present (H_1) and target absent (H_0) based on an observed data vector $\overline{R}$. Here $\overline{R}$ may be any subset of the measured quantities $\{ \hat{I}_{mn}, \hat{Q}_{mn} : 1 \leq m \leq M, 1 \leq n \leq N \}$ where the index m represents the subframe number and the index n represents the pixel number within a subframe. The Neyman-Pearson criterion constrains the probability of false alarm, $P_F = \Pr\{ \text{declare } H_1 \mid H_0 \}$, to be less than or equal to some specified value P_F' and then minimizes the probability of miss, $P_M = \Pr\{ \text{declare } H_0 \mid H_1 \}$, subject to the constraint. Performing this constrained minimization results in a likelihood ratio test:

$$\Lambda(\overline{r}) \equiv \frac{p_{\overline{R}|H_1}(\overline{r} \mid H_1)}{p_{\overline{R}|H_0}(\overline{r} \mid H_0)} \begin{array}{c} H_1 \\ > \\ < \\ H_0 \end{array} \lambda, \qquad\qquad (4.1)$$

with λ chosen so $P_F = P_F'$.

If $\Lambda(r)$ is not a continuous random variable, P_F will not be a continuous function of λ . In this case, if the desired value of P_F is not one of the discrete values, we must randomize the decision rule to obtain the desired performance [4]. The reference describes the procedure

for a simple example. We will need to use this procedure in chapter 6 to analyze the performance of the range processor because the discrete range measurements, $\{ \hat{Q}_{mn} \}$, give rise to a discrete likelihood ratio and P_F function.

B. Unknown Parameters

Equation 4.1 is not completely general, since the densities often depend not only on the data $\overline{R}$, but also on some other unknown, non-random parameters. If it is impossible to express the likelihood ratio $\Lambda(r)$ independent of these parameters, we must first determine the maximum likelihood estimates of the parameters under H_0 and H_1 and then use these estimated values in the densities as if they are the true values. This procedure generates the generalized likelihood ratio test [4]:

$$\Lambda_g(\overline{r}) \equiv \frac{\max\limits_{\overline{A}}\{ \, p_{\overline{R}|H_1,\overline{A}}(\overline{r} \mid H_1, \overline{A}) \, \}}{\max\limits_{\overline{A}}\{ \, p_{\overline{R}|H_0,\overline{A}}(\overline{r} \mid H_0, \overline{A}) \, \}} \quad \begin{array}{c} H_1 \\ > \\ < \lambda, \\ H_0 \end{array} \qquad (\; 4.2 \;)$$

where $\overline{A}$ is the unknown parameter vector.

In this chapter we will specifically treat intensity and ranging radars and later treat Doppler radars by duality arguments. For the intensity and range radars we are analyzing, the unknown parameters are m_o, the actual subframe which contains the target, Q_{tmn}, the actual target bin number for the n-th pixel in the m-th subframe, CNR_t and CNR_b, the target and background carrier-to-noise ratios, respectively, and sometimes functions of these parameters (i.e., $Pr(\, \alpha_{0t})$, the probability of no target anomaly, a function of CNR_t).

Introducing the generalized likelihood ratio is a crucial step in this development. The unknown parameters involve the multipixel nature of the target. Introducing the generalized likelihood ratio in combination with the models of chapter 2 is the procedure which makes it possible to derive optimal or quasi-optimal processors for multipixel targets. Although the generalized likelihood ratio concept is not new [4], applying the concept to this problem is new and this is what allows us to derive these results for multipixel processors.

C. Subframe and Frame Statistics

This section presents the general method we will use to derive the frame statistics from the subframe statistics and treat the target true subframe location, m_o, as an unknown parameter.

We will have some frame level measurement vector, $\overline{R}^{(f)}$, which is a composite vector of M subframe measurement vectors, $\overline{R}_m^{(s)}$, where the superscripts (f) and (s) indicate frame and subframe level measurements, respectively. The generalized likelihood ratio test with unknown parameters m_o and $\overline{A}$ (for any remaining unknown parameters) is:

$$\Lambda_g^{(f)} = \frac{\displaystyle\max_{\overline{A},\, m_o} \{ \, p_{\overline{R}^{(f)}|H_1,\overline{A},m_o} (\, \overline{r}^{(f)} \mid H_1, \overline{A}, m_o) \, \}}{\displaystyle\max_{\overline{A},\, m_o} \{ \, p_{\overline{R}^{(f)}|H_0,\overline{A},m_o} (\, \overline{r}^{(f)} \mid H_0, \overline{A}, m_o) \, \}} \underset{H_0}{\overset{H_1}{\gtrless}} \lambda \quad , \quad (\, 4.3 \,)$$

Since the subframes do not overlap, the subframe measurements are statistically independent and those subframes not containing the target have the same statistics as if there is no target in the frame:

$$\Lambda_g^{(f)} = \frac{\displaystyle\max_{\overline{A}, m_o} \left\{ p_{\overline{R}_{m_o}^{(s)}|H_1,\overline{A}}(\, \overline{r}_{m_o}^{(s)} \mid H_1, \overline{A}\,) \prod_{\substack{m=1 \\ m \neq m_o}}^{M} p_{\overline{R}_m^{(s)}|H_0,\overline{A}}(\, \overline{r}_m^{(s)} \mid H_0, \overline{A}\,) \right\}}{\displaystyle\max_{\overline{A}, m_o} \left\{ \prod_{m=1}^{M} p_{\overline{R}_m^{(s)}|H_0,\overline{A}}(\, \overline{r}_m^{(s)} \mid H_0, \overline{A}\,) \right\}} \quad . \qquad (\ 4.4\ )$$

Since the denominator in equation 4.4 is independent of m_o, we can drop the m_o maximization in the denominator and take the denominator inside the m_o maximization in the numerator (being careful to keep the $\overline{A}$ maximizations separate):

$$\Lambda_g^{(f)} = \max_{m_o} \left\{ \frac{\displaystyle\max_{\overline{A}} \left\{ p_{\overline{R}_{m_o}^{(s)}|H_1,\overline{A}}(\, \overline{r}_{m_o}^{(s)} \mid H_1, \overline{A}\,) \cdot \prod_{\substack{m=1 \\ m \neq m_o}}^{M} p_{\overline{R}_m^{(s)}|H_0,A}(\, \overline{r}_m^{(s)} \mid H_0, \overline{A}\,) \right\}}{\displaystyle\max_{\overline{A}} \left\{ \prod_{m=1}^{M} p_{\overline{R}_m^{(s)}|H_0,\overline{A}}(\, \overline{r}_m^{(s)} \mid H_0, \overline{A}\,) \right\}} \right\} \cdot (\ 4.5\ )$$

Often the unknown parameter vector, $\overline{A}$, contains elements which affect the densities under H_1 or H_0, but not both. Examples are CNR_t which affects the density under H_1 but not H_0, and CNR_b which affects the density under H_0 but not H_1. Let's call such parameters "hypothesis separable" parameters. Then the vector $\overline{A}$ becomes ($\overline{A}_0$, $\overline{A}_1$) where the subscripts

indicate which hypothesis the parameters affect. If the parameters are hypothesis separable, we can rewrite the part of equation 4.5 inside the m_o maximization as:

$$\frac{\max\limits_{\bar{A}_1}\left\{ p_{\bar{R}^{(s)}_{m_o}|H_1,\bar{A}_1}(\bar{r}^{(s)}_{m_o} \mid H_1, \bar{A}_1)\right\} \cdot \max\limits_{\bar{A}_0}\left\{ \prod\limits_{\substack{m=1 \\ m \neq m_o}}^{M} p_{\bar{R}^{(s)}_m|H_0,\bar{A}_0}(\bar{r}^{(s)}_m \mid H_0, \bar{A}_0)\right\}}{\max\limits_{\bar{A}_0}\left\{ \prod\limits_{m=1}^{M} p_{\bar{R}^{(s)}_m|H_0,\bar{A}_0}(\bar{r}^{(s)}_m \mid H_0, \bar{A}_0)\right\}} . \quad (\ 4.6 \ )$$

The difference between the $\bar{A}_0$ maximizations in the numerator and denominator is one subframe term. If M is fairly large, both numerator and denominator will give nearly the same estimates for the parameter vector $\bar{A}_0$. If we make the estimate in the denominator and use the resulting vector $\bar{A}_0$ in the numerator, we will introduce only a small error, but all M - 1 terms where $m \neq m_o$ will cancel in the numerator and denominator leaving for equation 4.6:

$$\frac{\max\limits_{\bar{A}_1}\{ \ p_{\bar{R}^{(s)}_{m_o}|H_1,\bar{A}_1}(\bar{r}^{(s)}_{m_o} \mid H_1, \bar{A}_1) \ \}}{p_{\bar{R}^{(s)}_{m_o}|H_0,\hat{\bar{A}}_0}(\bar{r}^{(s)}_{m_o} \mid H_0, \hat{\bar{A}}_0)} \equiv \Lambda_g^{(s)}(\bar{r}^{(s)}_{m_o}) \equiv \Lambda_{gm_o}^{(s)}, \quad (\ 4.7 \ )$$

where $\hat{\bar{A}}_0$ is the estimate of vector $\bar{A}_0$ derived from measuremnets over the entire frame. Notice we have introduced a shorthand notation for the subframe generalized likelihood ratio, $\Lambda_{gm}^{(s)}$. Now we may write:

$$\Lambda_g^{(f)} = \max_m \{ \Lambda_{gm}^{(s)} \} . \qquad\qquad (\text{ } 4.8 \text{ })$$

Now it is clear the generalized likelihood ratio for the frame is simply the maximum of the generalized likelihood ratios for the M subframes. This fact makes it quite easy to find the frame level probabilities of false alarm and miss, $P_F^{(f)}$ and $P_M^{(f)}$, from the subframe level probabilities of false alarm and miss, $P_F^{(s)}$ and $P_M^{(s)}$. The procedure is as follows:

$$
\begin{aligned}
P_F^{(f)} &= \Pr\{ \ \Lambda_g^{(f)}(\ \bar{r}^{(f)} \ ) \geq \lambda \ | \ H_0 \ \} \\
&= 1 - \Pr\{ \ \Lambda_g^{(f)} < \lambda \ | \ H_0 \ \} \qquad\qquad (\text{ } 4.9 \text{ }) \\
&= 1 - \Pr\{ \ \max_m\{ \ \Lambda_{gm}^{(s)} \ \} < \lambda \ | \ H_0 \ \} .
\end{aligned}
$$

We will treat all M of the $\Lambda_{gm}^{(s)}$ as approximately independent and, under H_0, identically distributed. They are not exactly inndependent because, although the measurements $\bar{R}_m^{(s)}$ are independent, the $\hat{\bar{A}}_0$ value used in the denominator is derived from a maximization over measurements for the entire frame. If the maximum is less than some specific value, all M must be less than that value, so:

$$
\begin{aligned}
P_F^{(f)} &= 1 - \Pr\{ \ \Lambda_{gm}^{(s)} < \lambda \ | \ H_0 \ \}^M \\
&= 1 - [\ 1 - \Pr\{ \ \Lambda_{gm}^{(s)} \geq \lambda \ | \ H_0 \ \} \ ]^M \qquad\qquad (\text{ } 4.10 \text{ }) \\
&= 1 - [\ 1 - P_F^{(s)} \ ]^M .
\end{aligned}
$$

Here $P_F^{(s)}$ has an intuitively meaningful definition. It is the

probability of false alarm if we consider just a single subframe. A nearly identical analysis for $P_M^{(f)}$, again assuming independent $\Lambda_{gm}^{(s)}$ gives:

$$P_M^{(f)} = P_M^{(s)} [1 - P_F^{(s)}]^{M-1}$$

$$= P_M^{(s)} [1 - P_F^{(f)}]^{(\frac{M-1}{M})}, \qquad\qquad (4.11)$$

where

$$P_M^{(s)} = Pr\{ \Lambda_{gm}^{(s)} < \lambda \mid H_1 \} .$$

The physical interpretation of these equations is as follows. A miss occurs if none of the subframe statistics, $\Lambda_{gm}^{(s)}$ clears the threshold λ. A detection occurs if at least one of the $\Lambda_{gm}^{(s)}$ statistics clears the threshold, even if the subframe whose statistic clears the threshold does not actually contain the target. But the probability of a detection on the wrong subframe turns out to be quite small; this event is essentially a false alarm and its probability is bounded by $P_F^{(s)}$. Notice this argument depends only on $P_F^{(s)}$ being relatively small. It does not depend on the CNRs or any other parameters. Further, from equation 4.10, if M is large, $P_F^{(s)}$ may be small even if $P_F^{(f)}$ is not.

Notice since adequate performance generally requires $P_F^{(s)}$ to be fairly small, we can usually make the approximations:

$$P_F^{(f)} \simeq M P_F^{(s)}$$

and (4.12)

$$P_M^{(f)} \simeq P_M^{(s)} .$$

In words, equation 4.12 says for a fixed target size, N, $P_F^{(f)}$ rises linearly with an increase in the angular search area and $P_M^{(f)}$ is approximately independent of the angular search area.

D. Multiple Targets

Suppose we wish to consider the possibility of multiple targets in the frame. We will continue to assume targets align with subframe boundaries. We will also assume the number of subframes containing targets, M', is a small fraction of M. There are several possible ways to analyze this problem and define the corresponding false alarm and detection (or miss) events, each of which may make sense for a particular problem. We will form the generalized likelihood ratio for each subframe, perform a threshold test on each subframe, and declare target present or target absent for each subframe independent of all other subframes. That is, perform no maximization over the subframe generalized likelihood ratios before the threshold test. A false alarm occurs any time we declare a target in an empty subframe, even if there is a target elsewhere in the frame. A miss occurs anytime we declare target absent in a subframe containing a target even if we have correctly detected targets in other subframes.

With this processor, the probability of miss for any target is just the value $P_M^{(s)}$ already computed. Similarly, if we compute a frame level probability of false alarm $P_F^{(f)}$, it is

$$P_M^{(f)'} = 1 - [\ 1 - Pr\{ \ \Lambda_{gm}^{(s)} \geq \lambda \ | \ H_0 \ \} \ ]^{M-M'} \qquad (\ 4.13\ )$$

$$\simeq P_F^{(f)}$$

since M', the number of subframes containing targets, $\ll$ M by assumption.

The point of all this discussion is whatever results we derive for the single target in a frame are also useful for discussing performance with multiple targets in the frame. We need make only minor corrections to the single target performance numbers to make quantitative statements about multiple targets in a frame.

E. Measurement and Target Models

We will retain the pre-processor introduced in chapter 2 and continue working with only coarse range or Doppler data as in chapter 3. In this case, we already have the density functions we need from chapter 3. Now we will use these density functions in the generalized likelihood ratio tests from above to derive the processors for receivers measuring range, Doppler, intensity, or some combination of these signal dimensions. Since we have already established a range-Doppler duality and a range and Doppler analogy with range only measurements, the joint range-intensity measurement receiver is our most general case. We will do this case and then the range only and intensity only cases.

All these derivations use the target model introduced in chapter 2. In that model the target is range unresolved at an unknown range. It is vertical against a background sloping away at a known range. Neither target nor background CNRs are known. Targets align with subframe

boundaries and we wish to determine whether or not a target exists in a frame.

We will label each pixel with a subscript for subframe index, m, $1 \leq m \leq M$, and a pixel index, n, $1 \leq n \leq N$, as we did at the start of this chapter. For each pixel in a subframe, we measure the intensity, $\hat{I}_{bmn}$, at the known background range, Q_{bmn}. This gives rise to an exponential density function for $\hat{I}_{bmn}$. For each pixel we also measure the intensity in all non-background range bins and choose the maximum of those intensities. Call this maximum $\hat{I}_{tmn}$ and call the bin it occurs in $\hat{Q}_{tmn}$, the presumed target range. This gives rise to the statistics we derived in the last chapter for $\hat{I}_{tmn}$ and $\hat{Q}_{tmn}$. Of course, $\hat{I}_{bmn}$ is independent of both $\hat{I}_{tmn}$ and $\hat{Q}_{tmn}$, though $\hat{I}_{tmn}$ and $\hat{Q}_{tmn}$ are dependent random variables in general. This is the most general form of the model.

F. Joint Range-Intensity Processor

If there is no target present for a particular pixel, the system CNR will be CNR_b and the effective CNR_t is zero. There are Q range bins and, using the notation introduced in chapter 3, one of Q_B of them is the background range bin, so we do the maximization over only $Q_T = Q - Q_B$ bins to find $\hat{I}_{tmn}$ and $\hat{Q}_{tmn}$ for each pixel. We measure $\hat{I}_{bmn}$ at the known background range bin. The densities for the resulting measurements are:

$$p_{\hat{I}_{bmn}|H_0}(x_{bmn} \mid H_0) = a_b \, e^{-a_b x_{bmn}} \, u(x_{bmn}) ,$$

$$(4.14)$$

$$p_{\hat{I}_{tmn}, \hat{Q}_{tmn}|H_0}(x_{tmn}, q_{mn} \mid H_0) =$$

$$(1 - e^{-x_{tmn}})^{Q_T-1} e^{-x_{tmn}} u(x_{tmn}) , \quad 1 \le q_{mn} \le Q_T .$$

The background and target random variables are conditionally independent, so we simply multiply the two densities to find the joint density for the measurement vector ($\hat{I}_{bmn}$, $\hat{I}_{tmn}$, $\hat{Q}_{tmn}$) on each pixel under hypothesis H_0.

If there is a target for a particular pixel, the system CNR is CNR_t and the effective CNR_b is zero. The resulting densities are:

$$p_{\hat{I}_{bmn}|H_1}(x_{bmn} | H_1) = e^{-x_{bmn}} u(x_{bmn}) ,$$

$$p_{\hat{I}_{tmn},\hat{Q}_{tmn}|H_1}(x_{tmn}, q_{mn} | H_1) = \qquad\qquad (4.15)$$

$$a_t e^{-a_t x_{tmn}} (1 - e^{-x_{tmn}})^{Q_T-1} u(x_{tmn}) \delta_{q_{mn}Q_t} +$$

$$(1 - e^{-a_t x_{tmn}}) (1 - e^{-x_{tmn}})^{Q_T-2} e^{-x_{tmn}} u(x_{tmn}) (1 - \delta_{q_{mn}Q_t}) ,$$

$$1 \le q_{mn} \le Q_T .$$

The background and target random variables are still conditionally independent under hypothesis H_1.

Since all pixels are independent, the frame density is just the product of the M subframe densities and each subframe density is the product of N pixel densities from equation 4.14 and 4.15. Applying the general results of part C above, the frame generalized likelihood ratio is

$$\Lambda_g^{(f)} = \max\{ \Lambda_{gm}^{(s)} \} ,$$

where

$$\Lambda_{gm}^{(s)} = \max_{a_t, Q_t} \Bigg\{ \prod_{n=1}^{N} p_{\hat{I}_{tmn}, \hat{Q}_{tmn} | H_1, a_t, Q_t} (x_{tmn}, q_{mn} \mid H_1, a_t, Q_t)$$

$$\cdot \; p_{\hat{I}_{bmn} | H_1} (x_{bmn} \mid H_1) \Bigg\} \qquad (4.16)$$

$$\overline{\qquad \prod_{n=1}^{N} p_{\hat{I}_{tmn}, \hat{Q}_{tmn} | H_0} (x_{tmn}, q_{mn} \mid H_0) \qquad}$$

$$\cdot \; p_{\hat{I}_{bmn} | H_0, \hat{a}_b} (x_{bmn} \mid H_0, \hat{a}_b)$$

The estimate $\hat{a}_b$ is from the maximization over an entire frame, i.e.,

$$\max_{a_b} \Bigg\{ \prod_{m=1}^{M} \prod_{n=1}^{N} p_{\hat{I}_{bmn} | H_0, a_b} (x_{bmn} \mid H_0, a_b) \Bigg\}$$

occurs at $a_b = \hat{a}_b$. This gives

$$\hat{a}_b = \left[\frac{1}{M N} \sum_{m=1}^{M} \sum_{n=1}^{N} \hat{I}_{bmn} \right]^{-1} . \qquad (4.17)$$

The true value of the parameter a_b is the true mean of the sampled random variable, $\hat{I}_{bmn}$. The estimate of the parameter a_b is exactly what we would expect from intuitive notions and the law of large numbers: it is the sample mean for measurements of $\hat{I}_{bmn}$ over the entire frame.

Now we substitute the densities in equations 4.14 and 4.15 into equation 4.16, cancel terms in common in the numerator and denominator, take the logarithm of $\Lambda_{gm}^{(s)}$ to change the products to summations and use the monotonicity of the logarithm to justify bringing the logarithms inside

the maximizations. The result is:

$$\log \Lambda_{gm}^{(s)} = \max_{a_t,Q_t} \left\{ \sum_{n=1}^{N} \log \Lambda^{(p)}(x_{tmn},\ q_{mn},\ x_{bmn}) \right\} , \qquad (4.18)$$

where

$$\log \Lambda^{(p)}(x_{tmn},\ q_{mn},\ x_{bmn}) \equiv \Lambda_{mn}^{(p)} =$$

$$\log \left[\frac{ p_{\hat{I}_{tmn},\hat{Q}_{tmn},\hat{I}_{bmn}|H_1,a_t,Q_t}(x_{tmn},\ q_{mn},\ x_{bmn} \mid H_1,\ a_t,\ Q_t)}{ p_{\hat{I}_{tmn},\hat{Q}_{tmn},\hat{I}_{bmn}|H_0,\hat{a}_b}(x_{tmn},\ q_{mn},\ x_{bmn} \mid H_0,\ \hat{a}_b)} \right] =$$

$$[\log(a_t) + (1 - a_t) x_{tmn}] \ \delta_{q_{mn}Q_t} + \qquad\qquad (4.19)$$

$$[\log(1 - e^{-a_t x_{tmn}}) - \log(1 - e^{-x_{tmn}})] (1 - \delta_{q_{mn}Q_t}) -$$

$$[\log(\hat{a}_b) + (1 - \hat{a}_b) x_{bmn}] \ .$$

The (p) superscript indicates a pixel level likelihood ratio.

Consider a very large CNR_t (say, >60 dB) and $\hat{I}_{tmn} \approx CNR_t$, which then occurs with high probability. The logarithm of $\Lambda_{mn}^{(p)}$ is then approximately:

$$\Lambda_{mn}^{(p)} \approx - [\log(\hat{a}_b) + (1 - \hat{a}_b) x_{bmn}] +$$

$$[\log(a_t) + (1 - a_t) x_{tmn}] \ \delta_{q_{mn}Q_t} \ . \qquad (4.20)$$

Since we are interested in receivers we can analyze rather than strictly optimal receivers, we will use this approximation for all CNR_ts, even small ones (CNR_t >10 dB) where the large CNR_t and $\hat{I}_{tmn}$ assumptions are not

valid.

Now we perform the maximizations over Q_t and a_t in equation 4.19 so the subframe log likelihood ratio is:

$$\log \Lambda^{(s)}_{gm} = \max_{a_t, Q_t} \{ \sum_{n=1}^{N} \log \Lambda^{(p)}_{mn} \}$$

$$= N \left[\frac{j_m}{N} \left(\log(\hat{a}_{tm}) + \frac{1}{\hat{a}_{tm}} - 1 \right) - \right. \qquad (4.21)$$

$$\left. \log(\hat{a}_b) + (1 - \hat{a}_b) \bar{I}_{bm} \right] ,$$

where

$$j_m \equiv \sum_{n=1}^{N} \delta_{q_{mn} \hat{Q}_{tm}} \quad , \quad \bar{I}_{bm} \equiv \frac{1}{N} \sum_{n=1}^{N} x_{bmn} ,$$

$$\hat{a}_{tm} \equiv \left[\frac{\sum_{n=1}^{N} x_{tmn} \delta_{q_{mn} \hat{Q}_{tm}}}{\sum_{n=1}^{N} \delta_{q_{mn} \hat{Q}_{tm}}} \right]^{-1} , \quad \hat{a}_b \equiv \left[\frac{1}{M N} \sum_{m=1}^{M} \sum_{n=1}^{N} x_{bmn} \right]^{-1} .$$

Physically, j_m is the number of times the peak detector selected bin $\hat{Q}_{tm}$ as the maximum bin in subframe m. We will coin the term "hits": j_m is the number of hits in bin $\hat{Q}_{tm}$. Clearly, j_m is an integer in the interval [1, N] with larger values more probable for high CNR_t values. Physically, $\hat{a}_{tm}$ is the inverse of the average intensity for the hits in the presumed target bin $\hat{Q}_{tm}$. It is the same form as the estimate $\hat{a}_b$ (for a single subframe) except the uncertainty in target location has reduced the number of intensities to average over from N to j_m. The quantity $\bar{I}_{bm}$

is just the average background intensity for subframe m.

The only thing left undefined here is the procedure to determine $\hat{Q}_{tm}$. Mathematically, the procedure comes from the a_t and Q_t maximization terms in equation 4.21. Physically, the mathematics tells us bin $\hat{Q}_{tm}$ is the bin which has the largest average intensity for measurements over the entire frame. Figure 4.1 demonstrates the procedure for $Q_T = 6$ and $N = 5$. For each pixel we record $\hat{Q}_{tmn}$ and $\hat{I}_{tmn}$. For each bin we sum the intensities of all the hits in that bin number over the entire subframe and divide by the number of hits in that bin number to find the average intensity for that bin. We compute this average for all Q_T potential target range bins and select the maximum. The bin where this maximum occurs is $\hat{Q}_{tm}$, the number of hits in that bin is j_m, and the inverse of the average for that bin is $\hat{a}_{tm}$. If there is a target in the subframe and CNR_t is significant (> 10 dB), there is a high probability $\hat{Q}_{tm}$ will be the bin with the most number of hits, too. If CNR_t is very small or there is no target in the subframe, there may be, for instance, one bin with two hits and a smaller average intensity than some other bin with only one hit.

Equation 4.21 has a physically intuitive form. It is essentially the difference between the average intensity at the presumed target range and the average intensity at the known background range. Under H_1, j_m should be reasonably large (>N/2) and the $\hat{a}_t$ dependent terms are approximately $CNR_t - \log(CNR_t)$ which is > 1 with high probability. Meanwhile, the background terms will be close to zero with high probability. This gives a large log likelihood ratio. For hypothesis H_0 the target terms will be small and the background terms large, so the log

Bin #:   1   2   3   4   5   6   Pixel #:

```
|___|___|___|___X___|___|___|   1
```

$$\hat{I}_{tmn} = 3.21$$

```
|___|___|___|___|___|___X__|   2
```

$$\hat{I}_{tmn} = 1.13$$

```
|___|___|___|___X___|___|___|   3
```

$$\hat{I}_{tmn} = 2.47$$

```
|___|___|___|___X__|___|___|   4
```

$$\hat{I}_{tmn} = 1.89$$

$$\hat{I}_{tmn} = 0.71$$ X = "hit"

```
|___X___|___|___|___|___|___|   5
```

Sum each of Q_T = 6 bins/pixel over N = 5 pixels/subframe

$$\begin{cases} \hat{Q}_{tm} = 4 \\ j_m = 3 \\ \hat{a}_{tm} = 0.397 \end{cases}$$

```
|___X___|___|___XXX_|___X___|
```
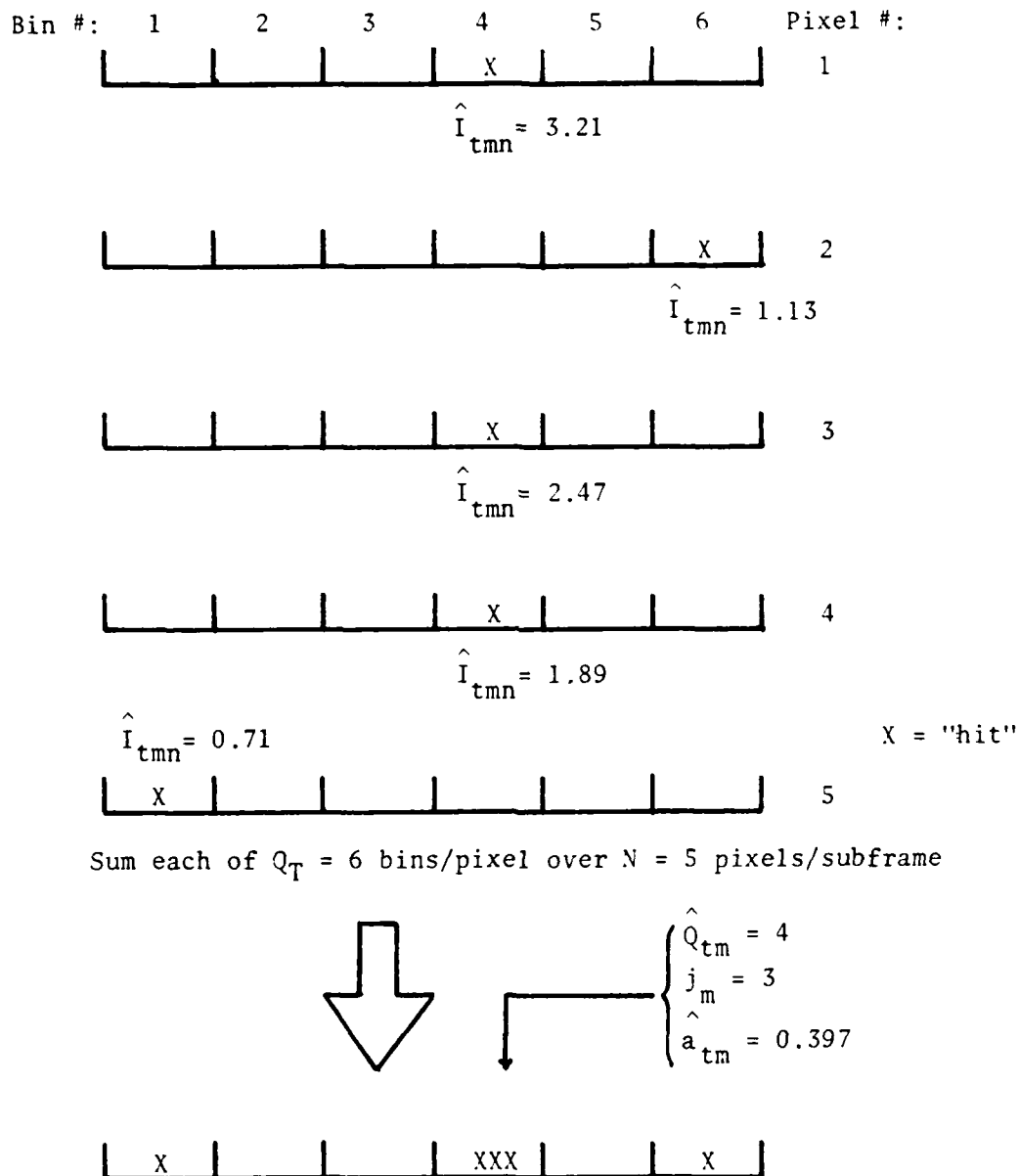
Figure 4.1

Subframe Bin Maximization to Determine $\hat{Q}_{tm}$

likelihood ratio will be small. If MN is large, we can treat $\hat{a}_b$ as an essentially exact estimate and thus make $\bar{I}_{bm}$ the only background dependent term. This simplifies the expression some since we can add, subtract, and multiply positive constants to a Neyman-Pearson test ratio without changing the performance (the as yet undetermined threshold shifts, however). An equivalent processor is:

$$\log \Lambda_{gm}^{(s)} = \frac{j_m}{N(1 - a_b)} \left(\log(\hat{a}_{tm}) + \frac{1}{a_{tm}} - 1 \right) - \bar{I}_{bm} \quad . \quad (4.22)$$

Here $\bar{I}_{bm}$ is a chi-squared random variable with 2N degrees of freedom since it is the sum of N exponential random variables [16]. However, $\hat{a}_t$ is a very complicated random variable and enters the expression in a very non-linear fashion. Random variable j_m is only slightly less difficult to generate a probability mass function for. This makes it very difficult to handle the performance even in approximate form. We could always calculate the processors performance by simulation methods, but we won't take this approach either. Instead, we will examine two simpler processors which measure range or intensity only. We will find their performances are easier to handle analytically or in approximate form. We should keep in mind, however, this joint range and intensity processor will out-perform the intensity only and the range only processors or any ad hoc combination of the two processors.

G. Intensity Only Processor

In this section we will investigate a receiver which measures only the intensity of the pre-processor output, $\hat{I}_{mn}$. We peak detect over all Q bins, but throw away $\hat{Q}_{mn}$ and we don't use the information about the range

to background. We use only the measured peak intensity I_{mn}. We will begin the intensity only processor analysis by examining the processor for a single pixel measurement:

$$\Lambda_g^{(p)}(x) = \frac{\max\limits_{a_t}\{\; p_{\hat{I}|H_1,a_t}(\,x\mid H_1,\,a_t\,)\;\}}{\max\limits_{a_b}\{\; p_{\hat{I}|H_0,a_b}(\,x\mid H_0,\,a_b\,)\;\}}$$

$$= \max_{a_t,a_b}\left\{\frac{p_{\hat{I}|H_1,a_t}(\,x\mid H_1,\,a_t\,)}{p_{\hat{I}|H_0,a_b}(\,x\mid H_0,\,a_b\,)}\right\}. \qquad (\,4.23\,)$$

If we make the large $\hat{I}_{mn}$, large CNR_t and CNR_b assumptions, as we did for the joint processor earlier, the conditional density for either hypothesis reduces to:

$$p_{\hat{I}|H_i,a_j}(\,x\mid H_i,\,a_j\,) \approx (\,1 - e^{-x}\,)\; e^{-a_j x}\, u(\,x\,) \qquad (\,4.24\,)$$

for $i = 0$, 1, and $j = b$ for $i = 0$, and $j = t$ for $i = 1$. Then the log likelihood ratio is:

$$\log \Lambda_g^{(p)}(x) = \max_{a_t,a_b}\{\,(\,a_b - a_t\,)\,x\,\}. \qquad (\,4.25\,)$$

Since the a_b and a_t values form a single multiplicative constant, they are irrelevant to a Neyman-Pearson processor _if_ we know the sign of $a_b - a_t$. Then the generalized likelihood ratio is also a uniformly most powerful (UMP) processor [4] and is simply:

$$\log \Lambda_g^{(p)}(x) = x \ .$$ (4.26)

Using the general results from earlier we now find the frame level processor for N pixel subframes is simply:

$$\log \Lambda_g^{(p)} = \max_m \{ \sum_{n=1}^{N} \log \Lambda_{gmn}^{(p)} \}$$

$$= \max_m \{ \sum_{n=1}^{N} x_{mn} \}$$ (4.27)

$$= \max_m \{ \log \Lambda_{gm}^{(s)} \} \ ,$$

where it is still critical that we know the sign of $a_b - a_t$. In general, however, we don't know the sign of $a_b - a_t$. Indeed, we may have either $CNR_b > CNR_t$ (called negative contrast), or $CNR_t > CNR_b$ (called positive contrast), or $CNR_b = CNR_t$ (no contrast or zero contrast). Nevertheless, in keeping with the idea of working with processors we can analyze, we will continue to use $\log \Lambda_{gm}^{(s)} = R_m^{(s)} = \sum_n \hat{I}_{mn}$ as our subframe statistic, and derive a way to handle the unknown contrast ratio.

Since we will generally be concerned with $N \sim 10$ or more pixels per subframe, we have a sum of a "large" number of independent random variables. This gives us a conditional Gaussian density for $R_m^{(s)}$, via the Central Limit Theorem. The conditional moments for $R_m^{(s)}$ are:

$$E[R_m^{(s)} \mid H_j^{(s)}] = N \mu_j, \qquad \text{var}[R_m^{(s)} \mid H_j^{(s)}] = N \sigma_j^2$$ (4.28)

for $j = t, b$, where μ_j and σ_j^2 are the conditional pixel mean and variance, respectively, and $H_t^{(s)}$ denotes the target subframe, and $H_b^{(s)}$ denotes a background subframe. After some straightforward but tedious calculations we get the conditional moment values:

$$\mu = \frac{Pr(\alpha_0)}{a} + [\ \mu(\ CNR = 0\ ) - \frac{1}{Q}\ ],$$

$$\mu(\ CNR = 0\ ) = \psi(\ Q + 1\ ) - \psi(\ 1\ ),$$

$$\sigma^2 = 2\frac{Pr(\alpha_0)}{a}[\ \psi(\ Q + a\ ) - \psi(\ a\ ) - \mu\ ] + \tag{4.29}$$

$$\left(\frac{Pr(\alpha_0)}{a}\right)^2 + \sigma^2(\ CNR = 0\ ) - \frac{1}{Q^2}\ ,$$

$$\sigma^2(\ CNR = 0\ ) = -[\ \psi'(\ Q + 1\ ) - \psi'(\ 1\ )\ ]\ ,$$

where $\psi(\ x\ )$ and $\psi'(\ x\ )$ are the first and second logarithmic derivatives of the gamma function, $\Gamma(\ x\ )$. The equations are valid for target and background with appropriate subscripts on the variables μ, σ, a, CNR, and α_0.

Since the subframes are independent, the frame processor falls into the same general form we derived in parts B and C above:

$$\hat\Lambda_g = \max_m \left\{ \frac{\max\limits_{\mu_t}(\ p_{R_m^{(s)}|H_1,\mu_t}(\ r_m^{(s)}\ |\ H_1,\ \mu_t\ )\ )}{p_{R_m^{(s)}|H_0,\hat\mu_b}(\ r_m^{(s)}\ |\ H_0,\ \hat\mu_b\ )} \right\}\ . \tag{4.30}$$

We will do the maximization in the numerator by differentiating the density with respect to μ_t directly and setting the derivative to zero:

$$\frac{d}{d \mu_t} [p_{R_m(s)|H_1,\mu_t} (r_m^{(s)} | H_1, \mu_t)] \Big|_{\mu_t = \hat{\mu}_{tm}} = 0 . \qquad (4.31)$$

The density for $R_m^{(s)} = \sum_n \hat{I}_{mn}$ is conditionally Gaussian with mean $N \mu_t$ and variance $N^2 \sigma_t^2$. However, σ_t^2 is a function of μ_t via the equations in 4.29. This dependence between μ_t and σ_t complicates the formula for $\hat{\mu}_{tm}$. With this functional dependence, the estimate is given implicitly by the equation:

$$\hat{\mu}_{tm} = \bar{\mu}_{tm} - \hat{\sigma}_{tm} \left[- \frac{1}{2 \hat{\sigma}_{tm}'} + \sqrt{\frac{1}{1 + 4\hat{\sigma}_{tm}'^2}} \right] \qquad (4.32)$$

where the value of $\hat{\sigma}_{tm}$ is the value of the equation for σ_t evaluated at $\mu_t = \hat{\mu}_{tm}$ and $\hat{\sigma}'_{tm}$ is the derivative of σ_t with respect to μ_t evaluated at $\hat{\mu}_{tm}$. If σ_t was not a function of μ_t (or CNR_t), the variance dependent terms in equation 4.32 would not be present and the estimate would be $\hat{\mu}_{tm} = \bar{\mu}_{tm} \equiv \sum_n \hat{I}_{mn}$, the sample mean. At very high CNR_t values, $\sigma_t \simeq \mu_t$, so the estimate reduces to:

$$\hat{\mu}_{tm} = \frac{2}{1 + \sqrt{5}} \bar{\mu}_{tm} = 0.618 \bar{\mu}_{tm} . \qquad (4.33)$$

For small CNR_t values, $\hat{\sigma}_t'$ and $\hat{\sigma}_t$ approach constant values and $\hat{\mu}_{tm}$ approaches the sample mean minus a constant bias. In keeping with our aim to use simple quasi-optimal processors, we will use the approximation $\hat{\mu}_{tm} = \bar{\mu}_{tm}$ since it is a reasonable approximation and has the advantage of being independent of CNR_t.

To obtain $\hat{\mu}_b$, we perform a similar differentiation except we use the

statistics for the entire frame: $\bar{R}^{(f)} = (R_1^{(s)}, \ldots, R_M^{(s)})$, where the $R_m^{(s)}$ random variables are conditionally independent jointly Gaussian random variables with identical means, $N \mu_b$, and variances, $N^2 \sigma_b^2$. Setting the derivative with respect to μ_b of

$P_{\bar{R}^{(f)}|H_0,\mu_b} (r^{(f)} | H_0, \mu_b)$ to zero and simplifying leaves the implicit equation for $\hat{\mu}_b$:

$$\sum_{m=1}^{M} (r_m^{(s)} - N \hat{\mu}_b) - M(\hat{\mu}_b + \kappa_1(\hat{a}_b))$$

$$[1 - \frac{1}{MN\hat{\sigma}_b^2} \sum_{m=1}^{M} (r_m^{(s)} - N \hat{\mu}_b)^2] = 0 , \qquad (4.34)$$

where $\kappa_1(\hat{a}) = \psi(Q + \hat{a}) - \psi(\hat{a})$ which is an increasingly weak function of $\hat{a}$ as CNR increases. Again, if σ_b^2 was not a function of μ_b through CNR_b, the last term would not appear and the equation would reduce to μ_b = the frame sample mean, as our intuition would lead us to guess. Even with the $\mu_b - \sigma_b$ relationship, the last term is small for large M. So, we can take $\hat{\mu}_b \simeq \bar{\mu}_b$ as an even better approximation for the background than for a target subframe.

With $\hat{\mu}_b$ and $\hat{\mu}_t$ set to their sample means for a frame and subframe, respectively, we can complete deriving the processor. The conditional densities are Gaussian under H_0 and H_1, so the log likelihood ratio is:

$$\log \Lambda_{gm}^{(s)} = \frac{1}{2} \log \frac{\hat{\sigma}_b^2}{\hat{\sigma}_{tm}^2} + \frac{(r_m^{(s)} - N\hat{\mu}_b)^2}{\hat{\sigma}_b^2} . \qquad (4.35)$$

We will drop the term involving the logarithm of the ratio of the

variances since this term is proportional to the logarithm of the contrast ratio and the other term is proportional to the contrast ratio directly. Then an equivalent processor for a Neyman-Pearson test is:

$$\log \Lambda^{(s)}_{gm} = \left| r^{(s)}_m - N \hat{\mu}_b \right| \quad . \tag{4.36}$$

This processor is very intuitively appealing. We choose as the target subframe that subframe which exhibits the largest contrast (positive or negative) relative to the computed background mean. The test is simply to compare this contrast to a threshold.

Notice that this processor is not quite in the form

$$\log \Lambda^{(f)}_g = \max_m \left\{ \log \Lambda^{(s)}_{gm} \right\} \tag{4.37}$$

as we would like since the quantity in the braces contains $\hat{\mu}_b$ which is a function of $R^{(s)}_m$ for all m. However, since MN is generally large, we know the variance of $\hat{\mu}_b$ must be fairly small since $\hat{\mu}_b$ is approximately the sample mean and the variance of the sample mean falls as $1 / MN$. Because of this, we will take $\hat{\mu}_b$ as exactly μ_b, that is, treat CNR_b as a known quantity. Then the log likelihood ratio is in the desired form. Numerical calculations with $\hat{\mu}_b = \mu_b \pm 3\sigma_b$ give indistinguishable results with MN = 128 x 128 pixels.

Although we have justified assuming conditional Gaussian statistics for $R^{(s)}_m$ via a Central Limit Theorem argument, we know for CNR $\to \infty$ the random variable $R^{(s)}_m / N \mu_i$ has conditional chi-squared statistics under

$H_i^{(s)}$ with mean 1 and 2N degrees of freedom. Let's compare this chi-squared density to a Gaussian density with mean 1 and variance $\sigma^2/N \mu^2$. We will do this comparison by calculating P_F versus λ' for both models with $\lambda' = \lambda / N \mu_b$ for P_F down to about 10^{-5}. This test allows us to compare the tails of the densities, which are of most interest to us, where the Central Limit Theorem arguments don't yield very accurate results. Figure 4.2 shows this comparison for M = 1000. Although the two models converge more as N gets larger, even at N = 100, the two are still very far apart for even fairly high false alarm rates like 10^{-4}. Of course, the problem is worse at more reasonable P_F values like 10^{-6} which are farther into the tails of the density.

Although we obviously cannot use the Gaussian statistics to analyze the processor's performance, we will continue to use the processor derived from the Gaussian statistics assumption because it is so intuitively appealing. For analysis purposes, we will use an approximation derived from the Chernoff bounds [4]. For CNR $\rightarrow \infty$, numerical calculations show this approximation differs from the exact results (the chi-squared statistics) by only a percent or two [18].

H.   Range Only Processor

In this section we will examine a processor which uses all the range information available and discards all the intensity information. For each pixel we measure the peak over all Q bins and record the bin number where the peak occurred, $\hat{Q}_{mn}$. We ignore the intensity of this peak.

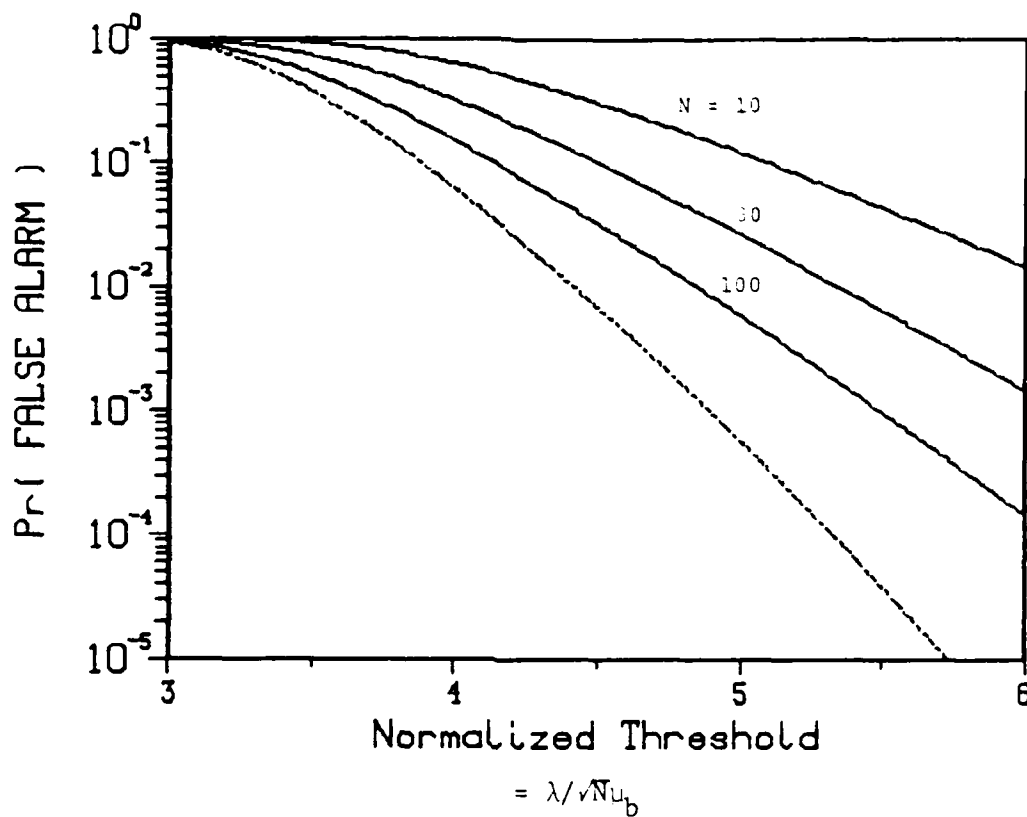We derive the range only processor using the same techniques we derived in

Figure 4.2

P_F for Two Intensity Statistic Models

—— Chi-Squared

--- Gaussian, any N value

section C above using the marginal coarse range probability mass functions
we derived in the previous chapter. As usual, we take each pixel and
subframe to be independent of the others. The resulting generalized
likelihood ratio test is:

$$
\Lambda_g^{(f)} = \max_m \left\{
\frac{\displaystyle \max_{\substack{Pr(\alpha_{0t}), \\ Q_t}} \prod_{n=1}^{N} Pr(\hat{Q}_{mn} = q_{mn} \mid H_1, Pr(\alpha_{0t}), Q_t)}{\displaystyle \prod_{n=1}^{N} Pr(\hat{Q}_{mn} = q_{mn} \mid H_0, Pr(\hat{\alpha}_{0b}))}
\right\}
\tag{4.38}
$$

where the denominator is evaluated with $Pr(\hat{\alpha}_{0b})$ which we in turn
derived from:

$$
\max_{Pr(\alpha_{0b})} \left\{ \prod_{m=1}^{M} \prod_{n=1}^{N} Pr(\hat{Q}_{mn} = q_{mn} \mid H_0, Pr(\alpha_{0b})) \right\}.
\tag{4.39}
$$

Taking the logarithm, substituting the probabilty mass function in,
differentiating with respect to $Pr(\alpha_{0b})$, and setting the derivative to
zero, we solve for:

$$
Pr(\hat{\alpha}_{0b}) = \frac{1}{M \, N} \sum_{m=1}^{M} \sum_{n=1}^{N} {}^{5}q_{mn}Q_{bmn} .
\tag{4.40}
$$

The estimate of $Pr(\alpha_{ob})$ is just the relative frequency of occurence of
anomaly events for the entire frame. If there is no target in the frame,
the estimate corresponds exactly to the intuitive notion of the

probability of no anomaly and the Law of Large Numbers [16]. If there is a target in the frame, the assumption we made of $M \gg 1$ makes the target contributions to the estimate of the background anomaly probability dilute, and hence we may use the same intuitive interpretation of the equation. Since MN is the number of pixels in a frame, it is usually quite large, so the estimate can be very accurate, particularly at small background CNRs. At higher CNRs, the estimate will be less accurate (because the summation will be smaller so statistical variations introduce larger relative errors). In the ensuing discussion, we will take the estimate to be exact and so treat the background CNR as known, as we did in the intensity only receiver.

Performing an identical maximization in the numerator gives the estimate

$$Pr(\hat{\alpha}_{0t}) = \frac{j_m}{N} \quad , \text{ where } \quad j_m \equiv \max_{1 \le Q_t \le Q_T} \left(\sum_{n=1}^{N} \delta_{q_{mn} Q_t} \right) . \quad (4.41)$$

Again, $Pr(\hat{\alpha}_{0t})$ corresponds to our intuitive notion of the probability of no anomaly. Here j_m is the number of hits in the range bin, from among the Q_T potential target range bins, with the most hits for the m-th subframe. However, since N is generally not very large (<100), the estimate may not be very accurate. Hence, we cannot take this estimate to be exact. Physically, j_m is the same as it was for the joint range and intensity processor we already examined and pictured in figure 4.1. Without the intensity information however, we choose Q_t in a different manner in equation 4.41. Now we simply choose as Q_t the bin with the most hits from among the Q_T potential target range bins in the subframe picture (the last line) in figure 4.1. We can see intuitively now why the range

only processor must under-perform the joint range and intensity
processor. The joint processor takes into account not only the number of
hits per bin, but also the average intensity for those hits. Since
anomalies occur in noise bins, they have intensities with mean 1, which is
always less than the target bin with mean $CNR_t + 1$. Thus, the joint
processor can weight the range bin measurements to make implicit guesses
at whether or not some hits correspond to anomalies. Without the
intensity information to help weight the decisions, the range only
processor will make poorer decisions, particularly at low CNRs where
anomalies occur more frequently.

If we substitute these quantities into equation 4.38, take the logarithm,
and define the number of hits at the known background ranges as:

$$k_m \equiv \sum_{n=1}^{N} \delta_{q_{mn}} Q_{bmn} , \qquad (4.42)$$

then the generalized log likelihood ratio processor is

$$\log \Lambda_g^{(f)} = \max_m \{ \log \Lambda_{gm}^{(s)} \} , \qquad \log \Lambda_{gm}^{(s)} = P_1 j_m - k_m + P_2 ,$$

$$P_1 \equiv \frac{\log \dfrac{(Q_T - 1) \, Pr(\hat{\alpha}_{0t})}{1 - Pr(\alpha_{0t})}}{\log \dfrac{(Q - 1) \, Pr(\alpha_{0b})}{1 - Pr(\alpha_{0b})}} , \qquad \text{and} \qquad (4.43)$$

$$P_2 \equiv N \cdot \frac{\log \frac{(Q-1)}{(Q_T-1)} \frac{(1 - Pr(\hat{\alpha}_{0t}))}{(1 - Pr(\alpha_{0b}))}}{\log \frac{(Q-1) Pr(\alpha_{0b})}{1 - Pr(\alpha_{0b})}} .$$

Notice that P_1 and P_2 are functions of $Pr(\hat{\alpha}_{0t})$ and so are functions of j_m. Because of this, we can plot P_1 and P_2 as functions of j_m for various values of CNR_b and get a feeling for how sensitive the processor is to the values of P_1 and P_2. Figures 4.3 and 4.4 show such plots for $Q = 100$ and $Q_B \ll Q \simeq Q_T$, a realistic condition for either a large range uncertainty, L_u, or a radar with good range resolution. Although both parameters can vary over a wide range, the probable values for j_m for reasonable target CNR values (> 10 dB) will place the parameters in a relatively narrow range. This being the case, an approximately equivalent processor for a Neyman-Pearson test is the much simpler formula:

$$\log \Lambda_{gm}^{(s)} \simeq j_m - k_m . \tag{4.44}$$

In fact, this processor is exactly optimal for known target CNR and zero contrast. We will use this processor for all CNRs since it is a fair approximation to the optimal processor and it is possible to analyze its performance without too much difficulty.

Physically, this processor determines whether the presumed target range bin or the background range bins had more hits and how many more. As CNR_t increases in the subframe containing the target, $\log \Lambda_{gm}^{(s)}$ grows more positive. As CNR_b increases in a background subframe, the statistic grows more negative. The processor looks for range measurements to clump or
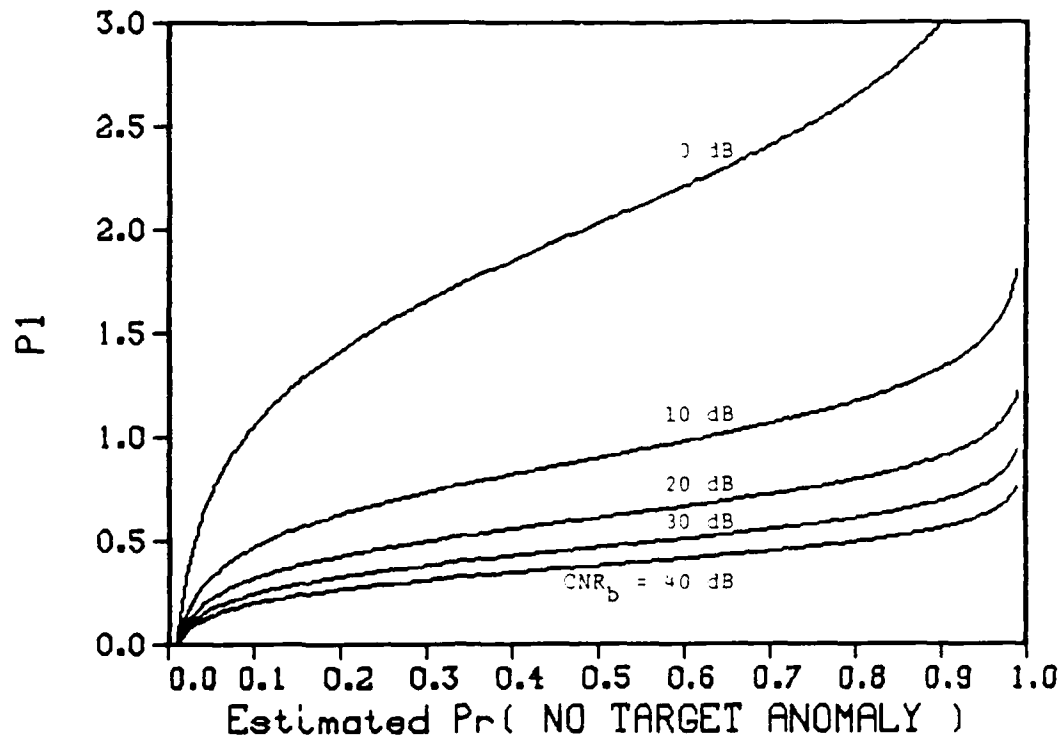
Figure 4.3
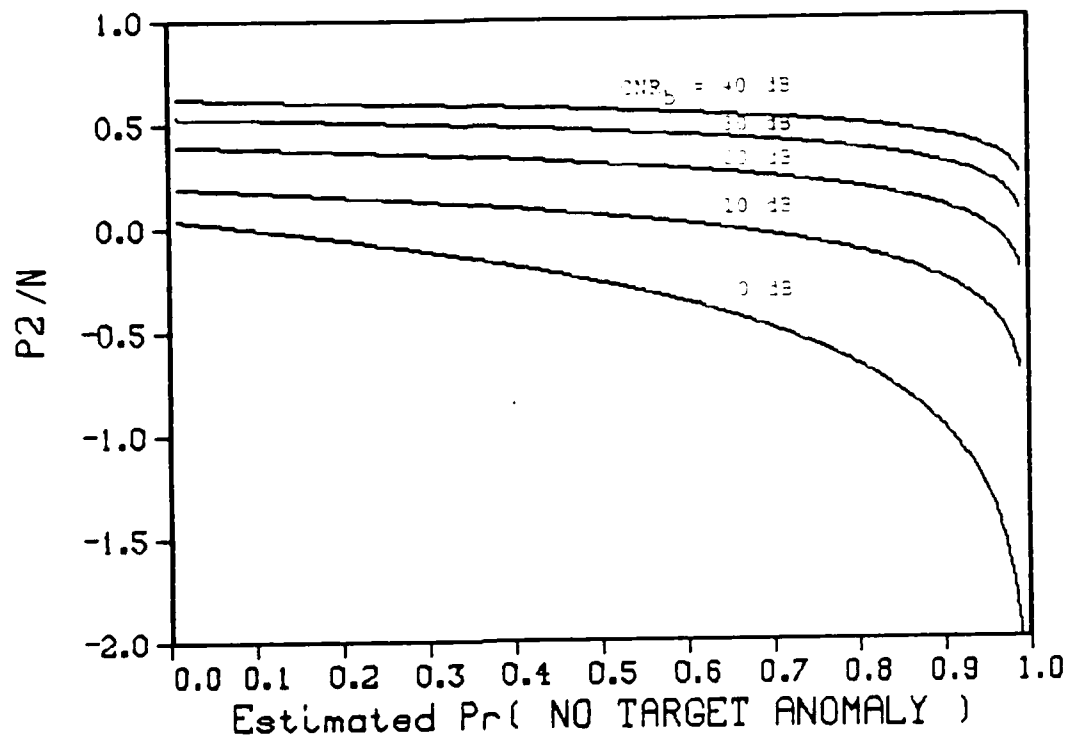
Parameter P_1 for Range Only Processor

Figure 4.4

Parameter P_2 for Range Only Processor

aggregate at the background ranges (the k_m term) and somewhere in the Q_T potential target range bins (the j_m term). It then makes a decision based on which clump is bigger and by how much. Colloquially, we can say that whereas the intensity only processor looks for the maximum intensity contrast, the range only processor looks for the maximum range contrast.

I. Other Processors

We have derived processors for intensity, range, and joint intensity and range measurements. We could also imagine incorporating Doppler measurements into these processors. However, our analysis in chapter 3 indicates we need do no further work on the processors because of the range-Doppler duality we encountered. Anywhere we treated range measurements, we could substitute Doppler measurements, or include joint range and Doppler measurements. The processors don't change form, although some parameters may change values. Because of this duality, we won't treat Doppler processors explicitly until chapter 6 where we will consider how the performance scales with changes in the system parameters that differ between range and Doppler radars.

Now that we have derived the processors we will use, we will derive performance measures for them in the next chapter.

V. Receiver Performance Derivations

Recall that we wish to find P_F and P_M for intensity only and range only receivers when they evaluate an entire frame of data. However, we already know we can easily get the frame level performance directly from the subframe level performance. Consequently, this chapter derives equations for $P_F^{(s)}$ and $P_M^{(s)}$ for a receiver measuring data only over a single subframe. The translation to frame level performance is direct. (For notational simplicity we don't use the (s) superscripts in this chapter nor the then superfluous m subscript. If there is cause for confusion, we will reintroduce the subscripts and superscripts.)

A. Intensity Only

Recall from the last chapter the quasi-optimal intensity only processor tests for subframe contrast:

$$\left| \sum_{n=1}^{N} \hat{I}_n - N \hat{\mu}_b \right| \underset{H_0}{\overset{H_1}{\underset{<}{>}}} \lambda \equiv N \mu_b \lambda' \; . \qquad (\,5.1\,)$$

If $N = 1$, we can analyze the processor exactly. The analysis is fairly simple and, using the exact statistics derived in chapter 3, the P_F and P_M, in terms of the threshold, are:

$$P_F = 1 - (1 - e^{-(1 + \lambda')\mu_b})^{Q-1} (1 - e^{-a_b(1 + \lambda')\mu_b}) +$$

$$(1 - e^{-(1 - \lambda')\mu_b})^{Q-1} (1 - e^{-a_b(1 - \lambda')\mu_b}) \, u(1 - \lambda')$$

$$P_M = (1 - e^{-(1 - \lambda') \mu_b})^{Q-1} (1 - e^{-a_t(1 - \lambda') \mu_b}) -$$

$$(1 - e^{-(1 - \lambda') \mu_b})^{Q-1} (1 - e^{-a_t(1 - \lambda') \mu_b}) \, u(1 - \lambda') ,$$

$$\lambda' > 0 . \tag{5.2}$$

Reasonable P_F performance ($<10^{-2}$) requires $\lambda' > 1$ and so

$$P_F \simeq \exp[- a_b \, \mu_b (1 + \lambda')] , \quad \text{which gives}$$

$$\lambda' \simeq - (1 + \log(P_F) / (a_b \, \mu_b)), \quad \text{and} \tag{5.3}$$

$$P_M \simeq 1 - \exp[\frac{a_t}{a_b} \log(P_F)] \; = \; 1 - (P_F)^{a_t/a_b} .$$

These equations are very similar to the equivalent equations for a processor which measures intensity at the known target range. The equation for the threshold, λ', in terms of P_F in 5.3 is identical to that for the known range processor with clutter [14]. The equation for P_M in terms of P_F in 5.3 is nearly the same as its (clutter free) analog for the known range processor. The only difference is the exponent to P_F which, for the known range processor, always exhibits an effective $CNR_b = 0$.

Notice that with zero contrast, the performance reverts to the guessing curve ($P_D = P_F$), as we would expect for a processor which searches for contrast. Similarly, there is an obvious asymmetry between performance for positive and negative contrasts of the same magnitude. This occurs because the density function is so asymmetric with a mode close to the origin and long tails out to positive infinity. Finally, notice that the

processor performance is independent of Q. This occurs because λ' is large enough to make the Q-dependent terms ~ 1.

Although the single pixel processor is not of much practical importance, the ability to make an exact analysis gives us information which may carry over to multipixel processors as well. We should not be surprised if multipixel processors don't perform well at negative contrasts and the performance is relatively insensitive to the value of Q.

When there are multiple pixels in a subframe, we have already noted the statistics are too complicated to analyze exactly and neither the Gaussian nor the chi-squared limits are accurate enough for general N and CNR values. Instead we use an approximate performance measure derived from the Chernoff bound [4]:

$$
\Pr\left\{ \sum_{n=1}^{N} \hat{I}_n \geq \lambda \mid H_i \right\} \simeq \exp[-N(s\dot{\gamma}_i(s) - \gamma_i(s)]
$$

$$
\cdot \frac{1}{2} \exp[\frac{1}{2} N s^2 \ddot{\gamma}_i(s)] \; \mathrm{erfc}(\sqrt{ \frac{1}{2} N s^2 \ddot{\gamma}_i(s) }), \qquad (5.4)
$$

$$
\gamma_i(s) \equiv \log(E[e^{s\hat{I}} \mid H_i]), \qquad i = t \text{ or } b, \qquad s \geq 0 .
$$

The parameter s is free, but the optimal choice is when $\dot{\gamma}_i(s) = \lambda$. The first exponential is just the Chernoff bound and the other two terms are the correction term. For $Ns^2 \ddot{\gamma}(s) > 9$, we can combine terms and approximate the correction term by:

$$
\frac{1}{2} \exp[\frac{1}{2} N s^2 \ddot{\gamma}_i(s)] \; \mathrm{erfc}(\sqrt{ \frac{1}{2} N s^2 \ddot{\gamma}_i(s) }) \simeq
$$

$$\frac{1}{\sqrt{2 \pi N s^2 \ddot{\gamma}_i(s)}} \qquad (\; 5.5 \;)$$

If the test in equation 5.4 is $\sum_n \hat{I}_n < \lambda$, the only change is in the sign of s in the equations, so s < 0.

For the multipixel intensity only processor we find that:

$$P_F = Pr\{ \; | \; \sum_{n=1}^{N} \hat{I}_n - N \; \mu_b \; | \; > \lambda \; | \; H_0 \; \}$$

$$= Pr\{ \; \sum_{n=1}^{N} \hat{I}_n > N \; \mu_b \; (\; 1 + \lambda' \;) \; | \; H_0 \; \} \; +$$

$$Pr\{ \; \sum_{n=1}^{N} \hat{I}_n < N \; \mu_b \; (\; 1 - \lambda' \;) \; | \; H_0 \; \} \quad ,$$

$$P_M = Pr\{ \; | \; \sum_{n=1}^{N} \hat{I}_n - N \; \mu_b \; | \; < \lambda \; | \; H_1 \; \} \qquad (\; 5.6 \;)$$

$$= Pr\{ \; \sum_{n=1}^{N} \hat{I}_n > N \; \mu_b \; (\; 1 - \lambda' \;) \; | \; H_1 \; \} \; +$$

$$Pr\{ \; \sum_{n=1}^{N} \hat{I}_n < N \; \mu_b \; (\; 1 + \lambda' \;) \; | \; H_1 \; \} \quad .$$

The conditional semi-invariant moment generating function, $\gamma_i(s)$, is:

$$\gamma_i(s) = \log(\; s \; [\; B(\; Q, \; a_i - s \;) - B(\; Q, \; - s \;) \;] \;) \; , \qquad (\; 5.7 \;)$$

$$i = b \text{ or } t,$$

where B(*) is the beta function:

$$B(x, y) \equiv \frac{\Gamma(x) \; \Gamma(y)}{\Gamma(x + y)} \; .$$

(5.8)

The s parameters in terms of the thresholds are:

$$\dot{\gamma}_i(s) = \mu_b(1 + \lambda') \; ,$$

(5.9)

$0 \leq s \leq a_i$ for the $> \lambda$ tests, $s \leq 0$ for the $< \lambda$ tests.

Going from this point to explicit numerical results requires much calculus and algebra, but there are no new theoretical developments, so we will skip these steps. In the next chapter we will present and discuss results of actual computations.

B. Range Only

We will handle the range only processor in a completely different fashion from the intensity only processor. From the last chapter, the processor is, again for a single subframe, one which searches for clumping of the range data in the background and target bins:

$$j - k \begin{array}{c} H_1 \\ > \\ < \\ H_0 \end{array} \lambda \; .$$

(5.10)

The P_F and P_M values are:

$$P_F = Pr\{ \; j - k \geq \lambda \; | \; H_0 \; \}$$

$$= \sum_{j = j_{min}}^{N} \sum_{k = 0}^{k_{max}} \Pr(J = j, K = k \mid H_0) \ ,$$

$$j_{min} = \max\{ 0, \lambda \} \ , \quad k_{max} = \max\{ 0, \min\{ N - j, \lambda - j \} \} \ ;$$

$$P_M = \Pr\{ j - k < \lambda \mid H_1 \} \tag{5.11}$$

$$= \sum_{k = k_{min}}^{N} \sum_{j = 0}^{j_{max}} \Pr(J = j, K = k \mid H_1) \ ,$$

$$k_{min} = \max\{ 0, - \lambda \} \ , \quad j_{max} = \max\{ 0, \min\{ N - k, k + \lambda \} \} \ .$$

Under both hypotheses we assume in case of a tie, $j - k = \lambda$, we choose hypothesis H_1. These are simple sums, but, of course, we need to find the joint probability mass functions first.

To find the joint probability mass function, start with a different mass function we can find relatively easily. We will divide the Q range bins into Q_T potential target bins and Q_B potential background bins as before. From the geometry discussed in chapter 3, we know these latter Q_B bins are always the most distant range bins for a particular subframe and, for a particular pixel, one of them is the known background range bin. Call J_i, $1 \leq i \leq Q_T$ the number of hits in the i-th potential target bin, K the number of hits in the correct background range bins (precisely which bin is "correct" depends on the pixel number within the frame), and L the number of hits in the $Q_B - 1$ background bins <u>not</u> at the correct background range. Under hypothesis H_0 we can write the joint mass function $\Pr(J_1 = j_1, \ldots, J_{Q_T} = j_{Q_T}, K = k, L = l \mid H_0)$ fairly easily. It is simply a multinomial:

$$\Pr(\ J_1 = j_1, \ \ldots, \ J_{Q_T} = j_{Q_T}, \ K = k, \ L = 1 \ | \ H_0 \ ) =$$

$$\frac{N!}{j_1! \ \cdots \ j_{Q_T}! \ k! \ 1!} \ \Pr(\ \alpha_{0b} \ )^k \ (\ Q_B - 1 \ )^1 \left[\frac{1 - \Pr(\ \alpha_{0b} \ )}{Q - 1} \right]^{N-k}$$

$$= \binom{N}{k} \ \Pr(\ \alpha_{0b} \ )^k \ \binom{N-k}{1} \ (\ Q_B - 1 \ )^1 \left[\frac{1 - \Pr(\ \alpha_{0b} \ )}{Q - 1} \right]^{N-k}$$

$$\cdot \ \frac{(\ N - k - 1 \ )!}{j_1! \ \cdots \ j_{Q_T}!} \ , \qquad\qquad (\ 5.12 \ )$$

for $\{ \ j_1, \ \ldots, \ j_{Q_T} \ , \ k, \ 1 \ \}$ non-negative integers obeying $j_1 + \ldots + j_{Q_T} = N - k - 1$. Now define $J = \max\{ \ J_i \ | \ i = 1, \ \ldots, \ Q_T \ \}$. To convert the mass function for the J_i's to a mass function for J we must sum over all combinations of the J_i's subject to the stated constraints and the additional constraint all $j_i \leq j$:

$$\Pr(\ J = j, \ K = k, \ L = 1 \ | \ H_0 \ ) = \qquad\qquad (\ 5.13 \ )$$

$$\sum_{j_1 = 0}^{j} \ \cdots \ \sum_{j_{Q_T} = 0}^{j} \ \Pr(\ J_1 = j_1, \ \ldots, \ J_{Q_T} = j_{Q_T}, \ K = k, \ L = 1 \ | \ H_0 \ )$$

$$= \binom{N}{k} \ \Pr(\ \alpha_{0b} \ )^k \ \binom{N-k}{1} \ (\ Q_B - 1 \ )^1 \left[\frac{1 - \Pr(\ \alpha_{0b} \ )}{Q - 1} \right]^{N-k} C_{j,N-k-1}^{(Q_T)}$$

$$C_{j,N-k-1}^{(Q_T)} \equiv \underbrace{\sum_{j_1 = 0}^{j} \ \cdots \ \sum_{j_{Q_T} = 0}^{j}}_{j_1 + \ldots + j_{Q_T} = N - k - 1} \ \frac{(\ N - k - 1 \ )!}{j_1! \ \cdots \ j_{Q_T}!} \ .$$

In words, $C_{j,N-k-1}^{(Q_T)}$ is the number of ways to order the elements of all the

sets $\{ J_i \mid i = 1,\ldots, Q_T \}$ such that we meet the constraints stated above. Now sum over 1 to get the mass function we want:

$$Pr(J = j, K = k \mid H_0) = \binom{N}{k} \; Pr(\alpha_{0b})^k \left[\frac{1 - Pr(\alpha_{0b})}{Q - 1} \right]^{N - k}$$

$$\sum_{1 = 0}^{N-j-k} \binom{N - k}{1} \; (Q_B - 1)^1 \; C_{j, N-k-1}^{(Q_T)} \qquad\qquad (5.14)$$

Evaluating $C_{j, N-k-1}^{(Q_T)}$ is computationally cumbersome, but once we have the C-values the remainder of the calculation is straightforward. Under hypothesis H_1 the procedure is similar though not the exact dual. To start, we assume the maximum, J, occurs in the correct (true target) range bin. This assumption simplifies the derivation and we will shortly see the error it introduces, for N and CNR_t values of interest, is very small. Call the event in which the maximum J_i occurs in the correct bin β_0 and the event in which the maximum J_i occurs in the wrong bin β_1. Then the mass function we start from is:

$$Pr(J = j, K = k, \beta_0 \mid H_1) = \sum_{1 = 0}^{N-j-k} Pr(J = j, K = k, L = 1, \beta_0 \mid H_1)$$

$$= \binom{N}{j} \; \binom{N - j}{k} \; Pr(\alpha_{0t}) \left[\frac{1 - Pr(\alpha_{0t})}{Q - 1} \right]^{N - j}$$

$$\bullet \sum_{1 = 0}^{N-j-k} \binom{N-j-k}{1} \; (Q_B - 1)^1 \; C'^{(Q_T-1)}_{j, N-j-k-1} \; . \qquad\qquad (5.15)$$

The difference between C' and C is, since we have β_0, there is one less sum in the sequence of summations and there are only $Q_T - 1$ bins to consider. For $N = 10$ and $CNR_t = 10 \; \mathrm{dB}$, both fairly small values,
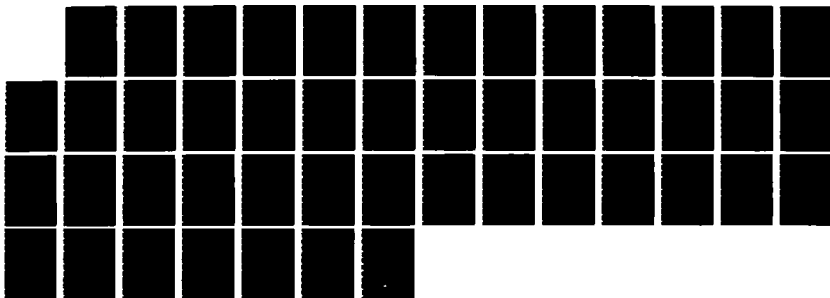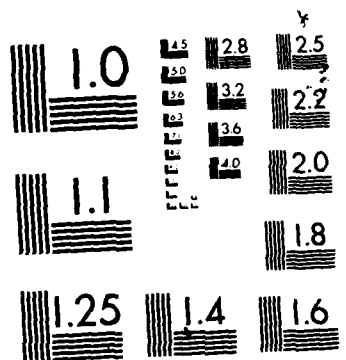
$\Pr(\beta_0 \mid H_1) \simeq 0.99966$. So, β_0 is essentially always true for cases of interest to us.

With these probability mass functions we can compute P_F and P_M directly using the equations in 5.11. However, P_F is not a continuous function of the threshold λ since the test statistic $\log \Lambda_{gm}^{(s)}$ is discrete. We touched on this problem at the beginning of chapter 4 and noted we could make P_F a continuous function of λ by randomizing the decision rule with a well known procedure. We will use this practice when computing P_F and P_M for the results in the next chapter so we can use P_F and P_M values in the range processor identical to those we used in the intensity processor. This will make it much easier to do comparisons between the two processors without introducing corrections to make the comparisons seem fair.

Now we have processors for range only and intensity only receivers and we have methods to compute their performance statistics. Actually performing the computations can be a complicated numerical procedure, but detailing the procedure would not contribute to the main point of this thesis and there are no novel numerical techniques necessary. Consequently, we will turn now to simply examining the results of these computations.

VI. RECEIVER PERFORMANCE RESULTS

We have taken our theoretical development from the single pixel speckle target IF waveform through a multipixel, multidimensional probability density function and derived quasi-optimal processors for two important receivers, the range only and intensity only measurement receivers. We have shown how to compute the P_D-P_F performance curves for these receivers in the last chapter. These theoretical developments are all we need to meet the original objectives of this thesis. Now we will present some actual numbers to demonstrate the relationships embodied in the processor and performance equations we derived in the last two chapters. In this chapter we will first derive relationships for how the CNR (target or background) scales with changes in various system parameters and then actually compute the performance curves for some cases of these processors and compare the range and intensity only receivers. As in previous chapters, we will perform our calculations only for a ranging radar and comment afterwards on how to carry the results over to Doppler and range-Doppler receivers.

A. System Parameter Interdependence

Our equations for system performance involve many parameters: M, the number of target sized subframes in one frame or field of regard; N, the number of pixels per subframe or on target; Q, the number of range bins per pixel; CNR_t, the target CNR; CNR_b, the background CNR; and ζ_{CNR}, which we will define as the contrast ratio, CNR_t/CNR_b. These parameters are not all independent and some depend on other system parameters which do not appear explicitly in the performance equations. However, the radar

equation, 3.17, determines how these parameters interact to affect performance:

$$CNR_i = \frac{\eta}{h\nu_o} \frac{P_T}{B} \rho_i \frac{A_P}{\pi L_i^2} e^{-2\alpha L_i} \varepsilon_{opt} , \qquad (6.1)$$

For simplicity of presentation, we will use $\alpha = 0$ and $\varepsilon_{opt} = 1$ and keep fixed $\eta/h\nu_o$ and target and background reflectivity ρ_i so that:

$$CNR_i = \left(\frac{\eta}{\pi h \nu_o} \rho_i \right) \frac{P_T}{B} \frac{A_P}{L_i^2} . \qquad (6.2)$$

Now consider how the choice of the parameters listed in the first sentence above affect the CNR through the radar equation, 6.2, and vice-versa. To do this, we will first review the models for the target and its environment and decide which elements of these models we will have reasonable control over and which we won't.

We will assume a fixed search volume and target size. The fixed search volume corresponds to a fixed angular uncertainty, Ω_u steradians, and fixed range uncertainty, L_u meters. These assumptions simply say the radar designer has no control over the size of the target or where it resides in space. For any given problem, however, the radar designer knows the fixed values of Ω_u, L_u, and the target size, Ω_t steradians. Notice we jumped from knowing the target _size_ to knowing the target _angular extent_ Ω_t. Formally, this requires knowing the target range, L, which we don't know. However, if we know there is only a small relative difference between the minimum and maximum L values, Ω_t will be

approximately constant for any L in the range of permitted values. We have assumed a known Ω_t all along by assuming a known N. A system where Ω_t is not known would require treating N as an unknown parameter in the fashion of chapter 3.

For a given L_u, we have

$$Q = \frac{L_u}{l_r} = \frac{2L_u}{ct_r} , \qquad\qquad (6.3)$$

where l_r is the bin size or range resolution in meters and t_r is the bin size or radar pulse width in seconds. Since all the performance equations depend only on Q, L_u does not enter the equations explicitly. For a given Ω_t, the value of N depends on the angular resolution, $\Delta\Omega$ steradians:

$$N = \frac{\Omega_t}{\Delta\Omega} , \qquad\qquad (6.4)$$

however, M remains constant at

$$M = \frac{\Omega_u}{\Omega_t} . \qquad\qquad (6.5)$$

Changing the radar parameters has no effect on M. Because this is true, and because performance depends on M in such a predictable fashion, we will not concern ourselves too much with M. We will fix M = 1000, as we did in chapter 5 for a single pixel, for the remainder of our work. This corresponds to a frame of about 30 by 30 subframes.

We should mention there is one complication with this assumption. Some of

our derivations assumed a large M value. Although we didn't define what we meant by large, cases of M $^-$ 10 are probably too small to allow the approximations to remain valid. We won't deal with this problem, but we should at least recognize it exists. Notice that N depends on $\Delta\Omega$ which in turn depends on the receiver aperture A_p, whereas Q depends on t_r which in turn sets the matched filter bandwidth B.

Now let's examine the B or Q dependence more carefully. We will let B = $1/t_r$ since we used a matched IF filter. P_T is the transmitter peak power and it is related to the transmitter average power, P_A, by

$$P_T = P_A \frac{T}{t_r} \qquad \longrightarrow \qquad \frac{P_T}{B} = P_T t_r = P_A T, \qquad (6.6)$$

where T is the pixel dwell time or inter-pulse time, and 1/T is the pulse repetition frequency (prf). There is a maximum pulse repetition frequency in a ranging radar that is set by the desire for unambiguous range information [1], [7]. If we want unambiguous range detection out to range L, we must have T > 2L/c; for L = 3 km this translates to T > 20 μsec. We will assume T takes on its minimum value, since larger values lead to longer frame imaging times, MNT.

If we assume our laser is average power limited, P_A is constant. Since T is also constant, P_T / B is a constant by equation 6.6. Hence, changing Q does not affect the system CNR.

If we assume our laser is peak power limited, P_T is constant and

$$B = \frac{1}{t_r} = \frac{c\,Q}{2\,L_u} \quad , \qquad\qquad (\ 6.7\ )$$

so the system CNR is proportional to 1/Q. In this case it is useful to define a quantity $Q^{(max)}$ as the largest number of range bins, corresponding to maximum bandwidth, $B^{(max)}$, operation of the radar. In terms of these maximum parameters we have:

$$B = \frac{c}{2L_u}\,Q^{(max)}\,\frac{Q}{Q^{(max)}} = B^{(max)}\,\frac{Q}{Q^{(max)}} \quad . \qquad (\ 6.8\ )$$

The value $Q^{(max)}$ exists because we have assumed all targets and background are not range resolved within a pixel. If we make t_r too small ($Q^{(max)}$ too large), we will start to resolve the fine range structure of the target. There is also an indirect N dependence in $Q^{(max)}$. For a given target, if N is small, each pixel will cover a larger area of the target which leaves more opportunities for the target to be range resolved. For large N, we have a larger $Q^{(max)}$. We won't deal with this weak N dependence in this thesis.

Turning to the N parameter, we use Fourier diffraction theory [21] and equation 6.4 to obtain

$$A_p = \frac{1.2\ \lambda^2}{\Delta\Omega} = \frac{1.2\ \lambda^2}{\Omega_t}\,N \quad , \qquad\qquad (\ 6.9\ )$$

where the factor 1.2 arises from the Airy disk radius, π , factors of 2, etc. If we define a maximum aperture $A_p^{(max)}$ and a corresponding maximum

N, $N^{(max)}$ we get:

$$A_P = \frac{1.2 \; \lambda^2 \; N^{(max)}}{\Omega_t} \; \frac{N^{(max)}}{N^{(max)}} = A_P^{(max)} \; \frac{N}{N^{(max)}} \; . \qquad (6.10)$$

Finally, in terms of the CNR at maximum aperture and maximum bandwidth,

$$CNR_i^{(0)} \equiv \frac{\eta}{h \nu_o} \; \rho_i \; \frac{A_P^{(max)}}{\pi \; L_i^2} \; \frac{P_T}{B^{(max)}} \; , \qquad (6.11)$$

we have the scaling laws

$$CNR_i = \begin{cases} CNR_i^{(0)} \; \dfrac{Q^{(max)}}{Q} \; \dfrac{N}{N^{(max)}} & : \quad P_T \text{ limited} \\[4mm] CNR_i^{(0)} \; \dfrac{N}{N^{(max)}} & : \quad P_A \text{ limited} \end{cases} \qquad (6.12)$$

These relationships are important for making reasonable comparisons between two processors with different resolution parameters imaging the same target and environment. We will return to these equations when we compare processors with different resolutions and in the last section of this chapter. For individual processors with fixed N and Q values, however, there is no need to bother with the scaling factors.

In all the following calculations, we will use $N^{(max)} = 40$ pixels and $Q^{(max)} = 10000$ bins.
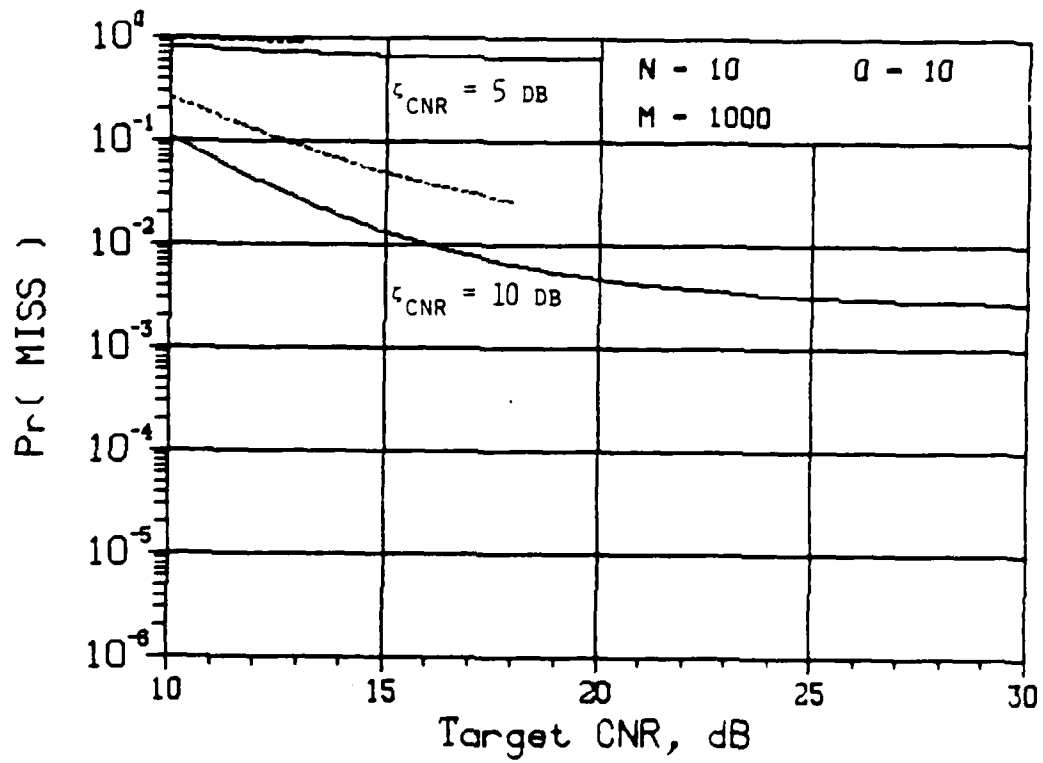
B. Intensity Processor

Recall the quasi-optimal intensity only processor searches the frame for the subframe which exhibits the most contrast relative to the computed background intensity. If that contrast exceeds a threshold, the processor declares a target present in the subframe with the maximum contrast:

$$\max\{ \, | \sum_{n=1}^{N} \hat{I}_{mn} - N \, \hat{\mu}_{b} \, | \, \} \overset{H_1}{\underset{H_0}{\gtrless}} \lambda \, . \qquad (\ 6.13\ )$$

Using the equations we derived in chapter 5, we can plot P_M versus CNR_t for this processor at given P_F, N, M, Q, and ζ_{CNR} values. Figure 6.1 shows the frame level performance results for N = 10 and 20 pixels, M = 1000, and Q = 10. For each plot there are two sets of two curves each. The top set is for ζ_{CNR} = +5 dB and the bottom set is for ζ_{CNR} = +10 dB. For each set, the top curve (dotted line) is for $P_F = 10^{-6}$ and the bottom curve is for $P_F = 10^{-3}$. For $\zeta_{CNR} \leq 0$ dB, all the curves are indistinguishable from $P_M = 1.0$. The value of Q = 10 is fairly arbitrary because, as we shall see shortly, Q is not very important to the performance of an intensity only processor. We expected this Q-insensitivity from our single pixel work in chapter 4.

The method used to generate the numbers in these curves has introduced two quirks in these plots which the reader will easily notice. In the N = 10 plot, figure 6.1 (a), the lines for $P_F = 10^{-6}$ don't extend to CNR_t = 30 dB. This is not a major problem since the curve has approximately reached its asymptotic value by the time the data stops anyway. In figure 6.1 (b)
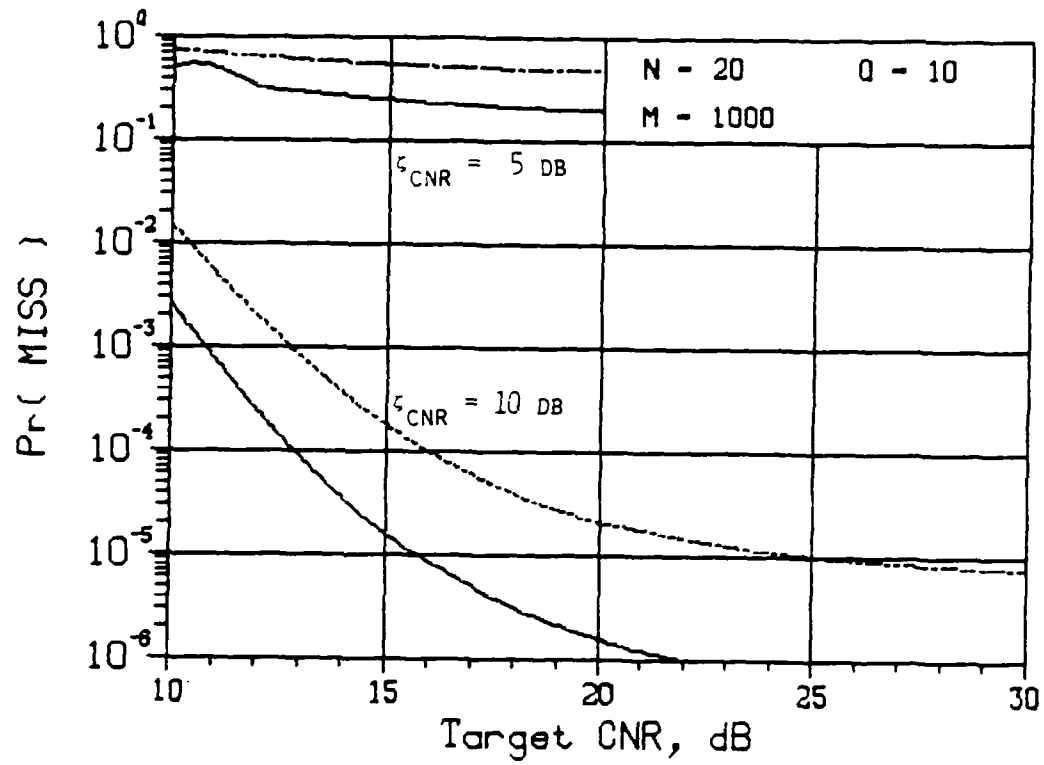
(a)

Figure 6.1

Frame Level Intensity Only Processor Performances

P_M -vs- CNR_t

(a) N = 10   (b) N = 20

—— P_F = 10^{-3} --- P_F = 10^{-6}

(b)

Figure 6.1

(cont'd)

for $P_F = 10^{-3}$ and $\zeta_{CNR} = 5$ dB, there is a bump in the curve at very low CNR_t values. This arises because the Chernoff bounds don't work well at estimating large probabilities. This is not a real problem since this region corresponds to very poor performance anyway.

The first thing to notice on these plots is the asymptotic behavior for large CNR_t. As $CNR_t \to \infty$, the P_M does not go to zero. If we use the unit mean chi-squared random variable with 2N degrees of freedom to model $R_m^{(s)}/E[R_m^{(s)}|H_i]$ for very large CNR_i values, $i = t, b$, we can more easily understand this behavior. Let's define a random variable $I_{mn}^{(0)}$:

$$I_{mn}^{(0)} \equiv \frac{\hat{I}_{mn}}{E[\hat{I}_{mn} \mid H_0]} \quad . \tag{6.14}$$

where $I_{mn}^{(0)}$ is a conditionally chi-squared random variable with 2 degrees of freedom and mean 1 under H_0, mean ζ_{CNR} under H_1. The sum of N conditionally chi-squared random variables with 2 degrees of freedom is another conditional chi-squared random variable with 2N degrees of freedom [16]. Now let us compute the relative distance between the two conditional means:

$$d \equiv \frac{\left| E[\sum_{n=1}^{N} I_{mn}^{(0)} \mid H_1] - E[\sum_{n=1}^{N} I_{mn}^{(0)} \mid H_0] \right|}{\mathrm{var}[\sum_{n=1}^{N} I_{mn}^{(0)} \mid H_0]} \tag{6.15}$$

$$= \mid 1 - \zeta_{CNR} \mid \ .$$

Notice for a fixed contrast ratio, the distance is fixed. As we increase

CNR_t with constant ζ_{CNR}, the densities converge to these chi-squared densities and the distance between the densities for the intensity processor's decision statistic under H_0 and H_1 don't spread farther apart. Consequently, the two hypotheses don't get any easier to distinguish as CNR_t increases at constant contrast, so, P_M approaches a nonzero asymptotic value.

Physically, we are at speckle limited performance. The CNRs are so large there is virtually no LO shot noise to contend with and the speckle induced intensity fluctuations alone make the target and background difficult to distinguish.

Equation 6.15 also helps explain what happens to performance as a function of ζ_{CNR}. For $\zeta_{CNR} = 1$, no contrast, the distance is zero. Since, intuitively, our processor searches for contrast, it is logical it would fail completely when there is no contrast. However, equation 6.15 also helps explain the asymmetry between performance for positive and negative contrasts of the same magnitude. For $\zeta_{CNR} > 1$, d grows linearly with ζ_{CNR}. However, for $\zeta_{CNR} < 1$, d $\rightarrow$ 1 as contrast increases in magnitude. This limiting value, a result of the asymmetry in the densities around their means, limits the performance for even very large negative contrasts.

Physically, for negative contrasts the mean target intensity is lower than the mean background intensity. However, the speckle induced intensity fluctuations in the background measurements often give intensities less than the mean and close to the target intensities. This makes the two

virtually impossible to distinguish.

Now let us examine the effect of Q and N, i.e., range and spatial resolution, on the performance. We will plot P_M versus Q or N for fixed P_F, M, and ζ_{CNR} for both laser power models. Figure 6.2 plots P_M versus Q for N = 10 and N = 20 at a $CNR_t^{(0)}$ of 16 and 20 dB. Figure 6.2(a) is for the constant average laser power model and figure 6.2(b) is for the constant peak laser power model. Figure 6.3 plots P_M versus N for Q = 10 and 1000 at $CNR_t^{(0)}$ of 16 and 20 dB. Figure 6.3(a) is for the constant average laser power model and figure 6.3(b) is for the constant peak laser power model. All plots hold constant M = 1000, $P_F = 10^{-6}$, and $\zeta_{CNR} = +10$ dB. These figures incorporate the performance corrections for different N and Q values we derived in section A of this chapter.

For the constant average laser power model, the performance is almost completely independent of Q as we expected from the single pixel equations. To the extent there is some dependence, the performance gets poorer as Q increases because of the increased probability of anomaly. For the constant peak laser power model, there is a Q dependence, but it is due to the CNR dependence on Q. As we decrease Q from the full bandwidth value $Q^{(max)}$, the CNR rises and performance improves until it saturates at the speckle limited values. The slight drop in performance at very low Q values for N = 10 is not real. It is a result of the lack of data at high CNR values mentioned in describing figure 6.1(a). (When I ran out of data for higher CNR_t values, I assumed the final data point had reached its asymptote. This assumption is not quite valid, as is obvious from figure 6.1(a).)
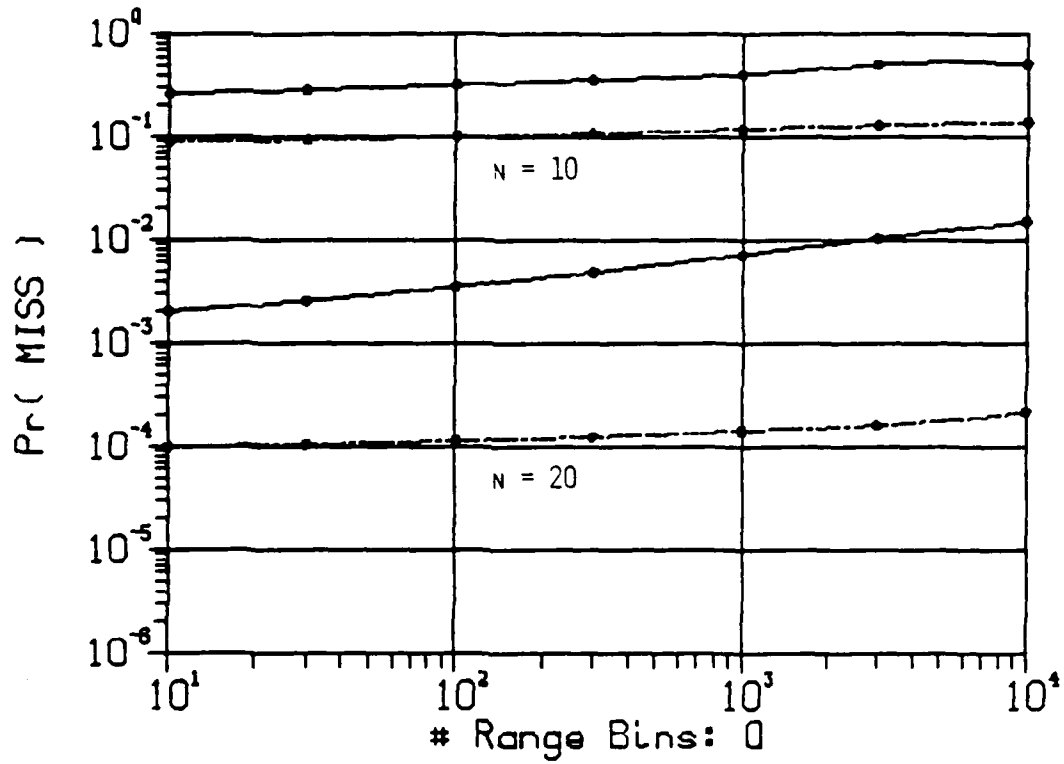
(a)

Figure 6.2

Frame Level Intensity Only Processor Performance

$$P_M \text{ -vs- } Q$$

(a) Constant P_A Model   (b) Constant P_T Model

—— $\text{CNR}_t^{(0)}$ = 16 dB   --- $\text{CNR}_t^{(0)}$ = 20 dB

(b)

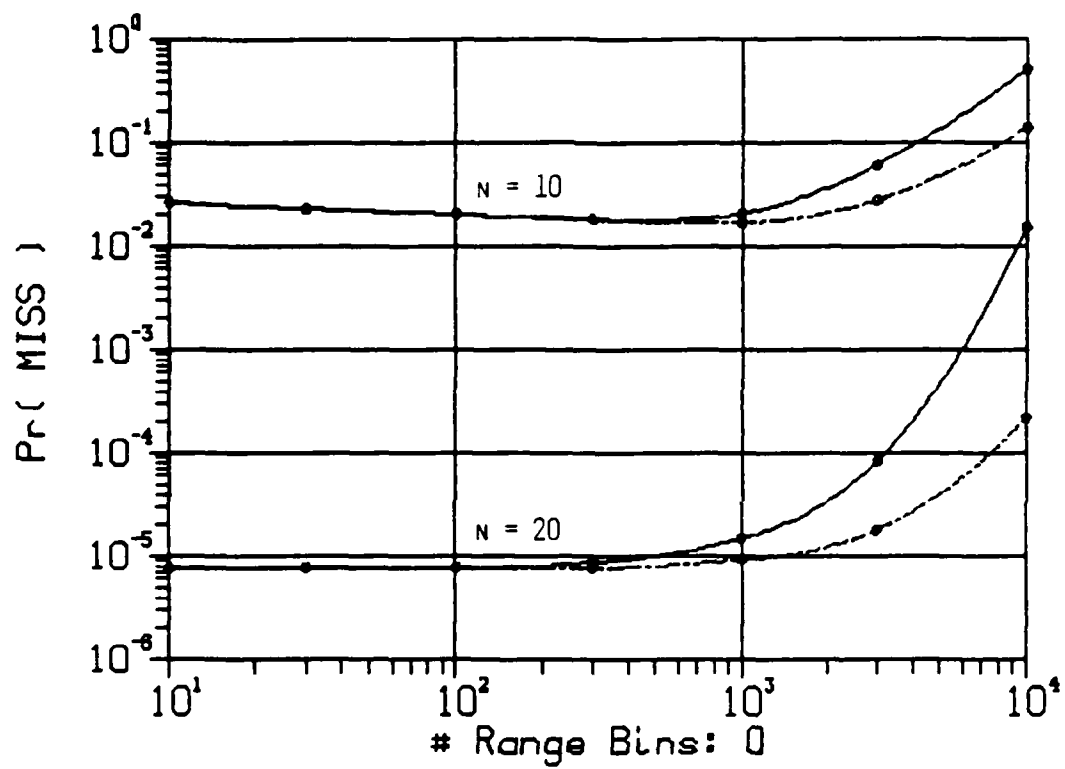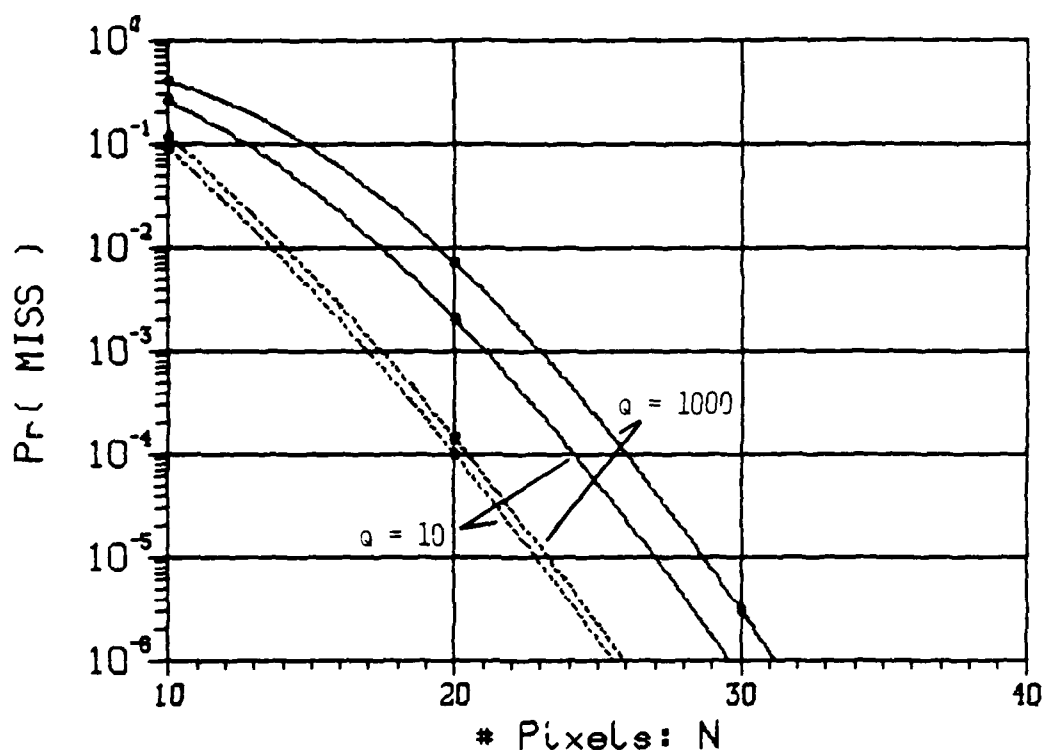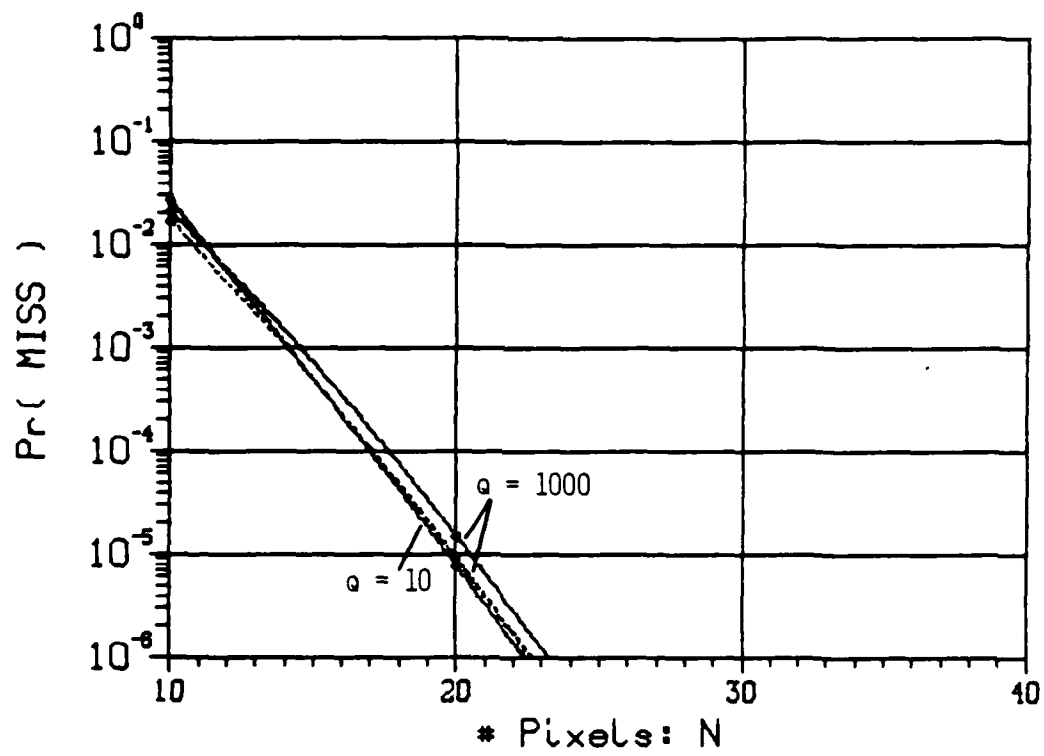Figure 6.2

(cont'd)

(a)

Figure 6.3

Frame Level Intensity Only Processor Performance:

$$P_M \text{ -vs- } N$$

(a) Constant P_A Model   (b) Constant P_T Model

—— $CNR_t^{(0)} = 16$ dB   --- $CNR_t^{(0)} = 20$ dB

(b)

Figure 6.3

(cont'd)

From the form of the Chernoff bound, we expect the performance to get exponentially better with increasing N and figure 6.3 bears this out for both models. Notice in the constant average laser power model the 4 dB change in $CNR_t^{(0)}$ makes a bigger performance difference than the 2 order of magnitude change in Q. For the constant peak laser power model, the Q = 10 curves coincide for both $CNR_t^{(0)}$ values because there is a 30 dB increase in CNR from $Q^{(max)} = 10000$ to Q = 10, so the processors are in their speckle limited regimes regardless of the 4 dB difference in the $CNR_t^{(0)}$ values. For the Q = 1000 case, there is only a 10 dB increase in CNR_t over the full bandwidth CNR, so the 4 dB change in CNR makes a small difference. These curves are still very close to each other and the speckle limited performance regime.

C. Range Processor

Recall the quasi-optimal range only processor determines the difference between the number of hits in the presumed target range bin and the number of hits in the known background range bins for each subframe. If the maximum of these differences exceeds a threshold, the processor declares a target present in the subframe where the maximum occurred:

$$\max_{m} \{ j_m - k_m \} \underset{H_0}{\overset{H_1}{\underset{<}{\overset{>}{\gtrless}}}} \lambda \, . \qquad\qquad (6.16)$$

Using the equations we derived in chapter 5, we can plot P_M versus CNR_t, Q, and N for the range only processor just as we did above for the intensity only processor. (Since Q_B enters the probability mass functions

for j and k, we would expect that performance is also a function of Q_B. In all ensuing examples we assume a square target with each horizontal line of pixels on the target at a different, adjacent range bin number from the adjoining line of pixels. Under this condition, N uniquely determines Q_B: $Q_B = \lceil \sqrt{N} \rceil$.) Figure 6.4 shows frame level P_M versus CNR_t performance for N = 10 and 20 pixels, M = 1000, and Q = 10. Each plot is for P_F values of 10^{-3} and 10^{-6} (dotted lines). For each P_F value there are curves for ζ_{CNR} = +10, 0, and -10 dB.

For this processor, $P_M \to 0$ as $CNR_t \to \infty$ for a fixed ζ_{CNR}. As both CNR_t and $CNR_b \to \infty$, the probabilities of anomaly, the probability of choosing the wrong range bin, for target and background $\to$ 0, so $E[\ j - k \mid H_0\ ] \to$ -N and $E[\ j - k \mid H_1\ ] \to$ +N. But $var[\ j - k \mid H_i\ ] \to$ 0 for i = 0, 1, so, if we define a d parameter as in equation (6.14), we find $d \to \infty$. The two hypotheses are easy to distinguish and the performance improves with increasing CNR_t at constant contrast. Physically, since the probability of anomaly goes to zero, the range estimates are always perfect and so there is infinite range contrast.

We can also explain the behavior as a function of ζ_{CNR} by examining the processor. The processor looks for range measurements from individual pixels to concentrate or clump together in one of two range bins, namely the target or the background bins. As CNR_i increases, the probability of anomaly, $Pr(\ \alpha_{1i}\ )$, drops so the clumping is more pronounced in bin Q_t for the target or bin Q_b for the background. If we fix CNR_t and vary ζ_{CNR}, we will change CNR_b. As ζ_{CNR} increases for a fixed CNR_t, CNR_b drops and $Pr(\ \alpha_{1b}\ )$ increases, so performance grows poorer. This is
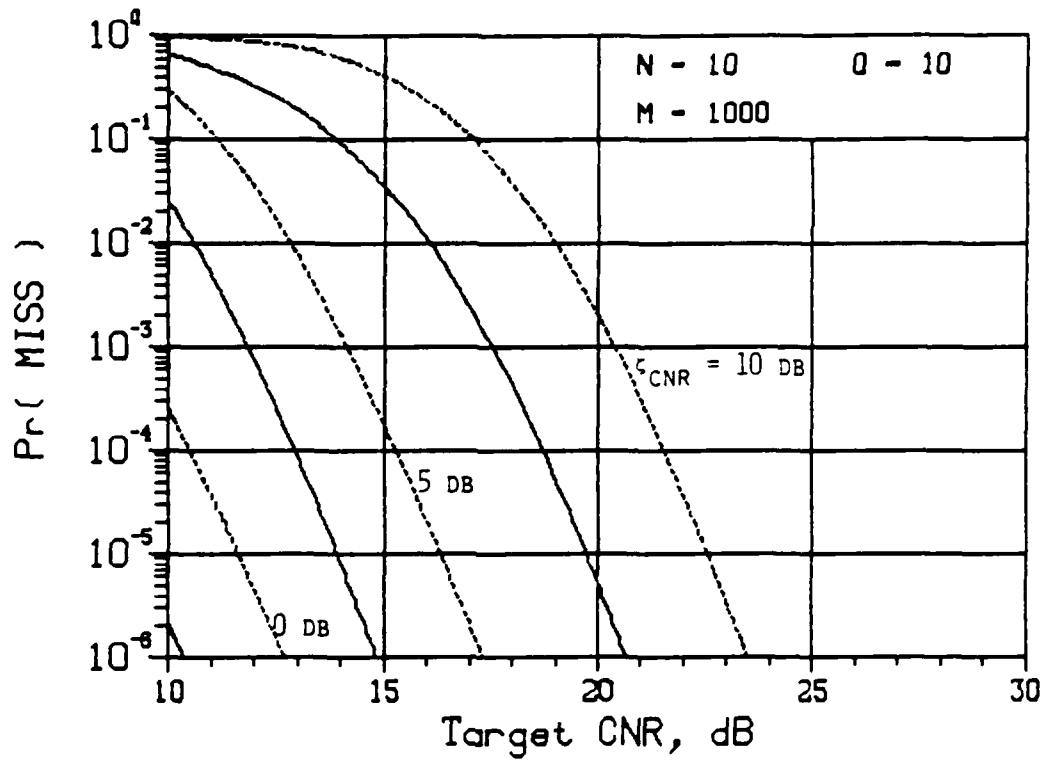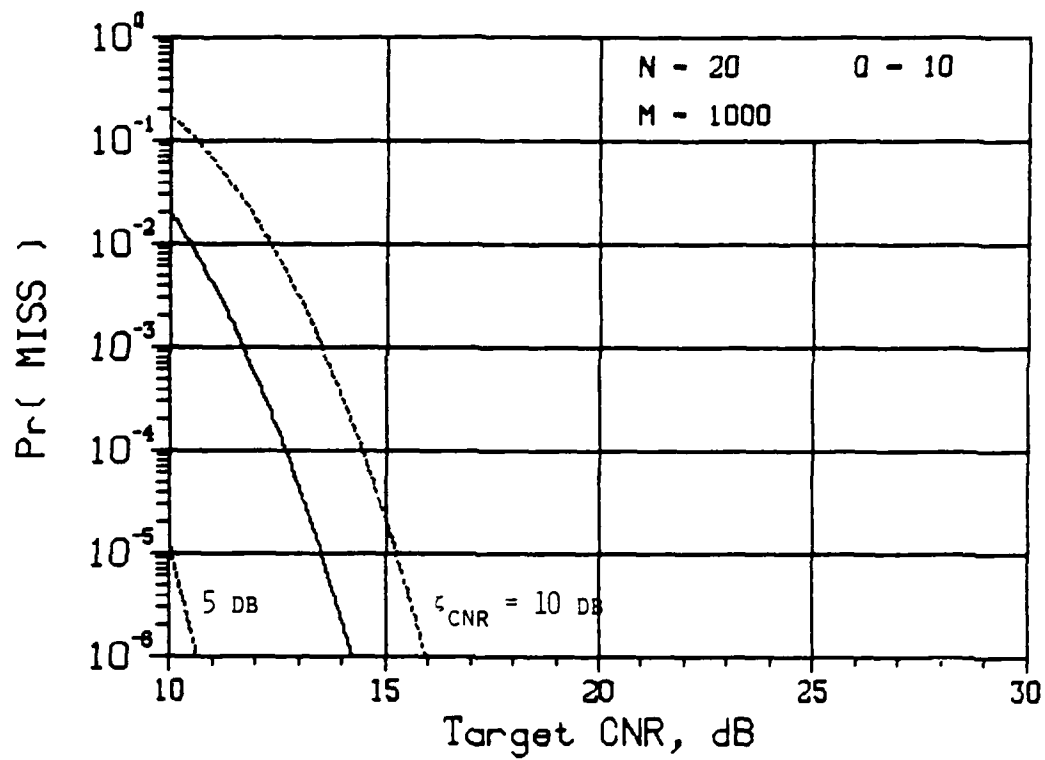
(a)

Figure 6.4

Frame Level Range Only Processor Performance:

$$P_M \text{ -vs- } CNR_t$$

(a) N = 10   (b) N = 20

—— $P_F = 10^{-3}$ --- $P_F = 10^{-6}$

(b)

Figure 6.4

(cont'd)

precisely what figure 6.4 shows: performance for a fixed CNR_t varies inversely with ζ_{CNR}.

Now let us examine the range only processor's performance as a function of Q and N. We will plot P_M versus Q and N for $P_F = 10^{-6}$, M = 1000, and $\zeta_{CNR} = +10$ dB for both laser power models. Figure 6.5 plots P_M versus Q for N = 10 and 20 pixels at $CNR_t^{(0)} = 16$ dB and 20 dB (dotted curves). Figure 6.5(a) is for the constant average laser power model and figure 6.5(b) is for the constant peak laser power model. Figure 6.6 plots P_M versus N for Q = 10 and 1000 at $CNR_t^{(0)} = 16$ dB and 20 dB (dotted curves) under the constant average laser power model.

Figure 6.5(a) shows performance for the constant average laser power model at first increases as Q increases and then falls slightly. There are two effects to consider to explain this behavior. As Q increases, so does Q_T. Since anomalies occur in random bin numbers, the larger is Q_T, the less likely it is that a random clumping of anomalies will be large enough to mistake for a target. This causes performance to improve. On the other hand, as Q_T increases, $Pr(\alpha_{1t})$ increases approximately logarithmically [4]:

$$Pr(\alpha_{1t}) \simeq a_t \left(\log(Q) - \frac{1}{2Q} + 0.577 \right) , \qquad (6.17)$$

which in turn reduces the processor's performance. These two effects combine to produce the behavior in figure 6.5(a). Under the constant peak laser power model, the increase in CNR_t as Q falls overwhelms the weaker Q dependence from the statistics. So, performance gets better very quickly for decreasing Q.
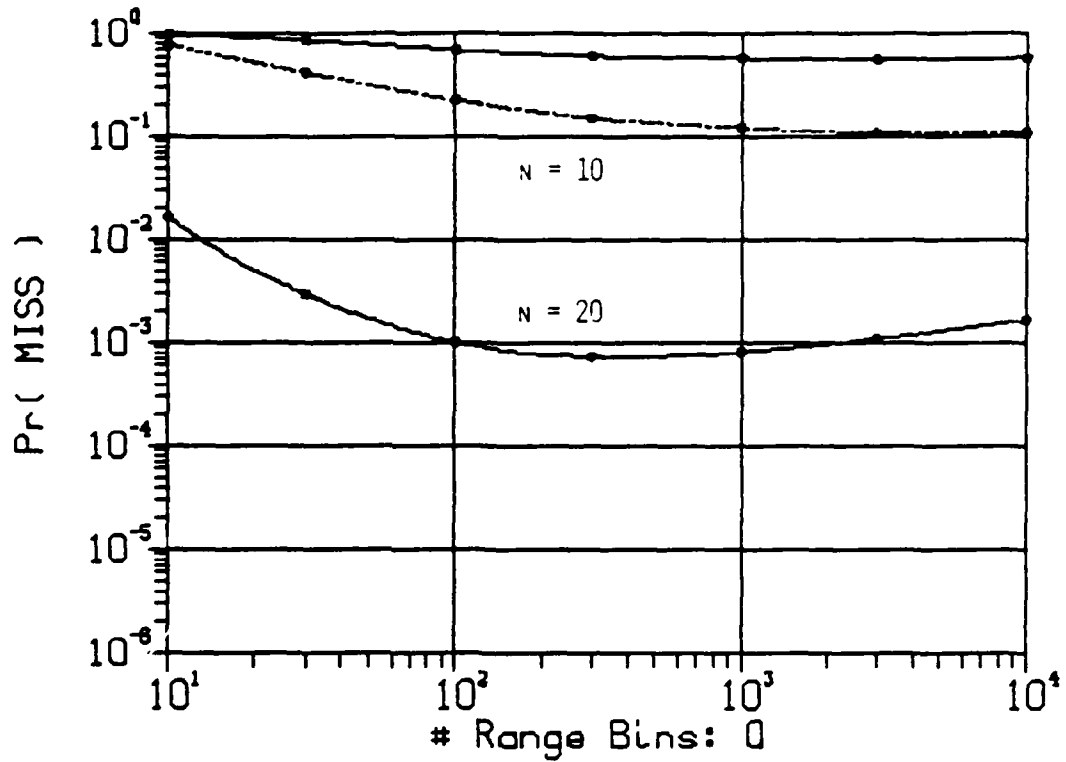
(a)

Figure 6.5

Frame Level Range Only Processor Performance:

$$P_M \text{ -vs- } Q$$

(a) Constant P_A Model   (b) Constant P_T Model

—— $CNR_t^{(0)} = 16$ dB   - - - $CNR_t^{(0)} = 20$ dB
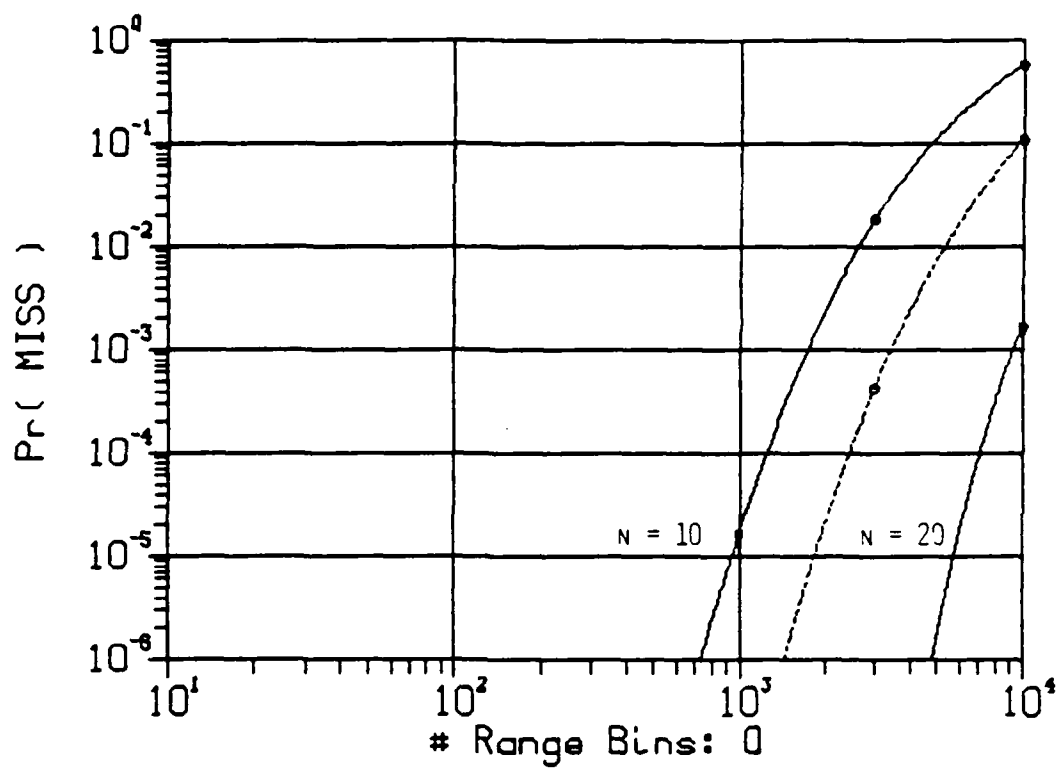
(b)

Figure 6.5

(cont'd)
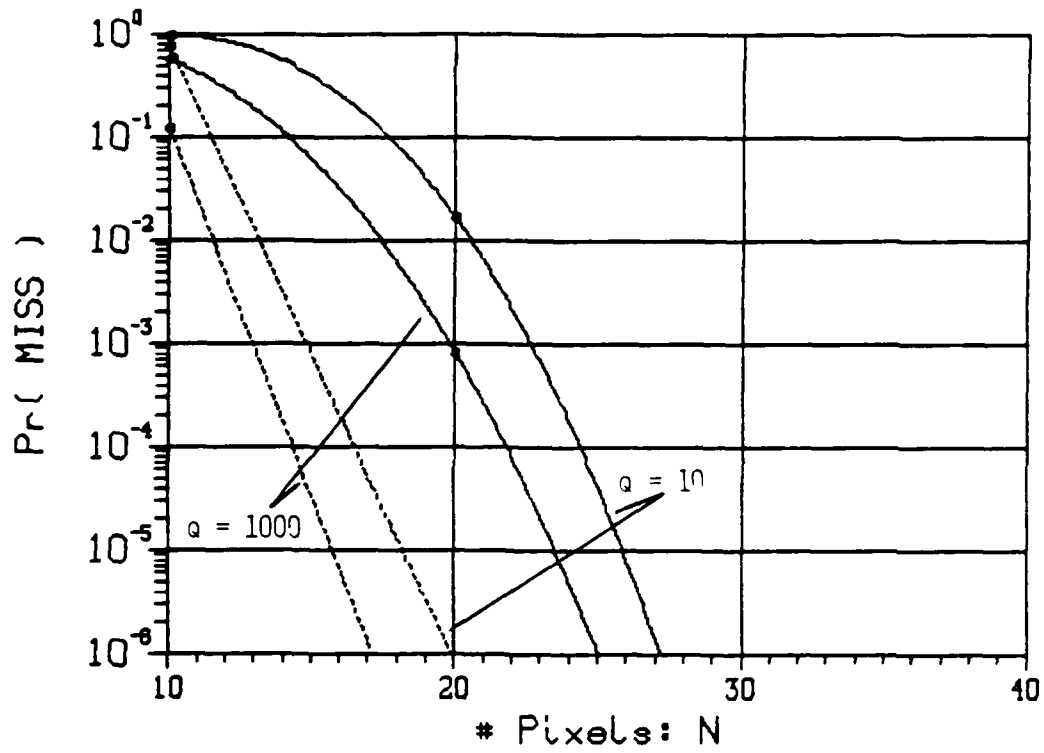
Figure 6.6

Frame Level Range Only Processor Performance:

P_M -vs- N

Constant P_A Model

—— $CNR_t^{(0)} = 16$ dB   --- $CNR_t^{(0)} = 20$ dB

Figure 6.6 shows that the range only processor's performance, under the constant average laser power model, as a function of N improves approximately exponentially in N. Since we are dealing with sums of random variables (we sum the number of hits in each bin over the subframe), the Chernoff bound applies to the tails of the range densities (although it would be difficult to generate one explicitly for this density). The Chernoff bound exhibits this exponential dependence on N for any density. Like the intensity only processor, we see the effect of the change in Q of two orders of magnitude is less important than a change of 4 dB in $CNR_t^{(0)}$. There is no curve for the constant peak laser power model because, for these parameter values, the 10 dB increase in CNR_t due to reducing Q from 10000 to 1000 is enough to drive all the P_M curves down below 10^{-6}.

D. Performance Comparisons

Now we want to compare detection performance of the range only and intensity only processors. There are many ways to perform these comparisons, some probably more suitable than others for any given problem. I have selected two methods of presentation. Both methods keep in mind our goal of expressing system performance in terms of system parameters and resolving power in the different measurement dimensions.

The first method is closely related to the way we presented results for the processors individually in sections B and C above. We will plot the quantity $\log_{10}(P_M^{(Intensity)} / P_M^{(Range)})$ as a function of Q and N, where the superscripts indicate the processor from which we derived the P_M value. Figure 6.7 shows such a plot for the constant average laser power
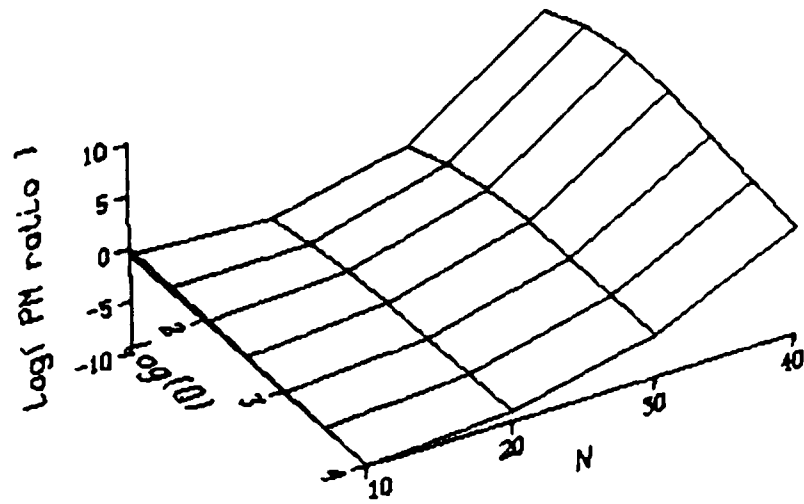
(a)
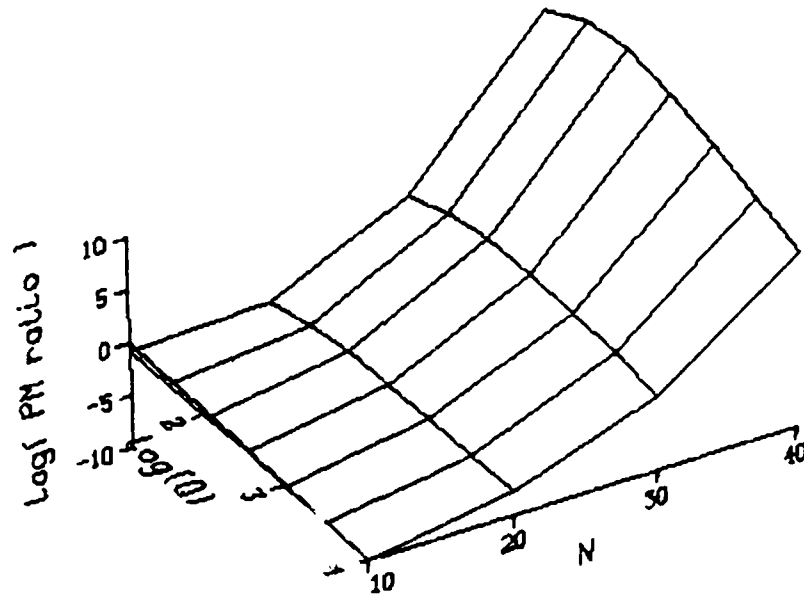
(b)

Figure 6.7

Ratio of P_M Values for Range Only and Intensity Only Processors,

Constant P_A Model

(a) $CNR_t^{(0)} = 16$ dB

(b) $CNR_t^{(0)} = 18$ dB

$P_F = 10^{-6}$, $\zeta_{CNR} = 10$ dB, $M = 1000$

model with $M = 1000$, $P_F = 10^{-6}$, $\zeta_{CNR} = +10$ dB, and $CNR_t^{(0)} = 16$dB and 18

dB. A positive value indicates the range processor outperforms the

intensity processor. It may be difficult to see on these plots, but the

intensity processor does slightly out-perform the range processor for low

N and Q values. We saw both processors improve exponentially with

increasing N, but these plots indicate the range only processor improves

faster than the intensity only processor, hence the surface always slopes

up for increasing N. Physically, this corresponds to performance

increasing more quickly as a result of range clumping in the range only

processor than as a result of averaging out the speckle intensity

variations in the intensity only processor. The concavity of a plot for a

cut along a constant N value reflects the behavior in figures 6.5(a) and

6.2(a). Since the intensity only processor is only very weakly dependent

on Q, the result is mostly due to the change in performance for the range

only processor as a function of Q. We have already discussed this

behavior in section C.

This method shows quite graphically how the two processors perform

relative to each other, however, we need a different plot for each $CNR_t^{(0)}$

and we get no indication of the absolute P_M for any point. Also, the

strong dependence of P_M on Q under the constant peak laser power model

makes it difficult to construct similar plots for that model.

Consider the other display method. Suppose we set certain performance

requirements: require meeting a P_F and P_M criteria at a given CNR_t and

ζ_{CNR}. Then we can simply check whether or not a processor meets these

requirements as a function of Q and N. Figures 6.8 and 6.9 show several

PF = 10^-6,   PM = 0.0010   PF = 10^-6,   PM = 0.0010
Target CNR = 20 dB, Contrast = 10 dB   Target CNR = 16 dB, Contrast = 10 dB

$\log_{10}(Q)$ $\log_{10}(Q)$

    1.0 1.5 2.0 2.5 3.0 3.5 4.0   1.0 1.5 2.0 2.5 3.0 3.5 4.0

 10   10

 20 ■ ■ ■ ■ ■ ■ ■   20 0 ■ ■ X X X X
N   N
 30 ■ ■ ■ ■ ■ ■ ■   30 ■ ■ ■ ■ ■ ■ ■

 40 ■ ■ ■ ■ ■ ■ ■   40 ■ ■ ■ ■ ■ ■ ■

X = Range Only meets requirements   X = Range Only meets requirements
0 = Intensity Only meets requirements   0 = Intensity Only meets requirements

(a)

PF = 10^-3,   PM = 0.0500   PF = 10^-3,   PM = 0.0500
Target CNR = 20 dB, Contrast =   5 dB   Target CNR = 16 dB, Contrast =   5 dB

$\log_{10}(Q)$ $\log_{10}(Q)$

    1.0 1.5 2.0 2.5 3.0 3.5 4.0   1.0 1.5 2.0 2.5 3.0 3.5 4.0

 10 X X X X X X X   10

 20 X X X X X X X   20 X X X X X X X
N   N
 30 ■ ■ ■ ■ ■ ■ ■   30 ■ ■ ■ ■ ■ ■ ■

 40 ■ ■ ■ ■ ■ ■ ■   40 ■ ■ ■ ■ ■ ■ ■

X = Range Only meets requirements   X = Range Only meets requirements
0 = Intensity Only meets requirements   0 = Intensity Only meets requirements

(b)

Figure 6.8

Range Only-Intensity Only Processor Performance Trades:

Constant P_T Model

(a) High Performance, High Contrast

(b) Low Performance, Low Contrast

PF = 10^-6,   PM = 0.0010   PF = 10^-6,   PM = 0.0010
Target CNR = 20 dB, Contrast = 10 dB   Target CNR = 16 dB, Contrast = 10 dB

$\log_{10}(Q)$ $\log_{10}(Q)$

```
     1.0 1.5 2.0 2.5 3.0 3.5 4.0            1.0 1.5 2.0 2.5 3.0 3.5 4.0

 10   X   X   X   X   X   X            10   X   X   X   X   X

 20   8   8   8   8   8   8   8        20   8   8   8   8   8   8   X
N                                    N
 30   8   8   8   8   8   8   8        30   8   8   8   8   8   8   8

 40   8   8   8   8   8   8   8        40   8   8   8   8   8   8   8
```

X = Range Only meets requirements   X = Range Only meets requirements
0 = Intensity Only meets requirements 0 = Intensity Only meets requirements

(a)

PF = 10^-3,   PM = 0.0500   PF = 10^-3,   PM = 0.0500
Target CNR = 20 dB, Contrast = 5 dB   Target CNR = 16 dB, Contrast = 5 dB

$\log_{10}(Q)$ $\log_{10}(Q)$

```
     1.0 1.5 2.0 2.5 3.0 3.5 4.0            1.0 1.5 2.0 2.5 3.0 3.5 4.0

 10   X   X   X   X   X   X   X        10   X   X   X   X   X   X

 20   X   X   X   X   X   X   X        20   X   X   X   X   X   X   X
N                                    N
 30   8   8   8   8   8   8   8        30   8   8   8   8   8   8   8

 40   8   8   8   8   8   8   8        40   8   8   8   8   8   8   8
```

X = Range Only meets requirements   X = Range Only meets requirements
0 = Intensity Only meets requirements 0 = Intensity Only meets requirements

(b)

Figure 6.9

Range Only-Intensity Only Processor Performance Trades:

Constant P_A Model

(a) High Performance, High Contrast

(b) Low Performance, Low Contrast

displays for M = 1000 and various performance requirements under the constant average and peak laser power model, respectively. It is quite easy to generate such displays for a given set of performance requirements. An "X" indicates the range processor meets the performance criteria for that Q and N while an "O" indicates the intensity processor meets the criteria. From the display a system engineer can, for instance, determine what combinations of N and Q will give a range or intensity processor which meets the necessary performance requirements.

Figure 6.8, for the constant average laser power model, shows the more significant impact of laser aperture size, A_p, (reflected in the N value) on performance relative to the resolution parameter Q. Generally the processor either meets requirements for a given N or not, regardless of Q. Figure 6.8(a) is for relatively high performance requirements: P_D = 99.9% at $P_F = 10^{-6}$ and fairly low $CNR_t^{(0)}$ values. At 16dB, we find the point N = 20 pixels, Q = 10 bins where the intensity only processor out-performs the range only processor. At higher Q values, $\geq$ 300, the intensity only processor fails, but the range only processor satisfies the requirements for $Q \geq 30$. If we increase the $CNR_t^{(0)}$ by only 4 dB, we can meet requirements with either processor as long as $N \geq 20$.

In figure 6.8(b) we relax the performance requirements somewhat to P_D = 95% at $P_F = 10^{-3}$, but we reduce the contrast to only 5 dB. Here the intensity only processors need at least N = 30 pixels to meet the relaxed requirements because they perform so poorly at low contrasts. The range only processors perform well enough, however, that for a 4 dB increase in $CNR_t^{(0)}$, we can cut angular resolution in half, from N = 20 pixels to N =

10 pixels and still meet requirements.

In figure 6.9(b), for the constant peak laser power model, the increase in CNR for reduced Q allows the processors to meet performance at lower N values. This effect is strong enough to change the Q dependence for the range only processor and make it perform better for small Q values. We saw this phenomenon in figure 6.5(b) as well.

E. Other Processors

Now it is worthwhile to say a few words about other types of processors and how to apply these results to them. We derived dualities for Doppler and range-Doppler processors in the last two sections of chapter 3. We can apply the results from this chapter to Doppler receivers as a result of those dualities, but we must take care in how we do the comparisons because of the system parameter interdependencies we worked with at the beginning of this chapter. In general, we have to consider each transmitter waveform separately and determine the effect on scaling parameters, particularly for range-Doppler systems where complex waveforms are often the norm.

For a Doppler only processor, we will use the long Gaussian pulse waveform we used in deriving the duality of chapter 3. We must determine how CNR scales with changing f_r, frequency resolution, and hence Q, for this waveform. We still have a pulsed Gaussian transmitter waveform, so the equations in 6.6 above still hold. Now, however, the frequency resolution is approximately $f_r \approx 1/t_r$ and the bandwidth is approximately $B = 1/t_r = f_r$. If F_u is the frequency uncertainty interval width, $Q = F_u/f_r = F_u/B$.

In an exact analogy with the ranging radar, we will assume the problem statement fixes F_u. In the ranging radar, we could make t_r arbitrarily small without worrying about L_u. In the Doppler radar, we must be a little concerned about making f_r too small. Although the design of Fourier transform devices like surface acoustic wave devices (SAWs) is somewhat afield of this thesis topic [22], there is a time-bandwidth (TW) product constraint on $F_u t_r$. However, high time-bandwidth product devices are available [22] so we will assume F_u is small enough that we can increase the frequency resolution without affecting F_u. Under this condition,

$$\frac{P_T}{B} = P_A T = \frac{P_T Q}{F_u} \ . \tag{6.18}$$

Now we can write how CNR depends on Q (the N dependence has not changed from the range radar analysis):

$$CNR_i = \begin{cases} CNR_i^{(0)} \ \dfrac{N}{N^{(max)}} \ \dfrac{Q}{Q^{(max)}} & : \ P_T \text{ limited} \\[4mm] CNR_i^{(0)} \ \dfrac{N}{N^{(max)}} & : \ P_A \text{ limited} \end{cases} \tag{6.19}$$

where $i = t$ or b.

Here $CNR_i^{(0)}$ still corresponds to CNR_i at $N = N^{(max)}$ and $Q = Q^{(max)}$. Now, however, by equation 6.18, $Q^{(max)}$ corresponds to minimum IF bandwidth instead of maximum IF bandwidth. If we defined a minimum Q value, $Q^{(min)}$, and defined $CNR_i^{(0)}$ at $N = N^{(max)}$ and $Q = Q^{(min)}$, then the scaling law for CNR_i would be the same as equation 6.12 for the ranging radar with $Q^{(max)}$ replaced by $Q^{(min)}$. Then the plots of figure 6.9 would still apply to the

Doppler only, constant P_T model analysis except the Q labels would reverse, running left to right from Q = 10000 to Q = 10 (i.e., take a mirror image of each plot through an axis at $\log_{10}(Q) = 2.5$). However, $Q^{(max)}$ still corresponds to maximum Doppler resolution which is a more physically meaningful quantity than $Q^{(min)}$. Analogous to the range radar case, there is a limit to how fine we can make the Doppler resolution. If we make the resolution too fine, we will start to resolve the fine Doppler structures of the target like vibrations and rotations of various parts of the target within a pixel. This violates the unresolved Doppler assumption we used in the derivations. Consequently, we will use the definition of $CNR_i^{(0)}$ in terms of full aperture and minimum bandwidth.

Obviously, we can apply the constant P_A model results for a ranging radar directly to the case of a Doppler radar. The ranging radar constant P_T results don't translate to Doppler results so easily because the two radars have opposite CNR dependencies on Q. However, we can make plots like those in figures 6.8 and 6.9 for this new CNR dependence on Q. Figures 6.10 (a) and (b) plot the same performance and contrast cases as in figures 6.8 and 6.9 but for this new Q dependence. Now as we decrease the Doppler velocity resolution, the transmitted pulse must grow narrower and so the IF bandwidth must grow larger. This causes the CNR to drop. The data base used for all the plots in this chapter only goes down to $CNR_t = 10$ dB, so when Q falls low enough that CNR_t falls to below 10 dB, we assume the processor cannot meet the performance requirements. (Realistically, we don't expect much out of any processor at such low CNR levels.) Because the CNR_t values fall so quickly, figure 6.10 (c) plots the same performance and contrast cases as in figures 6.10 (a) and (b)

PF = 10^-6,   PM = 0.0010
Target CNR = 20 dB, Contrast = 10 dB

$$\log_{10}(Q)$$

```
     1.0 1.5 2.0 2.5 3.0 3.5 4.0

  10

  20                      X   ∎
N
  30                      ∎   ∎

  40                  ∎   ∎   ∎
```

X = Doppler Only meets requirements
0 = Intensity Only meets requirements

PF = 10^-6,   PM = 0.0010
Target CNR = 16 dB, Contrast = 10 dB

$$\log_{10}(Q)$$

```
     1.0 1.5 2.0 2.5 3.0 3.5 4.0

  10

  20                          X
N
  30                      X   ∎

  40                      ∎   ∎
```

X = Doppler Only meets requirements
0 = Intensity Only meets requirements

(a)

PF = 10^-3,   PM = 0.0500
Target CNR = 20 dB, Contrast = 5 dB

$$\log_{10}(Q)$$

```
     1.0 1.5 2.0 2.5 3.0 3.5 4.0

  10                      X

  20                  X   X
N
  30                  X   ∎

  40              X   ∎   ∎
```

X = Doppler Only meets requirements
0 = Intensity Only meets requirements

PF = 10^-3,   PM = 0.0500
Target CNR = 16 dB, Contrast = 5 dB

$$\log_{10}(Q)$$

```
     1.0 1.5 2.0 2.5 3.0 3.5 4.0

  10

  20                          X
N
  30                      X   ∎

  40                      ∎   ∎
```

X = Doppler Only meets requirements
0 = Intensity Only meets requirements

(b)

Figure 6.10

Doppler Only-Intensity Only Processor Performance Trades:

Constant P_T Model

(a) High Performance, High Contrast

(b) Low Performance, Low Contrast

(c) High $CNR_t^{(0)}$ Cases

PF = 10^-3,   PM = 0.0500   PF = 10^-6,   PM = 0.0010
Target CNR = 30 dB, Contrast =   5 dB   Target CNR = 30 dB, Contrast = 10 dB

$$\log_{10}(Q)$$ $$\log_{10}(Q)$$

	1.0	1.5	2.0	2.5	3.0	3.5	4.0
10					X	X	X
20			X	X	X	X	
30			X	■	■	■	
40		■	■	■	■	■	

N

	1.0	1.5	2.0	2.5	3.0	3.5	4.0
10						X	X
20				X	■	■	■
30				■	■	■	■
40		■	■	■	■	■	

N

X = Doppler Only meets requirements   X = Doppler Only meets requirements
0 = Intensity Only meets requirements   0 = Intensity Only meets requirements

(c)

Figure 6.10

(Cont'd)

except for $CNR_t^{(0)}$ = 30 dB so we can get more points on the plot before CNR_t falls below 10 dB.

A drop in Q from 10000 to 1000 reduces the system CNR by 10 dB. This effect dominates the performance plots in figure 6.10. This effect is strong enough to overwhelm the much weaker underlying Q dependences in the processors which we plotted in figures 6.2 (a) and 6.5 (a). Both processors exhibit degraded performance for decreased Q. For any fixed N value, however, the Doppler only processor always performs at least as well as the intensity only processor in these cas~s.

The poorer performance of the intensity only processor at low contrasts is still readily apparent in these plots. If we have only 5 dB of contrast, even at $CNR_t^{(0)}$ = 30 dB we need at least N = 30 to achieve the performance standards with the intensity only processor. At the same $CNR_t^{(0)}$ value, the Doppler only processor meets performance requirements at N = 10 for both performance and contrast cases.

The plots in figure 6.10 give us additional insight into the effect of changing bandwidth over that gained from the plots in figure 6.9. In figure 6.9, the change in bandwidth only improved an already reasonable CNR. Here, the change (increase) in bandwidth reduces the CNR and we can see quite dramatically the effect the falling CNR has on performance.

We will conclude this section and the chapter by doing a brief analysis of the range and Doppler case using the thumbtack ambiguity function of figure 3.3, where T is the duration of the waveform and B is its

bandwidth. With this case we have a bit more difficulty being specific about the relationships between CNR and T and B because we have not specified the waveform explicitly and we cannot specify the duty cycle, t_r/T in our notation, based solely on the ambiguity function. (Actually, the ambiguity function uniquely determines the waveform, but there is no general procedure for inverting an ambiguity function to find the corresponding transmitted waveform.) Microwave radars often use coded pulses, up-chirps, down-chirps, and combinations of these waveforms [20]. We will assume a duty cycle of 1 (or at least a duty cycle independent of T and B) so the P_A-limited and P_T-limited cases are identical. This is a good assumption at least for the CW chirped waveforms. Now we will define two Q related values: $Q_F = F_u T$, the number of Doppler bins, and $Q_L = L_u B$, the number of range bins, with $Q = Q_F Q_L$ (see figure 3.4). For a unity duty cycle,

$$\frac{P_T}{B} = \frac{P_A}{B} = \frac{P_T \, 2 \, L_u}{Q_L \, c} \quad ,$$

$$CNR_i = CNR_i^{(0)} \, \frac{N}{N^{(max)}} \, \frac{Q_L^{(max)}}{Q_L} \quad , \tag{6.19}$$

exactly as for the ranging radar with constant P_T. There is another consideration, however, which won't permit us to use the ranging radar analyses directly when changing the value of Q or Q_L. When computing performance numbers, we must use the value $Q = Q_F Q_L$ since it is this total Q which influences the peak detector and $Pr(\alpha_0)$. However, when we change Q and examine the effect on the performance through the scaled CNR, we must scale only on changes in Q_L with no scaling for changes in Q_F.

This brief analysis is meant only to show how the scaling laws can be used in a range and Doppler analysis. For specific waveforms, more precise analyses are possible. However, we should still expect to see different dependences on Q_L and Q_F in the scaling laws while the performance equations remain a function only of Q.

VII. SUMMARY AND CONCLUSIONS

In this thesis we have attacked the problem of obtaining analytical
expressions for the performance of laser radars as a function of several
signal dimensions for multipixel targets. To derive such expressions, we
proposed a reasonable model for real targets and their environments in the
form of a vertical target against a sloping background at unknown range
and location. We derived an expression for the IF signal in the radar for
a single pixel based on the diffuse speckle target model and used the
components of our target and environment model to incorporate the range
and spatial information. We derived near optimal intensity, range, and
joint range and intensity measurement processors sacrificing optimality
for simplicity where necessary without over-simplifying the model. We
were able to derive performance measures for two of the processors and
compute the performance as a function of the radar parameters and
resolutions. Finally, we examined some specific cases of the results and
explained physically what phenomena were at work to give the observed
results.

What we found qualitatively was that the range only processor generally
outperforms the intensity only processor. This comes as no surprise to
researchers in this field. However, we were also able to make
quantitative statements, and this is something new to this area of
research. For a given set of parameters, we can say which processor will
perform better and by how much. We can deduce the regions where an
intensity only processor outperforms a range processor and by how much.
We made quantitative statements about how sensitive performance is to any

of the system parameters we investigated (N, Q, CNR_t, and ζ_{CNR}).

Although we achieved our stated goal for the thesis, there are several areas where future work could extend the results. The most important of these areas involve relaxing assumptions and making the models even more realistic.

The first assumption which we might relax is the assumption the target aligns exactly with a subframe. Although this assumption is probably the most physically unappealing of all, it may be the least important. We saw (equation 4.7) the system performance depends on the performance for a single subframe of data. Once we have the performance or statistics for a single subframe, the overall system performance comes directly from maximizing over the subframes. If we take a window the size and shape of the target and slide it around the frame (like the dotted target outline in figure 2.5) collecting a subframe statistic for each possible window location, we would collect about MN subframes statistics, each statistically correlated with N other subframe statistics. Consequently, the difference between this model and the target aligned with the subframe model is simply maximizing over MN dependent random variables or over M independent random variables. Whether we maximize over independent subframes or statistically dependent subframes tells us nothing new about laser radars per se. Furthermore, the number of subframes is independent of any of the radar parameters (chapter 6, section A). The one factor which does change is the statistics of the subframes if the target is not aligned exactly with the subframes. However, in the absence of noise, the maximum contrast in either intensity or range space must occur when the

window aligns with the true target location. All these factors considered, it may be more productive to concentrate on better characterizations of the subframe statistics rather than better models for the subframe maximization procedure.

For the subframe model we used, the most important extension of the work is probably an analysis of the joint intensity and range processor in chapter 4, section F. This will probably involve simulation, but there may yet be further analytical steps an investigator could take.

The final general area for future work on the models is in the model for the target and its environment. Here there are several ways the models could improve.

First, there are still parameters which we should have treated as unknown in a completely general model. Two of these are the target size and the target shape. Treating target size as an unknown parameter will involve adding N to the set of unknown parameter in vector $\overline{A}$ in chapter 4. Assuming an unknown target shape will be a bit more difficult to incorporate into the generalized likelihood ratio models. One potential method is to define a standard set of shapes and maximize over the discrete members of that set.

Second, if the background is not smooth, our assumption of known range to background is no longer valid. Then a ranging radar with very good range resolution, 1_r, might make many more errors because it used the wrong bins for counting the background hits, K. One solution to this problem could

be to assume the background is only reasonably smooth and expand the size of the set of background range bins. That is, increase Q_B for the same Q, then perform a maximization over the Q_B bins similar to the target maximization to get a value for k. However, since the correct bin number changes from one scan line to the next and may now also change within a scan line since the background is not smooth, this maximization will be much more difficult to define and perform.

Third, both target and background could have non-uniform reflectivity, so CNR_t and CNR_b would be functions of angular location (vary by pixel). We have assumed throughout the thesis the CNRs are independent of position: the target and background have uniform reflectivity. Particularly for the background, which is much larger than the small targets we used in this thesis, this assumption is probably not valid in any real problem of interest.

REFERENCES

1.   Bachman, C. G., _Laser Radar Systems and Techniques_, Artech House, Dedham, MA, 1979.

2.   Biron, D. G. and Edwards, B. E., "Moving Target Imaging Radar Utilizing both Intensity and Velocity Information," _Technical Digest of Conference on Lasers and Electro-Optics_, paper TB-6, Optical Society of America, Phoenix, AZ, 1982.

3.   Goodman, J. W., "Statistical Properties of Laser Speckle Patterns," _Laser Speckle and Related Phenomena_, J. C. Dainty (ed), Springer Verlag, Berlin, 1975.

4.   Van Trees, H. L., _Detection, Estimation, and Modulation Theory, Part I_, John Wiley and Sons, New York, 1968.

5.   Sullivan, D. R., "Active 10.6 um Image Processing," _Image Processing for Missile Guidance_, Proceedings SPIE 238, 1980.

6.   Lee, C. C., "Modified Distance Transform and Linking Algorithm for Image Skeletonization," _Coherent Infrared Radar Systems and Applications II_, Proceedings SPIE 415, 1983.

7.   Harney, R. C., _Conceptual Design of an Multifunction Infrared Radar for the Tactical Aircraft Ground Attack Scenario_, MIT Lincoln Labs, Project Report TST-25, 25 August 1978.

8.   Harney, R. C. and Hull, R. J., "Compact Infrared Radar Technology," _CO_2 Laser Devices and Applications_, Proceedings SPIE 227, 1980.

9.   Gschwendtner, A. B., Harney, R. C., and Hull, R. J., "Coherent IF Radar Technology," _Optical and Laser Remote Sensing_, D. K. Killinger and A. Mooradian (eds), Springer-Verlag, Berlin, 1983.

10. Gagliardi, R. M. and Karp, S., _Optical Communications_, John Wiley and Sons, New York, 1976.

11. Goodman, J. W., "Some Effects of Target-Induced Scintillation on Optical Radar Performance," _Proceedings of the IEEE_, _53_:11, November 1965.

12. Reinhold, R. W., _Reflectivity Determination Using a Peak Detecting Coherent Laser Radar_, SM Thesis, Dept of Electrical Engineering, MIT, June 1985.

13. Mesite, P. L., _Laser Speckle and Clutter Effects on Moving Targets Observed with an Optical Radar_, SM Thesis, Dept of Electrical Engineering, MIT, September 1983.

14. Shapiro, J. H., B. A. Capron, and R. C. Harney, "Imaging and Target Detection with a Heterodyne-Reception Optical Radar," Applied Optics 20:19, 1 October 1981.

15. Siegman, A. E., "The Antenna Properties of Optical Heterodyne Receivers," Proceedings of the IEEE, 54:10, October 1966.

16. Papoulis, A., Probability, Random Variables, and Stochastic Processes, McGraw-Hill, New York, 1965.

17. Shapiro, J. H., "Target Reflectivity Theory for Coherent Laser Radars," Applied Optics 21:18, 15 September 1982.

18. Mark, M. B., Multipixel Multidimensional Laser Radaer System Analysis, PhD Thesis Proposal, Dept of Electrical Engineering, MIT, Nov 1985.

19. Van Trees, H. L., Detection, Estimation, and Modulation Theory, Part III, John Wiley and Sons, New York, 1968.

20. Skolnik, M. I., Introduction to Radar Systems, McGraw-Hill, New York, 1980.

21. Goodman, J. W., Fourier Optics, McGraw-Hill, New York, 1968.

22. Arsenault, D. R., and Dolat, V. S., "Compact Multiple-Channel SAW Sliding-Window Spectrum Analyzer," 1981 Ultrasonics Symposium, IEEE, New York, 1981.

23. Shapiro, J. H., Reinhold, R. W., and Park, D., "Performance Analyses for Peak-Detecting Laser Radars," Proceedings of the SPIE, 663, 1986.

24. Papurt, D. M., Shapiro, J. H., and Lau, S. T., "Measured Turbulence and Speckle Effects in Laser Radar Target Returns," Proceedings of the SPIE, 415, 1983.

BIOGRAPHICAL NOTE

Martin B. Mark was born 17 December 1957 in Indianapolis, Indiana. He graduated from Purdue University at West Lafayette, IN, with a BSEE degree in 1979 and was also commissioned a Second Lieutenant in the United States Air Force through the ROTC program. His first assignment was to the Air Force Institute of Technology (AFIT) at Wright-Patterson AFB, OH, where he received an MSEE degree through the Electro-Optics program in 1980. He was then assigned to Air Force Space Division at Los Angeles AFS, CA, where he was a Satellite Development Manager for almost three years. AFIT then selected him for attendance at a civilian institution of his choice to pursue a PhD in electrical engineering and he gained admission to MIT. After receiving his PhD, Capt Mark reported to the USAF Academy in Colorado Springs, CO, for duty as an Assistant Professor of Electrical Engineering. Capt Mark is married to the former Miss Lynn Sharet.

END

11-86

DTIC